BioMed Research International

New Approaches, Findings, and Diagnostics in Medical and Surgical Retina

Guest Editors: Jerzy Nawrocki, Ron Adelman, and Didier Ducournau

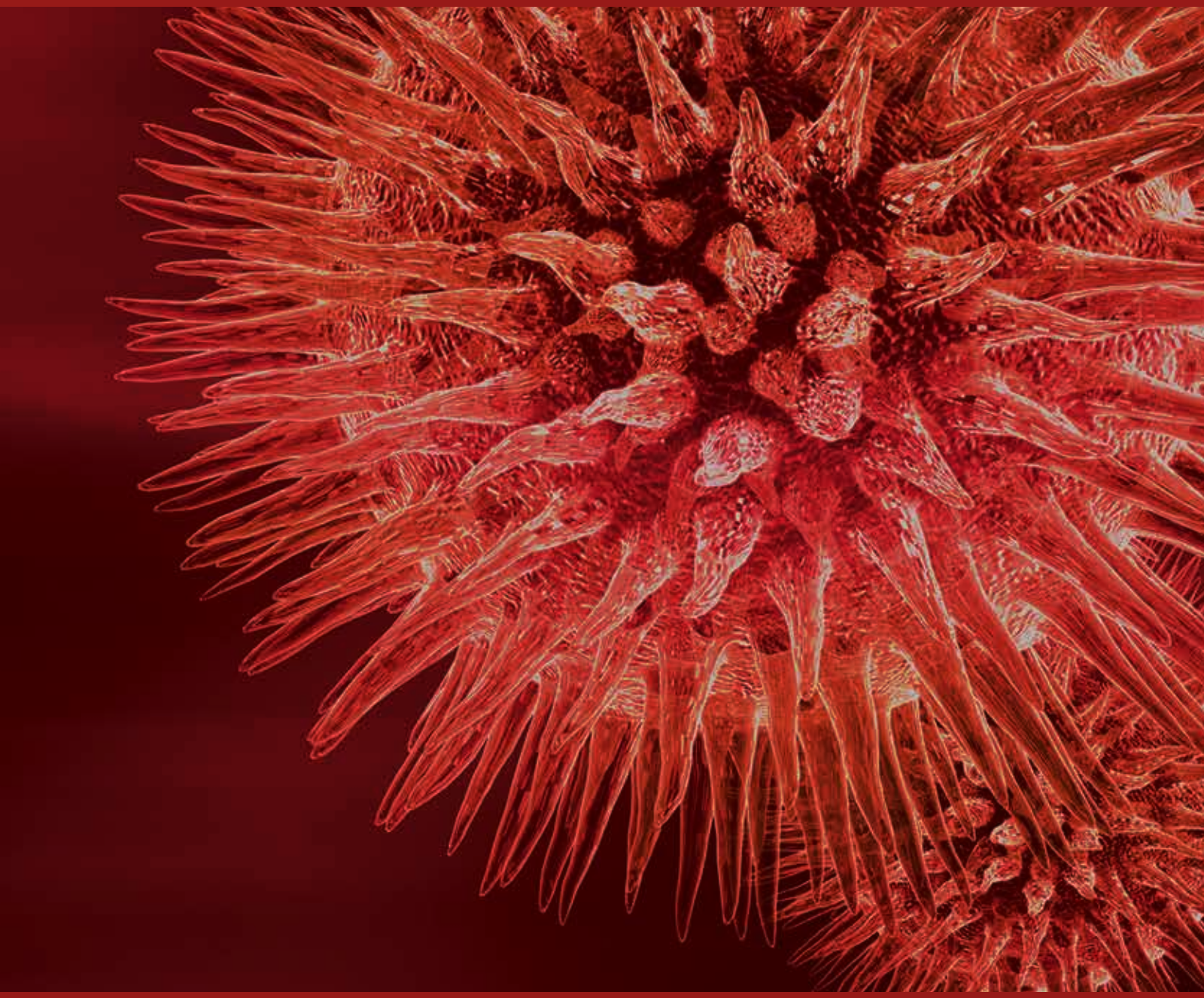

New Approaches, Findings, and Diagnostics in Medical and Surgical Retina

BioMed Research International

New Approaches, Findings, and Diagnostics in Medical and Surgical Retina

Guest Editors: Jerzy Nawrocki, Ron Adelman,
and Didier Ducournau

Contents

Hindawi Publishing Corporation
BioMed Research International
Volume 2015, Article ID 193561, 1 page
http://dx.doi.org/10.1155/2015/193561

Editorial

New Approaches, Findings, and Diagnostics in Medical and Surgical Retina

Jerzy Nawrocki,[1] Ron Adelman,[2] and Didier Ducournau[3]

[1] *Ophthalmic Clinic Jasne Blonia, Lodz, Poland*
[2] *Yale University Eye Center, New Haven, CT, USA*
[3] *Clinique Sourdille, Nantes, France*

Correspondence should be addressed to Jerzy Nawrocki; jerzy_n@poczta.onet.pl

Received 11 August 2014; Accepted 11 August 2014

The retina is a very innovative subspecialty of ophthalmology and ophthalmologists are continuing to play major roles in keeping this an exciting and dynamic field.

The amazing developments in OCT imaging, the use of smaller and smaller gauge instruments, and advances in cutting tools and pump systems all reflect the dedication of surgeons and the ophthalmic industry to improve patient outcomes through better diagnostics, machinery, software, and the technical aspects of surgical practice. The new investigations presented in this special issue focus on some of these current innovations. For example, the study by A. L. Sabater et al., on the effects of Brilliant Blue G-assisted internal limiting membrane peeling for idiopathic macular hole on the thickness of the macular retinal ganglion cell-inner plexiform layer, illustrates how new developments in OCT devices and software continue to provide new tools for ophthalmic examination. S. Koinzer et al. suggest a new OCT based classification system, which could enable comparison of differently created photocoagulation lesions across different studies and predictive estimation of clinical effects of photocoagulation. M. Pfister et al. have examined how we go about our surgical tasks at the detailed level of comparing reaction times for hand-powered versus foot-powered switch operations. The very latest development in OCT, Swept Source OCT, has been used by J. Michalewski et al. to measure choroidal thickness and volume.

Interestingly, some of the new studies presented in this issue show that older techniques remain as important today as ever. The electroretinogram can be brought into the 21st Century by using DWT scalograms according to a paper by M. Gauvin et al. New drug therapies have changed the way that many diseases are treated yet the EVRS present two of the largest studies ever conducted, into DME and RVO both of which highlight that despite the acknowledged benefits of anti-VEGF injections, vitrectomy with ILM peeling might provide the best visual outcomes for patients suffering from these diseases. D. Cohen et al. demonstrate the benefits of primary scleral buckling when dealing with posterior segment open-globe injuries.

This special issue brings you innovation in action: new applications for well-known techniques, modern imaging and technical systems, novel methods of acquiring and dealing with data, and complex statistical analysis. Retina specialists are seriously involved in constant research and development. Some of the papers presented here state the need for further investigation in order to develop their findings and peer-reviewed publications have a key role to play. They not only give us the opportunity to share our latest research but also provide a springboard to push that research ever onwards, leading to the development of new strategies to treat retinal diseases. I hope that you will enjoy the articles here and that they might encourage all of you to join in the many studies that are currently underway and to aim to publish your own material.

Jerzy Nawrocki
Ron Adelman
Didier Ducournau

Hindawi Publishing Corporation
BioMed Research International
Volume 2015, Article ID 870987, 8 pages
http://dx.doi.org/10.1155/2015/870987

Research Article

Strategy for the Management of Macular Edema in Retinal Vein Occlusion: The European VitreoRetinal Society Macular Edema Study

Ron A. Adelman,[1] Aaron J. Parnes,[2] Silvia Bopp,[3] Ihab Saad Othman,[4] and Didier Ducournau[5]

[1] *Yale Eye Center, 40 Temple Street No. 3d, New Haven, CT 06510, USA*
[2] *Eyecare Medical Group, 53 Sewall Street, Portland, ME 04102, USA*
[3] *Augenklinik Universitätsallee Bremen GmbH, Parkallee 301/Universitätsallee, 28213 Bremen, Germany*
[4] *Cairo University, Cairo University Road, Oula, Giza, Egypt*
[5] *European VitreoRetinal Society, 8 rue Camille Flammarion, 44000 Nantes, France*

Correspondence should be addressed to Ron A. Adelman; ron.adelman@yale.edu

Received 17 April 2014; Revised 28 June 2014; Accepted 30 June 2014

Academic Editor: Jerzy Nawrocki

Objective. To compare the efficacy of different therapies in the treatment of macular edema associated with retinal vein occlusion (RVO). *Design*. This is a nonrandomized, multicenter collaborative study. *Participants*. 86 retina specialists from 29 countries provided clinical information, including choice of treatment and outcome, on 2,603 patients with macular edema including 738 cases of RVO. *Methods*. Reported data included the type and number of treatments performed, visual acuities, and other clinical and diagnostic findings. *Main Outcome Measures*. The mean increase in visual acuity and mean number of treatments performed. *Results*. 358 cases of central retinal vein occlusion (CRVO) and 380 cases of branch retinal vein occlusion (BRVO) were included in this investigation. Taking all RVO cases together, pars plana vitrectomy with internal limiting membrane (ILM) peeling alone resulted in an improvement in vision greater than other therapies. Those treated with intravitreal antivascular endothelial growth factor (anti-VEGF) injection alone showed the second greatest improvement in vision. Dexamethasone intravitreal implant alone and intravitreal triamcinolone alone both resulted in modest visual gains. *Conclusions*. In the treatment of macular edema in RVO, vitrectomy with ILM peeling may achieve visual improvement and may be a good option for certain cases. Anti-VEGF injection is the most effective of the nonsurgical treatments.

1. Introduction

In population based studies, the age- and sex-standardized prevalence of retinal vein occlusion (RVO) was 5.2 per 1000 with an estimated 16.4 million adults affected by RVO, mostly branch retinal vein occlusion. RVO is the second leading cause of retinal vascular disease after diabetic retinopathy with its prevalence increasing with age, varying with race or ethnicity, and not differing based on gender [1]. Untreated RVO frequently results in vision impairment and significant ocular complications. Macular edema is present in the majority of cases with central retinal vein occlusion (CRVO) and develops in 5–15% of eyes with branch retinal vein occlusion (BRVO) [2, 3].

The treatment of macular edema due to RVO has seen significant changes over the past decade. New treatments and combination therapies continue to emerge with several showing positive results. As directed by the Central and Branch Vein Occlusion Study Groups, for many years macular edema in CRVO was observed, while in BRVO grid laser photocoagulation was applied [4, 5]. Corticosteroids, both intra- and extraocular, have long been used to treat edema with RVO, and the SCORE study results validated this therapy for edema in CRVO while confirming grid

laser photocoagulation as superior treatment for edema in BRVO [6, 7]. More recently, treatment with dexamethasone intravitreal implant has shown longer-lasting results in the treatment of this edema [8].

The arrival of antivascular endothelial growth factor (VEGF) agents has not only changed the landscape of treatment of edema in RVO but also reshaped the treatment of most of retinal vascular disease. The use of intravitreal ranibizumab has been extensively studied and is very effective in the treatment of edema due to RVO [9–16]. More recently, intravitreal aflibercept injection for treating macular edema in CRVO has shown promising outcomes [17, 18]. Literature examining combination therapy including anti-VEGF agents is not as abundant. While focal and grid laser photocoagulation is routinely used to supplement anti-VEGF injections, the possible benefit of this combined treatment has not been thoroughly studied. It has been suggested that the addition of grid laser photocoagulation to anti-VEGF therapy to treat edema in BRVO can lead to a better visual outcome and decrease the number of injections needed than if laser was not utilized [19, 20]. A separate prospective investigation found that the addition of a dexamethasone intravitreal implant to anti-VEGF injections also leads to a decrease in the number of injections needed and better vision in the combination group compared to monotherapy [21].

Pars plana vitrectomy (PPV) with peeling of the internal limiting membrane (ILM) has been an option in the treatment of edema in RVO for many years [22, 23]. More recent investigations have shown improvement of edema in both BRVO and CRVO following treatment with PPV [24–27]. The efficacy of combination therapy including vitrectomy is not completely understood. Considering the complexity and cost of comparative prospective studies, it is expected that comprehensive investigations analyzing three or more monotherapies and numerous possible combination treatments for edema in RVO are not feasible. An alternative to such large and prohibitively expensive randomized study with five or more treatment arms needs to be evaluated.

European VitreoRetinal Society (EVRS) was founded in 2001 and has over 1,900 retina specialists in its membership [28, 29]. A clinical study was conducted where EVRS members were asked to record information regarding individual cases of macular edema from 2008 to 2011, the treatments performed, and the outcomes attained. 86 retina specialists from 29 countries provided information on 2,603 cases of macular edema over the study period. Each case had at least 6 months follow-up. In this report, we will discuss the treatment and results of those cases with macular edema specifically due to RVO.

2. Methods

The EVRS macular edema study was a nonrandomized, multicenter study, which analyzed the treatment outcomes following different therapeutic interventions and treatment combinations for each etiology resulting in macular edema. This paper focuses on cases of edema due to RVO and their treatment outcomes.

During the reporting period from 2008 to 2011, participating EVRS members entered information regarding individual cases of macular edema. The clinical details for each case were entered into an online questionnaire on the EVRS website. Eighty-six retina specialists reported 2,603 cases of macular edema with 6 months to 2 years of follow-up at the conclusion of the study. The results were analyzed by the French INSEE (National Institute of Statistics and Economic Studies).

The clinical details reported from each case included the type and number of treatment(s) utilized, the pre- and post-treatment visual acuities, the specific dates of treatments and visual assessments, and lens status. Macular optical coherence tomography (OCT) measurements were not reported by the surgeons in this investigation. Any complications were also reported including increased or new cataract, increased intraocular pressure, retinal detachment, vitreous hemorrhage, choroidal detachment, and macular hole. After having cleaned the database, the global working sheet was sent to each contributor, masking the name of the other contributors, so that cleaning accuracy could be agreed upon.

This study was conducted in 29 countries and the regulations and Institutional Review Board requirements varied at each location. Given this, every physician involved in the study was responsible for following the rules and regulations of each individual country and institution. Also, the design and ethical aspects of the study have been approved by the EVRS Ethics Committee.

The study encountered a few problems. Following stratification of the macular edema etiologies, a smaller number of subgroups in the RVO cohort limited the ability to achieve statistical significance for each of them. There were 358 cases of macular edema associated with CRVO and 380 cases associated with BRVO. As there is no universal standard in management of macular edema in RVO, treatment complexity and the use of numerous combination therapies in each subgroup hindered a meaningful comparison due to further division of the subgroups to monotherapy and treatment combinations cohorts. To overcome these limitations and difficulties, the results are presented as trend lines displaying change in visual acuity over time to compare treatment outcomes. The trend lines represent data points plotted according to a mean number of lines of vision improvement (in LogMAR) at a specific follow-up visit (in months from initial treatment). Second order polynomial regression trend lines were used, as they best illustrate the effect of treatment in this complex setting. To limit error, only data points averaged from three or more cases were included in the analysis. Finally, a separate analysis was done to display final visual improvement according to pretreatment visual acuity. Trend lines are useful in comparing therapeutic groups. A trend line combining the results for all treatments of RVO was compared to plotted results for individual treatments and their average pretreatment visual acuities.

3. Results

Of the 2,603 cases of macular edema presented, four etiologies of macular edema had numbers large enough to study

Table 1: Baseline demographic patient data for CRVO.

	Number of cases	Mean pretreatment Va LogMAR (Snellen)	Standard deviation	Mean number of treatments
Anti-VEGF alone	111	1 (0.1)	0.48	5.01
PPV with ILM peeling alone	80	1.07 (0.09)	0.51	1.00
Dexamethasone implant alone	20	0.77 (0.17)	0.48	1.43
Triamcinolone alone	14	1.23 (0.06)	0.44	1.00

CRVO: central retinal vein occlusion.
VEGF: vascular endothelial growth factor.
PPV: pars plana vitrectomy.
ILM: internal limiting membrane.

Table 2: Baseline demographic patient data for BRVO.

	Number of cases	Mean pretreatment Va LogMAR (Snellen)	Standard deviation	Mean number of treatments
Anti-VEGF alone	140	0.72 (0.2)	0.42	3.83
PPV with ILM peeling alone	48	0.87 (0.13)	0.42	1.00
Dexamethasone implant alone	17	0.59 (0.25)	0.27	1.49
Triamcinolone alone	13	0.76 (0.18)	0.38	1.00

BRVO: branch retinal vein occlusion.
VEGF: vascular endothelial growth factor.
PPV: pars plana vitrectomy.
ILM: internal limiting membrane.

Table 3: Baseline demographic patient data for all RVO.

		Number of cases	Mean pretreatment Va LogMAR (Snellen)	Standard deviation	Mean number of treatments
Monotherapy	Anti-VEGF alone	251	0.85 (0.14)	0.47	4.45
	PPV with ILM peeling alone	128	1 (0.10)	0.49	1.00
	Dexamethasone implant alone	37	0.68 (0.25)	0.4	1.64
	Triamcinolone alone	27	1.04 (0.09)	0.48	1.00
Combination therapy	Anti-VEGF (1) + grid (2)	72	0.80 (0.16)	0.45	(1) 4.58 (2) 0.88
	Anti-VEGF (1) + triamcinolone (2)	37	0.96 (0.11)	0.49	(1) 3.16 (2) 1.04
	Anti-VEGF (1) + grid (2) + triamcinolone (3)	27	0.78 (0.17)	0.41	(1) 2.79 (2) 1.52 (3) 1.07
	Triamcinolone (1) + PPV with ILM peeling (2)	23	0.90 (0.13)	0.47	(1) 1.15 (2) 1.00

RVO: retinal vein occlusion.
VEGF: vascular endothelial growth factor.
PPV: pars plana vitrectomy.
ILM: internal limiting membrane.

totaling 2,159 patients. 358 were CRVO, 380 were BRVO, 870 were diabetic macular edema, and 551 were epiretinal membranes. The focus of this paper is cases of CRVO and BRVO and the baseline demographic patient data is displayed in Tables 1 and 2, respectively. The baseline demographic patient data for all RVO combined is displayed in Table 3.

The initial investigation analyzed the effects of monotherapy on edema in RVO and compared their efficacy. The change in visual acuity over time in response to each monotherapy on edema in CRVO and BRVO is displayed as separate second order polynomial regression trend lines in Figures 1 and 2, respectively. The trend lines for anti-VEGF therapy can be followed out to 24 months where treatment leads to an improvement of 3.958 lines of vision on the LogMAR chart in CRVO and 3.2415 lines in BRVO. The trend lines for PPV with ILM peeling displayed improvement in visual acuity at 24 months with a gain higher than other therapies. The trend lines for dexamethasone intravitreal implant and triamcinolone monotherapy, which are truncated due to the fact that fewer than three cases were reported at the later

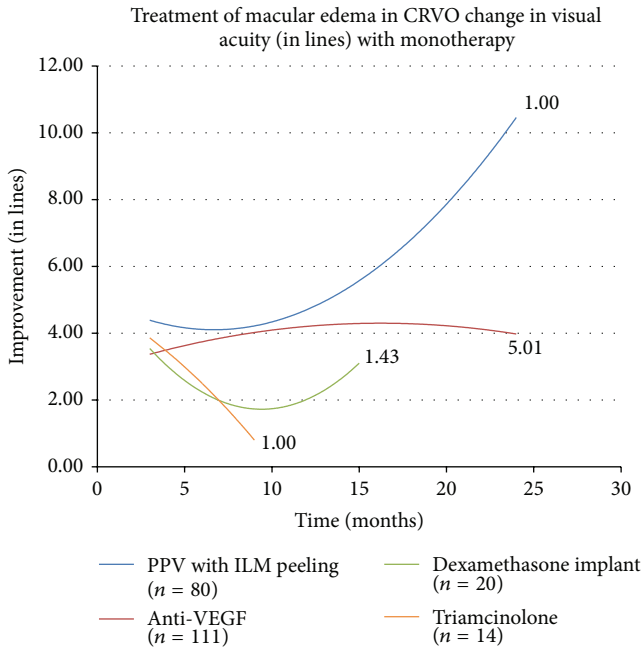

Figure 1: CRVO is central retinal vein occlusion, PPV is pars plana vitrectomy, ILM is internal limiting membrane, and VEGF is vascular endothelial growth factor.

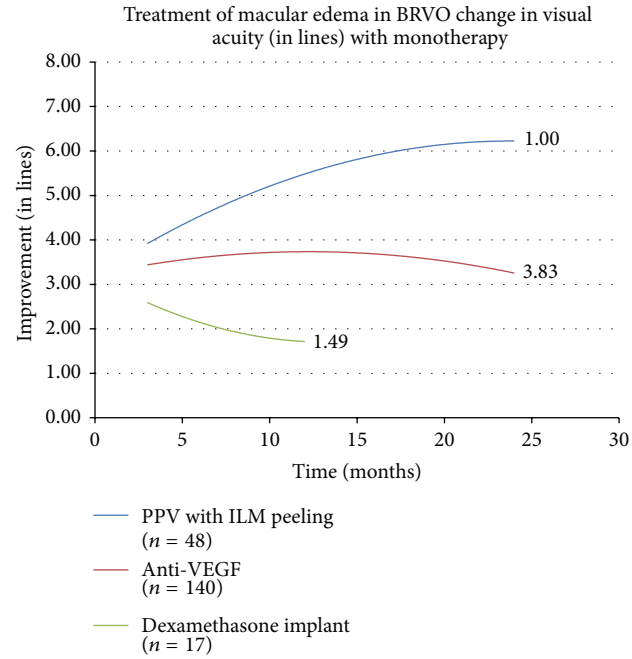

Figure 2: BRVO is branch retinal vein occlusion, PPV is pars plana vitrectomy, ILM is internal limiting membrane, and VEGF is vascular endothelial growth factor.

follow-up periods, showed a modest improvement. The numbers adjacent to the trend lines indicate mean number of treatments for each therapeutic intervention.

The effect of each monotherapy on all cases of RVO combined was then analyzed and the trend lines are displayed in Figure 3. The trend line for anti-VEGF therapy can be followed out to 24 months where treatment leads to an improvement of 3.740 lines. The trend line for PPV with ILM peeling again displayed the best improvement in visual acuity. The trend line for dexamethasone intravitreal implant, which again is truncated due to a lack of cases reported at later follow-up times, showed a modest improvement. Also for all RVO, treatment with intravitreal triamcinolone monotherapy showed a modest gain at 9 months.

Next, combination therapy with anti-VEGF agents was evaluated and compared in all RVO combined (Figure 4). The addition of grid laser photocoagulation to anti-VEGF therapy, combination therapy of intravitreal triamcinolone with anti-VEGF treatment, and combination of anti-VEGF therapy, intravitreal triamcinolone, and grid laser were studied. None of these combination therapies matched the gains observed with anti-VEGF treatment alone.

Visual improvement was then evaluated by looking at the percentage of patients achieving greater than or equal to 3 and 6 lines of vision recovery. In this analysis, the final visual acuity reading available was compared to the recorded pretreatment acuity. Monotherapy with either anti-VEGF treatment or PPV with ILM peeling for edema in all cases of RVO was compared using this data (Table 4). 61.7% of the anti-VEGF group and 75.4% of the vitrectomy group gained at least 3 lines of vision. This was a statistically significant difference with vitrectomy showing a better result over anti-VEGF therapy ($P = 0.008$). 26.0% of the anti-VEGF group and 48.4% of the vitrectomy group gained at least 6 lines of vision. PPV with ILM peeling again showed good outcomes ($P = 10^{-5}$).

Another presentation of the data displays treatment outcomes based on final visual improvement according to pretreatment visual acuity (Figure 5). This allows for a comparison of each treatment taking into account the initial visual acuities and the overall combined results for all treatments of RVO seen as a single second order regression trend line. Following the analysis of all possible mono- and combination therapies for edema in RVO, the plotted data points represent the top eight treatments, in terms of visual improvement. PPV with ILM peeling displayed the largest improvement in vision. This therapy was followed by, in order of descending amount of vision gain (LogMAR), anti-VEGF treatment alone, PPV with ILM peeling in combination with triamcinolone, and triamcinolone therapy alone.

4. Discussion

New treatments and subsequent combination therapies for macular edema in RVO have provided the present-day retina specialist with choices arguably more ample and complex than those of the previous generation. While these recently suggested treatments are welcome, their role with regard to appropriate first-line and subsequent therapy is not clear. The simple fact that only 11 of the 738 patients with RVO had their edema treated with grid laser photocoagulation monotherapy shows a major shift in treatment philosophy

Table 4: Final visual improvement for anti-VEGF injection and PPV with ILM peeling monotherapies.

	Anti-VEGF (n = 246)	PPV with ILM peeling (n = 126)	P value
≥3 lines improvement	61.7%	75.4%	0.008
≥6 lines improvement	26.0%	48.4%	10^{-5}

VEGF: vascular endothelial growth factor.
PPV: pars plana vitrectomy.
ILM: internal limiting membrane.

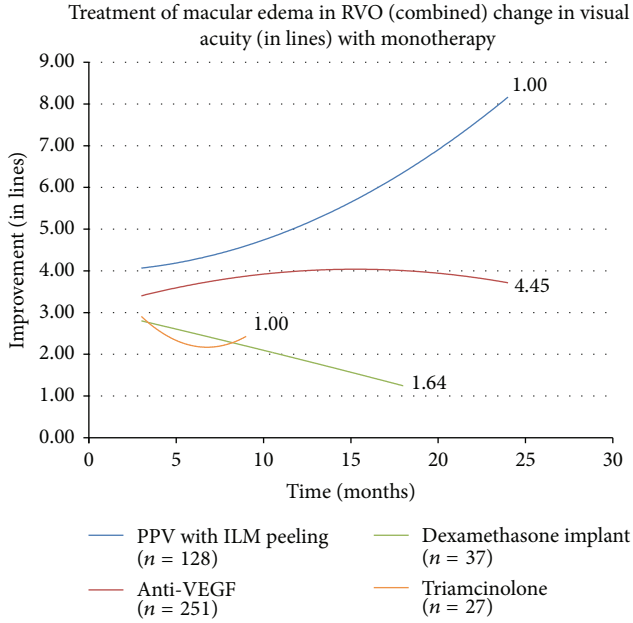

Figure 3: RVO is retinal vein occlusion, PPV is pars plana vitrectomy, ILM is internal limiting membrane, and VEGF is vascular endothelial growth factor.

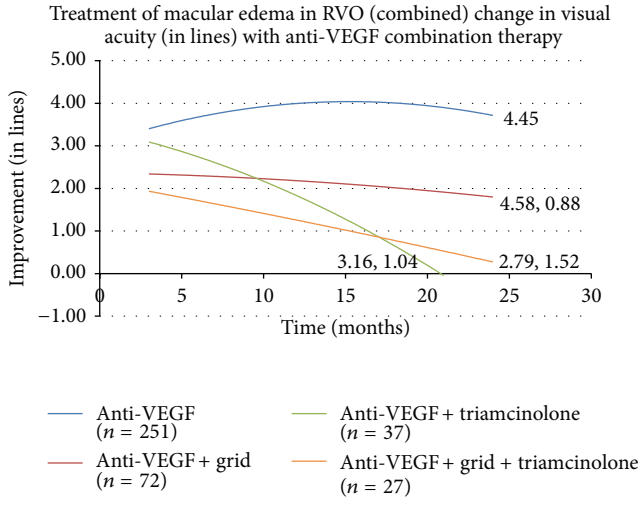

Figure 4: RVO is retinal vein occlusion and VEGF is vascular endothelial growth factor.

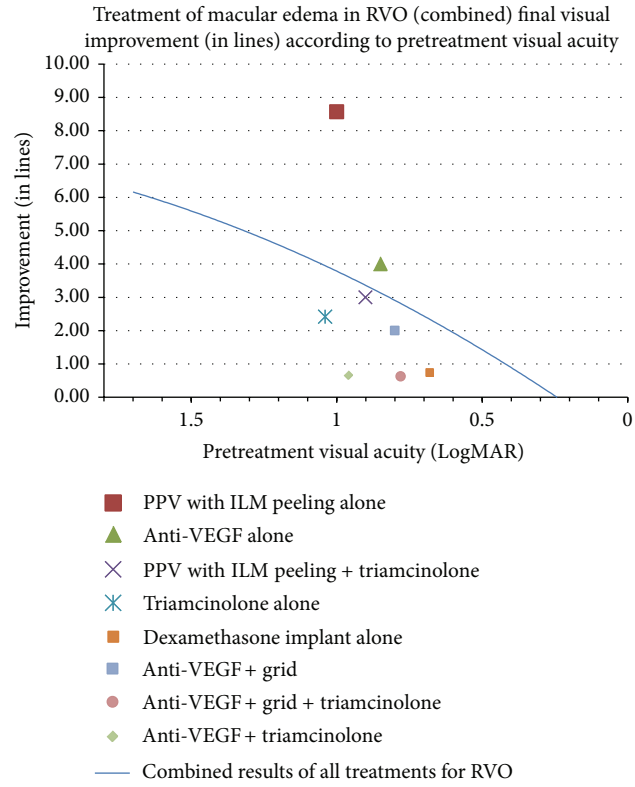

Figure 5: RVO is retinal vein occlusion, PPV is pars plana vitrectomy, ILM is internal limiting membrane, and VEGF is vascular endothelial growth factor.

of RVO. This small number did not allow for an analysis and signals a large shift in the international standard of care in recent years. Of course, a large-scale, prospective, and randomized study with treatment arms covering all possible mono- and combination therapies would be ideal to provide an answer. However, such study would likely be very costly and complex to conduct. In this investigation, we present an international nonrandomized multicenter trial evaluating current treatments for edema in RVO. Such study presents the real-life approach of a large number of ophthalmologists from a huge geographical area to the management of RVO.

When monotherapy for edema in RVO was analyzed, treatment with vitrectomy and ILM peeling gave the largest improvement in visual acuity. This held true when cases of CRVO and BRVO were evaluated both separately and in

combination. The improvement in vision with vitrectomy was better than other therapies at every time point. Overall, intravitreal anti-VEGF injection was the next most effective solo treatment with a gain of 3.7 lines of vision on the LogMAR chart at 24 months. Less improvement was seen with steroid monotherapy. The addition of grid laser, intravitreal triamcinolone, or both to anti-VEGF treatment did not improve visual outcomes compared to anti-VEGF alone. A traditional analysis showed a statistically significant benefit of vitrectomy over anti-VEGF therapy, in terms of percentage of cases gaining over 3 or 6 lines of vision. The problem with this type of analysis is that it does not take into account pretreatment vision. When initial visual acuity is included in the evaluation and results were adjusted based on initial visual acuity, vitrectomy with ILM peeling is still superior to other treatments and shows over twice the benefit of anti-VEGF injection. The results here suggest that vitrectomy with ILM peeling may provide good long-term benefit in the treatment of edema in RVO.

The significant improvement in edema and vision with vitrectomy seen here is likely the result of a number of factors. Posterior hyaloid removal may contribute to a decrease in edema because of the relief of any tractional component that may be present [30]. Spectral domain OCT has now been used to identify extrafoveal traction that may play a role in edema associated with RVO [31]. Also, improvement in vision may be attained with better preservation of the ellipsoid line and parallelism following PPV. Another possible factor noted in the literature is that vitreous removal may serve to improve oxygenation of the vitreous cavity and retina and prevent photoreceptor loss in RVO [32]. The removal of inflammatory and permeability mediators in the vitreous, including VEGF, may also play a role in improving edema in RVO [33]. A separate mechanism to explain the success of ILM removal involves the healing process it induces at the level of the Müller cells end-feet [34]. This minor injury causes an upregulation of epidermal growth factor receptor (EGF-R) which regulates the healing response. Stem cell proliferation occurs as a result of cell loss and EGF-R stimulates the filling of Müller cells with microfibrils of glial fibrillary acidic proteins (GFAPs) causing a vertical gliosis from the ILM to the external limiting membrane. This process of neural repair has been observed in both the central nervous system following traumatic injury and the retina in the setting of a retinal detachment [35–38].

While the evaluation of outcomes of this study in this manner may be useful, there are inherent limitations and significant disadvantages. Regarding the trend lines, even though several cases were available for each data point, generally fewer cases were available when plotting the data at two-year time point. Although trend lines are useful in comparing efficacy of a variety of treatment groups, they may not be very accurate in measuring the exact amount of improvement. Another limitation is the lack of randomization. However, the current study shows visual outcomes comparable to randomized clinical trials of anti-VEGF therapy for retinal vein occlusions.

The exact treatment parameters for each treatment group were determined by the investigators, leading to multiple treatment groups and smaller numbers to analyze for every mono- or combination therapy applied. In addition, the frequency and order of treatments were not standardized, leaving us with an ability to suggest a treatment, but without exact guidelines for execution. The smaller number of cases receiving each treatment necessitated the grouping of CRVO and BRVO cases together to achieve greater statistical significance. While the pathophysiology of macular edema is somewhat similar in both CRVO and BRVO, they do not necessarily respond exactly to the same treatment [4, 5]. This is a pitfall, however, given other studies that have shown relatively comparable outcomes with the same treatment; it may be reasonable to combine the cases [12, 13].

This study suggests that vitrectomy with ILM peeling may be a good treatment for macular edema due to RVO. The data suggests that vitrectomy may result in improvement in vision in some cases. Intravitreal anti-VEGF therapy is the most effective of the nonsurgical treatments. Future prospective, randomized clinical trials are needed to verify these results and establish a standard of care for the treatment of macular edema in RVO.

Disclosure

This paper was part of the European VitreoRetinal Society (EVRS) annual meeting, September 2012, and Macula Society annual meeting, 2013.

Conflict of Interests

The authors declare that there is no conflict of interests regarding the publication of this paper.

Acknowledgment

The authors are thankful for the European VitreoRetinal Society (EVRS) Macular Edema Study Group.

References

[1] S. Rogers, R. L. McIntosh, N. Cheung et al., "The prevalence of retinal vein occlusion: pooled data from population studies from the United States, Europe, Asia, and Australia," *Ophthalmology*, vol. 117, no. 2, pp. 313.e1–319.e1, 2010.

[2] R. L. McIntosh, S. L. Rogers, L. Lim et al., "Natural history of central retinal vein occlusion: an evidence-based systematic review," *Ophthalmology*, vol. 117, no. 6, pp. 1113.e15–1123.e15, 2010.

[3] S. L. Rogers, R. L. McIntosh, L. Lim et al., "Natural history of branch retinal vein occlusion: an evidence-based systematic review," *Ophthalmology*, vol. 117, no. 6, pp. 1094.e5–1101.e5, 2010.

[4] The Central Vein Occlusion Study Group, "Evaluation of grid pattern photocoagulation for macular edema in central vein occlusion," *Ophthalmology*, vol. 102, no. 10, pp. 1425–1433, 1995.

[5] "Argon laser photocoagulation for macular edema in branch vein occlusion," *The American Journal of Ophthalmology*, vol. 98, pp. 271–282, 1984.

[6] The SCORE Study Research Group, "A randomized trial comparing the efficacy and safety of intravitreal triamcinolone with

observation to treat vision loss associated with macular edema secondary to central retinal vein occlusion. The standard care vs corticosteroid for retinal vein occlusion (SCORE) study report 5," *Archives of Ophthalmology*, vol. 127, pp. 1101–1114, 2009.

[7] I. U. Scott, M. S. Ip, P. C. vanVeldhuisen et al., "A randomized trial comparing the efficacy and safety of intravitreal triamcinolone with standard care to treat vision loss associated with macular edema secondary to branch retinal vein occlusion: the standard care vs corticosteroid for retinal vein occlusion (SCORE) study report 6," *Archives of Ophthalmology*, vol. 127, no. 9, pp. 1115–1128, 2009.

[8] J. A. Haller, F. Bandello, R. Belfort Jr. et al., "Dexamethasone intravitreal implant in patients with macular edema related to branch or central retinal vein occlusion: twelve-month study results," *Ophthalmology*, vol. 118, no. 12, pp. 2453–2460, 2011.

[9] P. A. Campochiaro, G. Hafiz, S. M. Shah et al., "Ranibizumab for macular edema due to retinal vein occlusions: implication of VEGF as a critical stimulator," *Molecular Therapy*, vol. 16, no. 4, pp. 791–799, 2008.

[10] D. J. Pieramici, M. Rabena, A. A. Castellarin et al., "Ranibizumab for the treatment of macular edema associated with perfused central retinal vein occlusions," *Ophthalmology*, vol. 115, no. 10, pp. e47–e54, 2008.

[11] R. F. Spaide, L. K. Chang, J. M. Klancnik et al., "Prospective study of intravitreal ranibizumab as a treatment for decreased visual acuity secondary to central retinal vein occlusion," *The American Journal of Ophthalmology*, vol. 147, no. 2, pp. 298–306, 2009.

[12] P. A. Campochiaro, J. S. Heier, L. Feiner et al., "Ranibizumab for macular edema following branch retinal vein occlusion: six-month primary end point results of a phase III study," *Ophthalmology*, vol. 117, no. 6, pp. 1102.e1–1112.e1, 2010.

[13] D. M. Brown, P. A. Campochiaro, R. P. Singh et al., "Ranibizumab for macular edema following central retinal vein occlusion. Six-month primary end point results of a phase III study," *Ophthalmology*, vol. 117, no. 6, pp. 1124–e1, 2010.

[14] D. M. Brown, P. A. Campochiaro, R. B. Bhisitkul et al., "Sustained benefits from ranibizumab for macular edema following branch retinal vein occlusion: 12-month outcomes of a phase III study," *Ophthalmology*, vol. 118, no. 8, pp. 1594–1602, 2011.

[15] P. A. Campochiaro, D. M. Brown, C. C. Awh et al., "Sustained benefits from ranibizumab for macular edema following central retinal vein occlusion: Twelve-month outcomes of a phase III study," *Ophthalmology*, vol. 118, no. 10, pp. 2041–2049, 2011.

[16] J. S. Heier, P. A. Campochiaro, L. Yau et al., "Ranibizumab for macular edema due to retinal vein occlusions: long-term follow-up in the HORIZON trial," *Ophthalmology*, vol. 119, no. 4, pp. 802–809, 2012.

[17] D. M. Brown, J. S. Heier, W. L. Clark et al., "Intravitreal aflibercept injection for macular edema secondary to central retinal vein occlusion: 1-year results from the phase 3 COPERNICUS study," *The American Journal of Ophthalmology*, vol. 155, no. 3, pp. 429.e7–437.e7, 2013.

[18] F. G. Holz, Y. Ogura, J. Roider et al., "Intravitrial aflibercept injection for macular edema in central retinal vein occlusion: 1-year results of the phase 3 GALILEO study," *Ophthalmology*, vol. 121, no. 1, pp. 202–208, 2014.

[19] R. Azad, K. Vivek, Y. Sharma, P. Chandra, S. Sain, and A. Venkataraman, "Ranibizumab as an adjunct to laser for macular edema secondary to branch retinal vein occlusion," *Indian Journal of Ophthalmology*, vol. 60, no. 4, pp. 263–266, 2012.

[20] S. Donati, P. Barosi, M. Bianchi, M. A. Oum, and C. Azzolini, "Combined intravitreal bevacizumab and grid laser photocoagulation for macular edema secondary to branch retinal vein occlusion," *European Journal of Ophthalmology*, vol. 22, no. 4, pp. 607–614, 2012.

[21] M. A. Singer, D. J. Bell, P. Woods et al., "Effect of combination therapy with bevacizumab and dexamethasone intravitreal implant in patients with retinal vein occlusion," *Retina*, vol. 32, no. 7, pp. 1289–1294, 2012.

[22] T. Sekiryu, T. Yamauchi, H. Enaida, Y. Hara, and M. Furuta, "Retina tomography after vitrectomy for macular edema of central retinal vein occlusion," *Ophthalmic Surgery and Lasers*, vol. 31, no. 3, pp. 198–202, 2000.

[23] S. Saika, T. Tanaka, T. Miyamoto, and Y. Ohnishi, "Surgical posterior vitreous detachment combined with gas/air tamponade for treating macular edema associated with branch retinal vein occlusion: retinal tomography and visual outcome," *Graefe's Archive for Clinical and Experimental Ophthalmology*, vol. 239, no. 10, pp. 729–732, 2001.

[24] M. Raszewska-Steglinska, P. Gozdek, S. Cisiecki, Z. Michalewska, J. Michalewski, and J. Nawrocki, "Pars plana vitrectomy with ILM peeling for macular edema secondary to retinal vein occlusion," *European Journal of Ophthalmology*, vol. 19, no. 6, pp. 1055–1062, 2009.

[25] H. Noma, H. Funatsu, T. Mimura, S. Eguchi, and K. Shimada, "Visual acuity and foveal thickness after vitrectomy for macular edema associated with branch retinal vein occlusion: a case series," *BMC Ophthalmology*, vol. 10, no. 1, article 11, 2010.

[26] D. H. Park and I. T. Kim, "Long-term effects of vitrectomy and internal limiting membrane peeling for macular edema secondary to central retinal vein occlusion and hemiretinal vein occlusion," *Retina*, vol. 30, no. 1, pp. 117–124, 2010.

[27] N. Baharivand, A. Hariri, A. Javadzadeh, E. Heidari, and K. Sadegi, "Pars plana vitrectomy and internal limiting membrane peeling for macular edema secondary to retinal vein occlusion," *Clinical Ophthalmology*, vol. 5, no. 1, pp. 1089–1093, 2011.

[28] R. A. Adelman, A. J. Parnes, D. Ducournau et al., "Strategy sfor the management of uncomplicated retinal detachments: the European vitreo-retinal society retinal detachment study report 1," *Ophthalmology*, vol. 120, no. 9, pp. 1804–1808, 2013.

[29] R. A. Adelman, A. J. Parnes, J. O. Sipperley, and D. Ducournau, "Strategy for the management of complex retinal detachments: the European vitreo-retinal society retinal detachment study report 2," *Ophthalmology*, vol. 120, no. 9, pp. 1809–1813, 2013.

[30] T. Hikichi, S. Konno, and C. L. Trempe, "Role of the vitreous in central retinal vein occlusion," *Retina*, vol. 15, no. 1, pp. 29–33, 1995.

[31] M. R. Martinez and A. Ophir, "Extrafoveal traction in retinal vein occlusion using spectral domain optical coherence tomography," *Graefe's Archive for Clinical and Experimental Ophthalmology*, vol. 249, no. 6, pp. 811–820, 2011.

[32] E. Stefansson, R. L. Novack, and D. L. Hatchell, "Vitrectomy prevents retinal hypoxia in branch retinal vein occlusion," *Investigative Ophthalmology and Visual Science*, vol. 31, no. 2, pp. 284–289, 1990.

[33] Y. Okunuki, Y. Usui, N. Katai et al., "Relation of intraocular concentrations of inflammatory factors and improvement of macular edema after vitrectomy in branch retinal vein occlusion," *The American Journal of Ophthalmology*, vol. 151, no. 4, pp. 610.e1–616.e1, 2011.

[34] S. Wolf, U. Schnurbusch, P. Wiedemann, J. Grosche, A. Reichenbach, and H. Wolburg, "Peeling of the basal membrane in

the human retina: ultrastructural effects," *Ophthalmology*, vol. 111, no. 2, pp. 238–243, 2004.

[35] S. Shibuya, O. Miyamoto, T. Itano, S. Mori, and H. Norimatsu, "Temporal progressive antigen expression in radial glia after contusive spinal cord injury in adult rats," *GLIA*, vol. 42, no. 2, pp. 172–183, 2003.

[36] G. E. Goings, V. Sahni, and F. G. Szele, "Migration patterns of subventricular zone cells in adult mice change after cerebral cortex injury," *Brain Research*, vol. 996, no. 2, pp. 213–226, 2004.

[37] G. P. Lewis and S. K. Fisher, "Up-regulation of glial fibrillary acidic protein in response to retinal injury: its potential role in glial remodeling and a comparison to vimentin expression," *International Review of Cytology*, vol. 230, pp. 263–290, 2003.

[38] J. D. Unterlauft, W. Eichler, K. Kuhne et al., "Pigment epithelium-derived factor released by Müller glial cells exerts neuroprotective effects on retinal ganglion cells," *Neurochemical Research*, vol. 37, no. 7, pp. 1524–1533, 2012.

Hindawi Publishing Corporation
BioMed Research International
Volume 2015, Article ID 352487, 9 pages
http://dx.doi.org/10.1155/2015/352487

Research Article

Strategy for the Management of Diabetic Macular Edema: The European Vitreo-Retinal Society Macular Edema Study

Ron Adelman,[1] Aaron Parnes,[2] Zofia Michalewska,[3] Barbara Parolini,[4] Claude Boscher,[5] and Didier Ducournau[6]

[1] *Yale University School of Medicine, New Haven, CT, USA*
[2] *Eyecare Medical Group, Portland, ME, USA*
[3] *Ophthalmic Clinic "Jasne Blonia", Lodz, Poland*
[4] *Department of Ophthalmology, S. Anna Hospital, Brescia, Italy*
[5] *American Hospital of Paris, Paris, France*
[6] *EVRS, Nantes, France*

Correspondence should be addressed to Ron Adelman; ron.adelman@yale.edu

Received 17 April 2014; Accepted 30 June 2014

Academic Editor: Jerzy Nawrocki

Objective. To compare the efficacy of different therapies in the treatment of diabetic macular edema (DME). *Design*. Nonrandomized, multicenter clinical study. *Participants*. 86 retina specialists from 29 countries provided clinical information on 2,603 patients with macular edema including 870 patients with DME. *Methods*. Reported data included the type and number of treatment(s) performed, the pre- and posttreatment visual acuities, and other clinical findings. The results were analyzed by the French INSEE (National Institute of Statistics and Economic Studies). *Main Outcome Measures*. Mean change of visual acuity and mean number of treatments performed. *Results*. The change in visual acuity over time in response to each treatment was plotted in second order polynomial regression trend lines. Intravitreal triamcinolone monotherapy resulted in some improvement in vision. Treatment with threshold or subthreshold grid laser also resulted in minimal vision gain. Anti-VEGF therapy resulted in more significant visual improvement. Treatment with pars plana vitrectomy and internal limiting membrane (ILM) peeling alone resulted in an improvement in vision greater than that observed with anti-VEGF injection alone. In our DME study, treatment with vitrectomy and ILM peeling alone resulted in the better visual improvement compared to other therapies.

1. Introduction

Diabetic macular edema (DME) is the leading cause of visual impairment in diabetic patients and according to some data is the leading cause of blindness among working age individuals in industrialized countries. The 10-year incidence of DME in diabetics was reported to be 20–40% [1]. Given the increasing incidence of diabetes, DME may become a leading cause of vision loss requiring treatment by ophthalmologists. A meta-analysis extrapolated to the world diabetes population in 2010 estimated that approximately 93 million people may have some form of diabetic retinopathy (DR), and 28 million may have sight-threatening stages of DR [2].

The optimal treatment of DME is evolving. Focal and grid laser photocoagulation's place as the gold standard of therapy for DME, as established in the Early Treatment of Diabetic Retinopathy Study (ETDRS), is threatened but still has a role in therapy [3].

New therapies continue to be developed and proven with an ever-growing swath of literature detailing positive clinical results. Antivascular endothelial growth factor (VEGF) agents have emerged as effective treatments and published data supports this tectonic shift [4–10]. The RISE and RIDE studies confirmed that intravitreal ranibizumab injection was superior to sham treatment and approximately 40% of patients treated monthly gained over 15 letters [6]. The RESOLVE study suggested that ranibizumab treatment was superior to laser (7.8 ETDRS letters gained versus –1.7 ETDRS letters lost) [9]. Similar results were obtained in

the BOLT study, when bevacizumab was administered (8 ETDRS letters gained versus −0.5 ETDRS letters lost in patients treated with laser) [8]. It must be considered that although the endophthalmitis rate was confirmed to be as low as 0.006% in the RIDE and RISE trials and 2% in the RESOLVE study, diabetic patients typically require multiple injections and are in general more susceptible to infections and endophthalmitis [6, 9].

The question of timing in combined ranibizumab and laser therapy was explored by the Diabetic Retinopathy Clinical Research Network (DRCR) [11]. Two-year data confirmed that ranibizumab with deferred laser photocoagulation (>24 weeks) gained 5.7 more ETDRS letters, when compared to laser with sham injection. The protocol also compared ranibizumab with prompt laser and triamcinolone with prompt laser but found them in some aspect inferior to ranibizumab with deferred laser. Patients with ranibizumab and deferred laser needed a mean of 11.4 injections over 24 months. DRCR suggested that the smaller number of total injections, as compared to other trials when ranibizumab was used as solo therapy, may have been due to the laser photocoagulation performed [11].

Other therapies, such as intravitreal corticosteroid injections or implants, subthreshold laser photocoagulation, pars plana vitrectomy with or without internal limiting membrane (ILM) peeling, and combined therapies have supported clinical research and are also widely used [12–18]. Despite a large amount of primary literature, direct comparisons examining the efficacy of surgical and medical treatments, or combination thereof, are inadequate.

Prospective clinical trials that do exist in the literature, for the most part, only compare two or three treatment modalities. Grid laser photocoagulation and anti-VEGF agents have been commonly compared in recent years as monotherapy or in combination with each other [19–24]. The majority of these studies actually favor intravitreal anti-VEGF therapy over laser. Direct comparisons between intravitreal triamcinolone and anti-VEGF agents have been made as well [25, 26]. Turning to a surgical option, when measured against grid laser photocoagulation and intravitreal triamcinolone injection in relatively small clinical trials, pars plana vitrectomy had the advantage [27, 28].

It is not surprising that conducting comprehensive comparative studies for the treatment of DME is time consuming and costly. Prospective, randomized studies with just a few clinical arms are difficult enough to organize. One can imagine that a clinical trial with 10 or more treatment groups encompassing all current therapeutic options, and the many combinations that could be made between them, would be very difficult and very expensive to conduct. Alternatives to such an implausible randomized study must be examined.

European Vitreo-Retinal Society (EVRS) is an organization of over 1,900 retina specialists founded in 2001, which previously conducted large trials examining the treatment of retinal detachments [29–32]. A clinical study was initiated and participating EVRS members were asked to record information regarding individual cases of macular edema and the treatments performed since 2008. A total of 86 retina specialists from 29 countries provided information on 2,603 cases of macular edema with at least 6-month follow-up. In this report we will discuss the treatment and results of those cases with macular edema specifically related to diabetes.

2. Methods

The EVRS Macular Edema Study was a nonrandomized, multicenter study in which the goal was to analyze the treatment of macular edema. The focus was on the results of varying treatments and treatment combinations for each etiology of the macular edema. This paper concentrates on cases of DME and their treatment outcomes.

The members of EVRS contributed to the study by reporting on individual cases of macular edema and their management from 2008 to 2011. A portal was created on the EVRS website where reporting questionnaires were available to be filled out for each patient treated. At the conclusion of the reporting period, the study organizers received complete data on 2,603 cases of macular edema from 86 retina specialists. Follow-up for these cases ranged from 6 months to 2 years. The results were analyzed independent of investigators by the French INSEE (National Institute of Statistics and Economic Studies).

Reported data for each case included the type and number of treatment(s) utilized, the pretreatment and posttreatment visual acuities, and the specific dates of treatments and visual assessments. Lens status was also recorded. Information regarding complications was reported including an increased or new cataract, increased intraocular pressure, retinal detachment, vitreous hemorrhage, choroidal detachment, and macular hole. Macular optical coherence tomography (OCT) measurements were not reported by the surgeons in this investigation. After having cleaned the database, the global working sheet was sent to each contributor, masking the name of the other contributors, so that cleaning accuracy could be agreed upon.

Considering that this study was performed in 29 countries, the regulations and institutional review board requirements were different in each location. Every participant was responsible to follow the rules and regulations of each individual country and institution. In addition, the EVRS Ethics and Study Design Committees have approved the design and ethical aspects of the study.

This method of reporting of cases of macular edema led to a few difficulties. The large number of etiologies causing macular edema was the first factor limiting the ability to achieve statistical significance. While information on 2,603 eyes with macular edema was reported; 870 of those cases were specifically associated with diabetes. A second, and more influential, factor affecting the number of cases needed to reach a statistically significant comparison was treatment complexity. The relatively large number of treatment options available for macular edema and the lack of standardization in the integration of these treatment regimens presented some challenge. Given these limitations, the statisticians decided to present the results as trend lines displaying improvement in visual acuity over time.

Table 1: Baseline demographic patient data.

	Number of cases	Mean pretreatment Va LogMAR (Snellen)	Standard deviation	Mean number of treatments
Monotherapy				
Anti-VEGF only	139	0.7 (0.2)	0.41	2.13
Threshold grid	97	0.39 (0.41)	0.32	1.66
PPV-ILM	61	0.86 (0.14)	0.52	1.00
Subthreshold grid	52	0.36 (0.44)	0.25	2.35
Triamcinolone	41	0.69 (0.2)	0.40	1.08
Combination therapy				
Anti-VEGF (1) + threshold grid (2)	130	0.64 (0.23)	0.40	(1) 1.85 (2) 1.44
Anti-VEGF (1) + subthreshold grid (2)	30	0.61 (0.25)	0.37	(1) 1.37 (2) 2.32
Triamcinolone (1) + threshold grid (2)	38	0.64 (0.23)	0.46	(1) 1.24 (2) 1.46
Triamcinolone (1) + anti-VEGF (2)	31	0.62 (0.24)	0.39	(1) 1.20 (2) 1.44
Triamcinolone (1) + PPV-ILM (2)	68	0.79 (0.16)	0.39	(1) 1.21 (2) 1.00

VEGF = vascular endothelial growth factor.
PPV-ILM = pars plana vitrectomy with internal limiting membrane peeling.

Regarding the analysis of collected data, the institute of statistics made two decisions. First, a second order polynomial regression trend line method was used, as opposed to a linear or third order polynomial regression trend line, because it better illustrates the effect of various treatments. A linear regression simply does not reflect what happens to vision following a single treatment in clinical practice nor does a third order regression where acuity would be depicted as fluctuating up and down in an unnatural and unexpected way. The presentation of visual acuity over time with a second order trend line allows one to analyze the effect of treatment on vision at specific intervals or according to pretreatment visual acuity. The second decision made was that, for each data point plotted to create the trend lines, a minimum of three cases would be needed for every follow-up interval. With this approach, only the averages of vision improvement with at least three cases would be included, and the impact of aberrant cases would be minimized.

Additional analysis was performed in order to display final visual improvement (LogMAR) according to pretreatment visual acuity. A trend line combining the results for all treatments of DME was compared to plotted results for individual treatments and their average pretreatment visual acuities.

Considering that this is not a randomized study, there is a risk of selection bias, with regard to the cases reported on by each physician. Based on recommendation by the institute of statistics, this risk was limited by always comparing the results obtained with different treatment modalities as opposed to presenting individual values of visual improvement at different time points along the trend lines. Furthermore, the large number of reported cases and participating physicians in each treatment group worked to reduce selection bias. The trend lines, therefore, can be used to classify the efficiency of each treatment and must be considered as indicators of comparative results. Usually trend lines are useful in comparing treatment groups. However, they are not a precise measure of exact number of lines of improvement in vision. Based on this presentation, a strategy for the treatment of DME could be proposed.

3. Results

The details regarding the treatment of 2,603 cases of macular edema were reported by 86 retina specialists in 29 countries. Of these reported cases, 2,159 comprised the four etiologies, which had numbers large enough to study. 870 had DME, 551 had epiretinal membranes, 380 had branch retinal vein occlusion, and 358 had central retinal vein occlusion. The focus of this paper is to compare different treatment options for DME. The baseline demographic patient data are displayed in Table 1.

3.1. Monotherapy. Initial visual acuity in eyes in which pars plana vitrectomy was performed was lower than in all the other treatment groups (0.86 LogMAR versus 0.7 LogMAR in the anti-VEGF group, 0.69 LogMAR in the triamcinolone group, 0.39 LogMAR in threshold grid, and 0.36 LogMAR in the grid subthreshold group). Our first goal was to analyze the results of monotherapy in DME and to compare the efficacy of various treatment modalities. The evolution of visual acuity over time in response to each treatment is displayed as separate second order polynomial regression trend lines in Figure 1. The numbers adjacent to the trend lines indicate mean number of treatments for each therapeutic intervention.

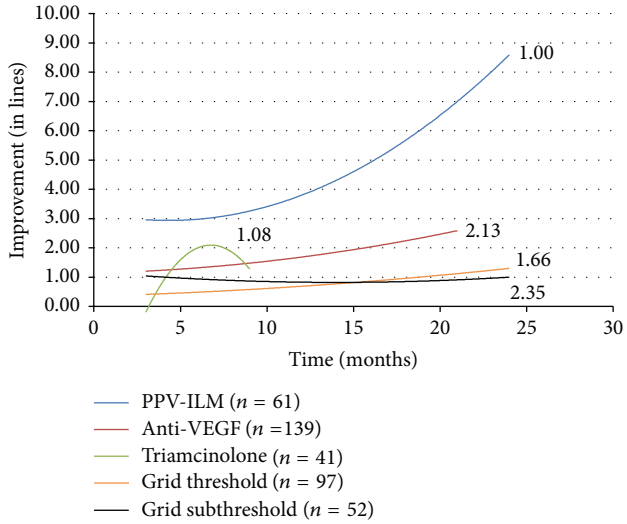

Figure 1: Change in visual acuity (in lines) with monotherapy. PPV-ILM = pars plana vitrectomy with internal limiting membrane peeling. VEGF = vascular endothelial growth factor.

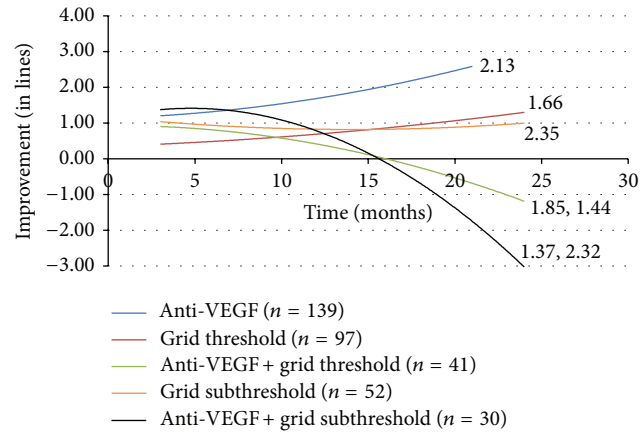

Figure 2: Change in visual acuity (in lines) with anti-VEGF combination therapy. VEGF = vascular endothelial growth factor.

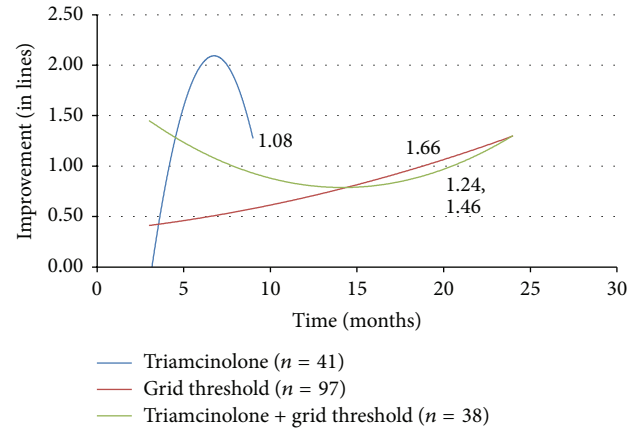

Figure 3: Change in visual acuity (in lines) with triamcinolone and threshold grid laser.

Pars plana vitrectomy with ILM peeling was performed in 61 eyes and resulted in a trend line displaying marked visual recovery about 2-3 times higher when compared to anti-VEGF therapy alone. This result was superior to all other treatment groups. The improvement in visual acuity continued to increase between 12 and 24 months after surgery.

Monotherapy with anti-VEGF injections was performed in 139 eyes. Following anti-VEGF therapy alone, final visual improvement was over two times greater than the gains observed with either threshold (97 eyes) or subthreshold grid laser (52 eyes) (2.589 lines of improvement on the LogMAR chart at 21 months versus 1.326 lines and 0.995 lines at 24 months, resp.). The results achieved in subthreshold grid laser treated eyes were not statistically different from those obtained with threshold grid laser. Improvement remained constant throughout the follow-up period in both groups.

Triamcinolone injections were performed in 41 eyes. The trend line illustrating the response to treatment with intravitreal triamcinolone is truncated due to the fact that fewer than three cases were reported at each follow-up period past nine months. The fact that the therapy was discontinued after this period may be explained by the decrease of the visual acuity trend line.

An additional issue to be considered is the number of treatments per eye. Patients treated with vitrectomy and ILM peeling received a mean of 1 treatment per 24 months. Patients treated with anti-VEGF injections received a mean of 3 treatments per 24 months and a mean of 2 triamcinolone injections was performed during the first 9 months.

3.2. Combination Therapy. The effect of the addition of grid laser photocoagulation to intravitreal anti-VEGF agent injection was compared to monotherapy (Figure 2). The improvement in visual acuity was similar to monotherapy at the 3 month mark. However, after 6 months the improvement in vision in the combination groups was lost and at 21 months vision worsening was observed with the addition of subthreshold grid laser to anti-VEGF therapy (loss of 3.017 lines of vision on the LogMAR chart). The addition of threshold grid laser to anti-VEGF injection resulted in a loss of vision at 24 months (loss of 1.199 lines).

The combination of laser photocoagulation and triamcinolone was also investigated. At 3 months, improvement was observed in combination therapy when compared to either laser or steroid monotherapy. However, at 24 months both combination therapy (1.290 lines) and threshold grid laser alone led to a similar vision gain (Figure 3).

The combination of intravitreal triamcinolone and anti-VEGF agents showed a temporary improvement in vision at 3 months when compared to monotherapy. However, combination therapy led to a negative result with an eventual vision loss at 24 months (loss of 3.052 lines) (Figure 4). The addition of triamcinolone injection to these cases receiving vitrectomy did not reach the level of visual improvement attained in those treated with ILM peeling alone (2.733 lines of gain) (Figure 5).

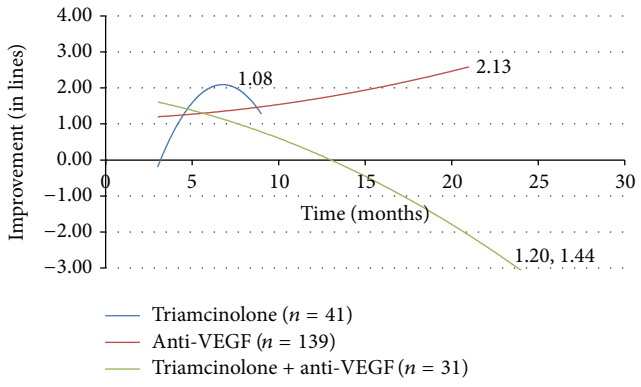

Figure 4: Change in visual acuity (in lines) with triamcinolone and anti-VEGF. VEGF = vascular endothelial growth factor.

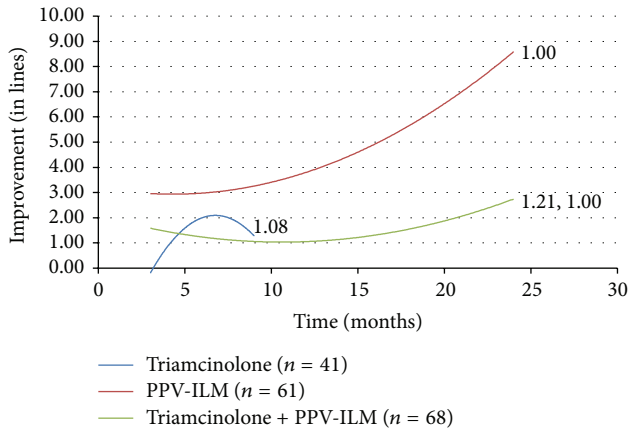

Figure 5: Change in visual acuity (in lines) with triamcinolone and PPV-ILM. PPV-ILM = pars plana vitrectomy with internal limiting membrane peeling.

Table 2: Final visual improvement for anti-VEGF injection and pars plana vitrectomy with ILM peeling monotherapy.

	Anti-VEGF (n = 102)	PPV-ILM (n = 58)	P value
≥3 line improvement	31.3%	55.2%	0.0031
≥6 line improvement	10.8%	29.3%	0.003

VEGF = vascular endothelial growth factor.
PPV-ILM = pars plana vitrectomy with internal limiting membrane peeling.

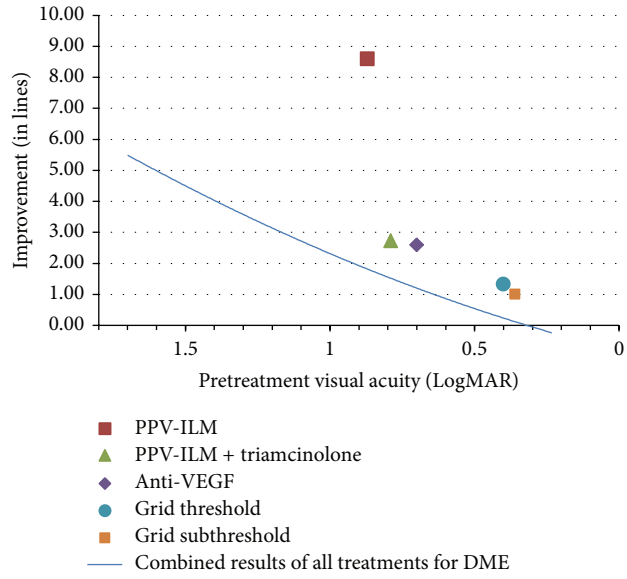

Figure 6: Final visual improvement (in lines) according to pretreatment visual acuity. PPV-ILM = pars plana vitrectomy with internal limiting membrane peeling. VEGF = vascular endothelial growth factor.

Visual improvement was then analyzed in terms of the percent of patients gaining three or six lines of vision. The last visual acuity reading available was compared to the recorded pretreatment visual acuity. The data of patients treated with either anti-VEGF injection or vitrectomy with ILM peeling alone were compared (Table 2). 31.3% of the anti-VEGF group and 55.2% of the vitrectomy group gained at least 3 lines of vision. This was a statistically significant difference. Vitrectomy with ILM peeling led to a significantly better result (P = 0.0031). 10.8% of those treated with anti-VEGF injection and 29.3% of patients receiving vitrectomy gained at least 6 lines of vision. Again, statistical significance was reached and ILM peeling had a more favorable outcome in this analysis.

A final presentation of the data compared different treatment outcomes based on final visual improvement according to pretreatment visual acuity. In Figure 6, data were plotted as improvement in vision, in LogMAR, and against pretreatment visual acuity. A single second order regression trend line represents the combined results of all treatments for DME in this study, giving us a baseline. After analyzing all of the possible mono- and combination therapies for DME, the plotted data points represent the top five treatments in terms of vision improvement. Vitrectomy with ILM peeling showed the largest recovery in vision. This treatment was followed by, in order of descending amount of vision gain (LogMAR), vitrectomy with ILM peeling combined with triamcinolone (2.7328), anti-VEFG injection (2.5894), threshold grid laser (1.3256), and subthreshold grid laser (0.9953).

3.3. Complications. Intraocular pressure rise was observed most frequently in eyes treated with triamcinolone (17%). In the other treatment groups, intraocular pressure increased in about 3%.

Secondary cataract formation was most frequently observed in the pars plana vitrectomy group (14% versus 8% in the other treatment groups). Retinal detachment was observed in 1 case in the pars plana vitrectomy group, 1 case treated with anti-VEGF, and 1 case following grid laser photocoagulation.

4. Discussion

The choice of treatment when dealing with DME has been complicated in recent years with the emergence of new

therapies, which allow for a large number of possible treatment schedules and combinations [3–28]. A prospective, randomized clinical trial could be done to address the efficacy of each treatment alone or in combination with another; however this sort of investigation would have many arms. Thus, the study would be almost prohibitively large, costly, and complex and would take years until results could be obtained. Here we present a nonrandomized, multicenter collaborative study to compare treatment effects among all available therapies.

When cases of DME treated with a single therapy were analyzed, monotherapy with vitrectomy and ILM peeling resulted in the largest improvement in vision. In comparison, treatment with pars plana vitrectomy and ILM peeling alone resulted in an improvement in vision two to three times greater than observed with anti-VEGF injection alone. Treatment with intravitreal anti-VEGF agents resulted in a better outcome than either type of grid laser, but vitrectomy still led to more vision improvement. Both methods of grid laser did not show overly positive results in improving visual acuity. It does appear that subthreshold grid laser has the same effect as threshold grid laser, which is consistent with the findings of other studies [27, 28]. These results suggest that if only a single therapy is to be considered to treat DME, vitrectomy with ILM peeling may be a good option for attaining visual acuity improvement over 24-month follow-up.

The more favorable outcomes observed with vitrectomy and ILM peeling alone versus other mainstream therapies certainly raise questions. Considering that surgery for DME is in many cases done as a last resort, why would this therapy alone result in significant visual improvement? A possible explanation could be that the majority of cases chosen for vitrectomy have already failed other treatments. Thus DME is chronic and photoreceptors are nonfunctional by the time that the operation is performed. In this situation, a better prognosis would be expected if a surgical option was opted for sooner.

The treatment of DME with anti-VEGF injection alone fared well with relatively good visual improvement; however the addition of any grid laser led to an overall negative outcome by the conclusion of the study. There are prior clinical trials supporting the assertion that the addition of grid laser to anti-VEGF therapy does not significantly improve outcomes [19, 21]. For example, the RESTORE study in 2011 did not show improvement with the addition of laser. Our results suggest that adding grid laser to a regimen of intravitreal anti-VEGF injections may not improve visual outcome. Prior studies have shown that outcomes for treatment of DME at 36 months with ranibizumab are maintained with frequent injections to optimally control edema and maximize vision. In our study the average number of intravitreal injections of anti-VEGF per patient was low which may reflect difficulty with frequent injections outside of randomized clinical trials. Also more extensive focal/grid laser therapy may have contributed in reduction of the number of injections [33].

Intravitreal triamcinolone is widely used to treat DME, especially in combination with other therapies. In this study, the efficacy of treating DME solely with triamcinolone injection is difficult to interpret given the truncated trend line with an insufficient number of cases to evaluate the effect on vision past nine months. This may reflect the general shift of therapy away from the use of triamcinolone injection to the use of anti-VEGF agents. There is sufficient data to comment on combination therapy with triamcinolone. While the addition of triamcinolone to threshold grid laser did not seem to help with vision improvement, the medication's addition to both anti-VEGF therapy and vitrectomy with ILM peeling actually led to worse results compared to cases where the steroid was not used. These results reflect the conclusions of clinical trials in the literature reporting no improvement with the addition of triamcinolone to anti-VEGF therapy or grid laser [22, 34–37]. The outcomes here suggest that triamcinolone injection may not be useful in augmenting treatment with grid laser, anti-VEGF injection, or ILM peeling.

A major issue that must be addressed is the fact that visual improvement should ideally be considered according to pretreatment vision level. It is less productive and less impactful to present the percentage of vision improvement greater than three lines where initial vision is not taken into account. ILM peeling was superior to anti-VEGF therapy in this comparison. However, this classical way of presenting data is not completely meaningful in this situation, since the improvement is dependent on pretreatment visual acuity. Certainly it is easier to achieve three lines of improvement if the initial vision is 20/400 than if it is 20/30. The true evaluation of results should relies on classification of the results according to pretreatment visual acuity. This was the impetus behind displaying final visual improvement for each therapy according to pretreatment visual acuity. According to this analysis, vitrectomy with ILM peeling resulted in better visual outcome for DME compared to other treatments.

The impact of vitrectomy on tractional diabetic macular edema is well known. Removal of the posterior hyaloid and release of traction result in an increase in tissue pressure and also a lowering of hydrostatic pressure gradient [38]. It is important to note that there is also evidence to support benefits of vitrectomy in nontractional edema. The oxygen level in the vitreous of diabetic patients is low [39]. There is evidence that demonstrate increased oxygen level in the vitreous cavity following vitrectomy [40]. Vitrectomy not only results in increased oxygen transport between the anterior and posterior segment, but also helps the removal of growth factors, such as vascular endothelial growth factor [41]. The net impact may result in improved macular edema. In addition, 3D spectral domain OCT now provides full-field macular images that can identify often overlooked extrafoveal traction that can contribute to DME that is labeled as nontractional by foveal features alone [42]. Also, PPV could result in better preservation of the ellipsoid line and parallelism and could therefore result in a better visual acuity.

Considering the success of ILM removal in improving retinal edema and vision in this study, a more detailed explanation regarding a possible mechanism of action is in order. Aside from the favorable changes with the removal of vitreous, peeling results in the removal of the ILM barrier as well as local glial proliferation including astrocytes, microglia, and the Müller cells endfeet. Prior investigations have shown that ILM peeling usually results in some Müller cell injury and

stimulation of healing process [41]. Minor Müller cell trauma has been extensively studied in retinal detachments where it results in an upregulation of epidermal growth factor receptor (EGF-R). EGF-R regulates the injury response where stem cell proliferation compensates for the loss of neural cells. More importantly, EGF-R stimulates the filling of Müller cells with microfibrils of glial fibrillary acidic proteins (GFAPs) causing a vertical glial proliferation from the ILM to the external limiting membrane. This mechanism was described in the central nervous system, where, following trauma, radial glia are formed to repair and reconnect synapses [43, 44]. This has also been observed in the retina where, in the case of detachment, an increase of GFAPs in Müller cells attenuates hypoxic damage and neuronal loss is reduced [45–47]. Besides retinal detachment, these protective mechanisms have been shown to be linked to ischemic retinal injury [48, 49]. These results suggest that, as we perform vitrectomy and ILM peeling, anti-inflammatory agents like triamcinolone may not be helpful in reducing edema as they can decrease the repair of glial cells.

Significant weaknesses and limitations do exist for this sort of investigation. Considering this study was not randomized with specific treatment groups, the exact sequence and timing of single treatment types or combination therapies were not standardized. Different doses of triamcinolone, different techniques of grid laser application, and varying numbers of intravitreal anti-VEGF injections may have been used, possibly impacting the results. With regard to the formulation of the trend lines, even though several cases were available for each data point, for the most part fewer cases were available when plotting the data points two years out from starting treatment. This may weaken the validity of extrapolated final visual improvement. Trend lines are useful in comparing efficacy of therapeutic options. However, they may not be very precise in measuring exact number of lines of improvement in vision. Another issue is that not all diabetic macular edemas are created equal. It is possible that combination therapy, such as the addition of triamcinolone to another treatment or grid laser to anti-VEGF injection, was chosen in those cases deemed to be particularly severe or difficult. Thus, it is not that the combination is necessarily worse, but it is that the results may be affected due to a selection of patients with particularly advanced disease receiving that treatment.

It is extremely difficult to compare different studies due to varying inclusion criteria, treatment options, and initial visual acuities. Retrospective studies are generally of less statistical and clinical value than prospective trials. This weakness may be lessened by using a large number of investigated subjects, which can results in a more significant statistical analysis. Considering that this study shows outcomes similar to prior prospective randomized clinical trials with regard to anti-VEGF therapy with laser and triamcinolone with other treatment options, it is reasonable to infer that other outcomes from this investigation, such as the role of vitrectomy in the treatment of diabetic macular edema, may be later confirmed with subsequent prospective randomized trial results [8, 12, 15, 16].

In summary, this comparative study suggested that vitrectomy with ILM peeling may be a good option for the treatment of selected patients with DME. As for combination therapy, adding grid laser to a regimen of intravitreal anti-VEGF injections may not be helpful. Also, the addition of intravitreal triamcinolone injection to grid laser, anti-VEGF injection, or vitrectomy/ILM peeling may not improve final visual acuity. Additional prospective, randomized studies are needed to determine the optimal treatment of DME and confirm these results.

Disclosure

The findings in this manuscript were presented at the European Vitreo-Retinal Society (EVRS) Annual Meeting in Dresden, Germany, September 2012 and at the Association for Research in Vision and Ophthalmology (ARVO) in Seattle, WA, May 2013.

Conflict of Interests

The authors declare that there is no conflict of interests regarding the publication of this paper.

Acknowledgment

Ron Adelman, Aaron Parnes, Zofia Michalewska, Barbara Parolini, and Didier Ducournau acknowledge the support of the European Vitreo-Retinal Society (EVRS) Macular Edema Study Group.

References

[1] R. Klein, B. E. K. Klein, S. E. Moss, M. D. Davis, and D. L. DeMets, "The Wisconsin epidemiologic study of diabetic retinopathy. IV. Diabetic macular edema," *Ophthalmology*, vol. 91, no. 12, pp. 1464–1474, 1984.

[2] J. W. Y. Yau, S. L. Rogers, R. Kawasaki et al., "Global prevalence and major risk factors of diabetic retinopathy," *Diabetes Care*, vol. 35, no. 3, pp. 556–564, 2012.

[3] Early Treatment Diabetic Retinopathy Study Research Group, "Photocoagulation for diabetic macular edema. Early treatment diabetic retinopathy study report number 1," *Archives of Ophthalmology*, vol. 103, pp. 1796–1806, 1985.

[4] C. Haritoglou, D. Kook, A. Neubauer et al., "Intravitreal bevacizumab (Avastin) therapy for persistent diffuse diabetic macular edema," *Retina*, vol. 26, no. 9, pp. 999–1005, 2006.

[5] J. F. Arevalo, J. G. Sanchez, A. F. Lasave et al., "Intravitreal Bevacizumab (Avastin) for Diabetic Retinopathy at 24-months: The 2008 Juan Verdaguer-Planas Lecture," *Current Diabetes Reviews*, vol. 6, no. 5, pp. 313–322, 2008.

[6] Q. D. Nguyen, D. M. Brown, D. M. Marcus et al., "Ranibizumab for diabetic macular edema: results from 2 phase iii randomized trials: RISE and RIDE," *Ophthalmology*, vol. 119, no. 4, pp. 789–801, 2012.

[7] Q. D. Nguyen, S. M. Shah, A. A. Khwaja et al., "Two-year outcomes of the ranibizumab for edema of the mAcula in diabetes (READ-2) study," *Ophthalmology*, vol. 117, no. 11, pp. 2146–2151, 2010.

[8] M. Michaelides, A. Kaines, R. D. Hamilton et al., "A prospective randomized trial of intravitreal bevacizumab or laser therapy in

the management of diabetic macular edema (BOLT study) 12-month data: report 2," *Ophthalmology*, vol. 117, no. 6, pp. 1078–1086, 2010.

[9] P. Massin, F. Bandello, J. G. Garweg et al., "Safety and efficacy of ranibizumab in diabetic macular edema (RESOLVE study): a 12-month, randomized, controlled, double-masked, multicenter phase II study," *Diabetes Care*, vol. 33, no. 11, pp. 2399–2405, 2010.

[10] D. V. Do, Q. D. Nguyen, D. Boyer et al., "One-year outcomes of the da VINCI study of VEGF trap-eye in eyes with diabetic macular edema," *Ophthalmology*, vol. 119, no. 8, pp. 1658–1665, 2012.

[11] Diabetic Retinopathy Clinical Research Network, M. J. Elman, H. Qin et al., "Intravitreal ranibizumab for diabetic macular edema with prompt versus deferred laser treatment: three-year randomized trial results," *Ophthalmology*, vol. 119, pp. 2312–2318, 2012.

[12] M. Soheilian, A. Ramezani, A. Obudi et al., "Randomized trial of intravitreal bevacizumab alone or combined with triamcinolone versus macular photocoagulation in diabetic macular edema," *Ophthalmology*, vol. 116, no. 6, pp. 1142–1150, 2009.

[13] I. Zucchiatti, R. Lattanzio, G. Querques et al., "Intravitreal dexamethasone implant in patients with persistent diabetic macular edema," *Ophthalmologica*, vol. 228, no. 2, pp. 117–122, 2012.

[14] P. A. Campochiaro, D. M. Brown, A. Pearson et al., "Sustained delivery fluocinolone acetonide vitreous inserts provide benefit for at least 3 years in patients with diabetic macular edema," *Ophthalmology*, vol. 119, no. 10, pp. 2125–2132, 2012.

[15] M. C. Gillies, F. K. P. Sutter, J. M. Simpson, J. Larsson, H. Ali, and M. Zhu, "Intravitreal triamcinolone for refractory diabetic macular edema: two-year results of a double-masked, placebo-controlled, randomized clinical trial," *Ophthalmology*, vol. 113, no. 9, pp. 1533–1538, 2006.

[16] J. B. Jonas, B. A. Kamppeter, B. Harder, U. Vossmerbaeumer, G. Sauder, and U. H. M. Spandau, "Intravitreal triamcinolone acetonide for diabetic macular edema: a prospective, randomized study," *Journal of Ocular Pharmacology and Therapeutics*, vol. 22, no. 3, pp. 200–207, 2006.

[17] T. Otani and S. Kishi, "A controlled study of vitrectomy for diabetic macular edema," *American Journal of Ophthalmology*, vol. 134, no. 2, pp. 214–219, 2002.

[18] T. Kimura, J. Kiryu, H. Nishiwaki et al., "Efficacy of surgical removal of the internal limiting membrane in diabetic cystoid macular edema," *Retina*, vol. 25, no. 4, pp. 454–461, 2005.

[19] P. Mitchell, F. Bandello, U. Schmidt-Erfurth et al., "The RESTORE study: ranibizumab monotherapy or combined with laser versus laser monotherapy for diabetic macular edema," *Ophthalmology*, vol. 118, no. 4, pp. 615–625, 2011.

[20] J. F. Arevalo, A. F. Lasave, L. Wu et al., "Intravitreal bevacizumab plus grid laser photocoagulation or intravitreal bevacizumab or grid laser photocoagulation for diffuse diabetic macular edema: results of the pan-american collaborative retina study group at 24 months," *Retina*, vol. 33, no. 2, pp. 403–413, 2013.

[21] S. J. Lee, E. T. Kim, and Y. S. Moon, "Intravitreal bevacizumab alone versus combined with macular photocoagulation in diabetic macular edema," *Korean Journal of Ophthalmology*, vol. 25, no. 5, pp. 299–304, 2011.

[22] M. Soheilian, A. Ramezani, A. Obudi et al., "Randomized trial of intravitreal bevacizumab alone or combined with triamcinolone versus macular photocoagulation in diabetic macular edema," *Ophthalmology*, vol. 116, no. 6, pp. 1142–1150, 2009.

[23] Diabetic Retinopathy Clinical Research Network, "Randomized trial evaluating ranibizumab plus prompt or deferred laser or triamcinolone plus prompt laser for diabetic macular edema," *Ophthalmology*, vol. 117, no. 6, pp. 1064–1077, 2010.

[24] G. Sobaci, G. Özge, C. Erdurman, H. A. Durukan, and Z. M. Bayraktar, "Comparison of grid laser, intravitreal triamcinolone, and intravitreal bevacizumab in the treatment of diffuse diabetic macular edema," *Ophthalmologica*, vol. 227, no. 2, pp. 95–99, 2012.

[25] T. C. Kreutzer, R. Al Saeidi, D. Kook et al., "Comparison of intravitreal bevacizumab versus triamcinolone for the treatment of diffuse diabetic macular edema," *Ophthalmologica*, vol. 224, no. 4, pp. 258–264, 2010.

[26] L. Paccola, R. A. Costa, M. S. Folgosa, J. C. Barbosa, I. U. Scott, and R. Jorge, "Intravitreal triamcinolone versus bevacizumab for treatment of refractory diabetic macular oedema (IBEME study)," *British Journal of Ophthalmology*, vol. 92, no. 1, pp. 76–80, 2008.

[27] N. Doi, T. Sakamoto, Y. Sonoda et al., "Comparative study of vitrectomy versus intravitreous triamcinolone for diabetic macular edema on randomized paired-eyes," *Graefe's Archive for Clinical and Experimental Ophthalmology*, vol. 250, no. 1, pp. 71–78, 2012.

[28] A. Yanyali, A. F. Nohutcu, F. Horozoglu, and E. Celik, "Modified grid laser photocoagulation versus pars plana vitrectomy with internal limiting membrane removal in diabetic macular edema," *The American Journal of Ophthalmology*, vol. 139, no. 5, pp. 795–801, 2005.

[29] R. A. Adelman, A. J. Parnes, and D. Ducournau, "Strategy for the management of uncomplicated retinal detachments: the european vitreo-retinal society retinal detachment study report 1," *Ophthalmology*, vol. 120, no. 9, pp. 1804–1808, 2013.

[30] R. A. Adelman, A. J. Parnes, J. O. Sipperley, and D. Ducournau, "Strategy for the management of complex retinal detachments: the European vitreo-retinal society retinal detachment study report 2," *Ophthalmology*, vol. 120, no. 9, pp. 1809–1813, 2013.

[31] Z. Michalewska, D. Ducournau, and R. A. Adelman, "How do vitrectomy parameters influence the results of rhegmatogenous retinal detachments repair? EVRS RD Study No. 3," *Acta Ophthalmologica*, vol. 92, no. 5, pp. e416–e417, 2014.

[32] R. A. Adelman, A. J. Parnes, Z. Michalewska, D. Ducournau, and European Vitreo-Retinal Society (EVRS) Retinal Detachment Study Group, "Clinical variables associated with failure of retinal detachment repair: the European vitreo-retinal society retinal detachment study report number 4," *Ophthalmology*, vol. 121, no. 9, pp. 1715–1719, 2014.

[33] D. V. Do, Q. D. Nguyen, A. A. Khwaja et al., "Ranibizumab for edema of the macula in diabetes study: 3-year outcomes and the need for prolonged frequent treatment," *JAMA Ophthalmology*, vol. 131, no. 2, pp. 139–145, 2013.

[34] V. Kumar, B. Ghosh, D. K. Mehta, and N. Goel, "Functional outcome of subthreshold versus threshold diode laser photocoagulation in diabetic macular oedema," *Eye*, vol. 24, no. 9, pp. 1459–1465, 2010.

[35] J. W. Lim, H. K. Lee, and M. C. Shin, "Comparison of intravitreal bevacizumab alone or combined with triamcinolone versus triamcinolone in diabetic macular edema: a randomized clinical trial," *Ophthalmologica*, vol. 227, no. 2, pp. 100–106, 2012.

[36] H. M. Marey and A. F. Ellakwa, "Intravitreal bevacizumab alone or combined with triamcinolone acetonide as the primary treatment for diabetic macular edema," *Clinical Ophthalmology*, vol. 5, no. 1, pp. 1011–1016, 2011.

[37] H. Y. Lee, S. Y. Lee, and J. S. Park, "Comparison of photocoagulation with combined intravitreal triamcinolone for diabetic macular edema," *Korean Journal of Ophthalmology*, vol. 23, no. 3, pp. 153–158, 2009.

[38] T. J. Wolfensberger and Z. J. Gregor, "Macular edema—rationale for therapy," *Developments in Ophthalmology*, vol. 47, pp. 49–58, 2010.

[39] N. M. Holekamp, Y.-B. Shui, and D. Beebe, "Lower intraocular oxygen tension in diabetic patients: possible contribution to decreased incidence of nuclear sclerotic cataract," *American Journal of Ophthalmology*, vol. 141, no. 6, pp. 1027–1032, 2006.

[40] N. M. Holekamp, Y. B. Shui, and D. C. Beebe, "Vitrectomy surgery increases oxygen exposure to the lens: a possible mechanism for nuclear cataract formation," *The American Journal of Ophthalmology*, vol. 139, no. 2, pp. 302–310, 2005.

[41] S. Wolf, U. Schnurbusch, P. Wiedemann, J. Grosche, A. Reichenbach, and H. Wolburg, "Peeling of the basal membrane in the human retina: ultrastructural effects," *Ophthalmology*, vol. 111, no. 2, pp. 238–243, 2004.

[42] A. Ophir, M. R. Martinez, P. Mosqueda, and A. Trevino, "Vitreous traction and epiretinal membranes in diabetic macular oedema using spectral-domain optical coherence tomography," *Eye*, vol. 24, no. 10, pp. 1545–1553, 2010.

[43] S. Shibuya, O. Miyamoto, T. Itano, S. Mori, and H. Norimatsu, "Temporal progressive antigen expression in radial glia after contusive spinal cord injury in adult rats," *GLIA*, vol. 42, no. 2, pp. 172–183, 2003.

[44] G. E. Goings, V. Sahni, and F. G. Szele, "Migration patterns of subventricular zone cells in adult mice change after cerebral cortex injury," *Brain Research*, vol. 996, no. 2, pp. 213–226, 2004.

[45] G. P. Lewis and S. K. Fisher, "Up-regulation of glial fibrillary acidic protein in response to retinal injury: its potential role in glial remodeling and a comparison to vimentin expression," *International Review of Cytology*, vol. 230, pp. 263–290, 2003.

[46] J. D. Unterlauft, W. Eichler, K. Kuhne et al., "Pigment epithelium-derived factor released by Müller glial cells exerts neuroprotective effects on retinal ganglion cells," *Neurochemical Research*, vol. 37, no. 7, pp. 1524–1533, 2012.

[47] M. Wang, W. Ma, L. Zhao, R. N. Fariss, and W. T. Wong, "Adaptive Müller cell responses to microglial activation mediate neuroprotection and coordinate inflammation in the retina," *Journal of Neuroinflammation*, vol. 8, article 173, 2011.

[48] A. Madinier, "Microglial and BDNF impact on the induction of the postischemic neuroplasticity," Thesis 2011, http://www.theses.fr/2011DIJOS037/document.

[49] I. L. McAllister, S. Vijayasekaran, S. D. Chen, and D. Y. Yu, "Effect of triamcinolone acetonide on vascular endothelial growth factor and occludin levels in branch retinal vein occlusion," *The American Journal of Ophthalmology*, vol. 147, no. 5, pp. 838–846, 2009.

Hindawi Publishing Corporation
BioMed Research International
Volume 2014, Article ID 458631, 8 pages
http://dx.doi.org/10.1155/2014/458631

Research Article

Evaluation of Macular Retinal Ganglion Cell-Inner Plexiform Layer Thickness after Vitrectomy with Internal Limiting Membrane Peeling for Idiopathic Macular Holes

Alfonso L. Sabater,[1] Álvaro Velázquez-Villoria,[1] Miguel A. Zapata,[2,3] Marta S. Figueroa,[3,4] Marta Suárez-Leoz,[5] Luis Arrevola,[6] María-Ángeles Teijeiro,[6] and Alfredo García-Layana[1,3]

[1] *Department of Ophthalmology, Clínica Universidad de Navarra, 31008 Pamplona, Spain*
[2] *Department of Ophthalmology, Hospital Universitario Vall d'Hebrón, 08035 Barcelona, Spain*
[3] *Red Temática de Investigación Cooperativa en Oftalmología (RETICS-Oftared RD12/0034), Instituto de Salud Carlos III, Madrid, Spain*
[4] *Department of Ophthalmology, Hospital Universitario Ramón y Cajal, 28034 Madrid, Spain*
[5] *Clínica Oftalmológica Suárez Leoz, 28010 Madrid, Spain*
[6] *Clínica Baviera, 28046 Madrid, Spain*

Correspondence should be addressed to Alfredo García-Layana; aglayana@unav.es

Received 9 May 2014; Accepted 13 June 2014; Published 7 July 2014

Academic Editor: Jerzy Nawrocki

Purpose. To evaluate macular retinal ganglion cell-inner plexiform layer (GCIPL) thickness changes after Brilliant Blue G-assisted internal limiting membrane peeling for idiopathic macular hole repair using a high-resolution spectral-domain optical coherence tomography (SD-OCT). *Methods*. 32 eyes from 32 patients with idiopathic macular holes who underwent vitrectomy with internal limiting membrane peeling between January 2011 and July 2012 were retrospectively analyzed. GCIPL thickness was measured before surgery, and at one month and at six months after surgery. Values obtained from automated and semimanual SD-OCT segmentation analysis were compared (Cirrus HD-OCT, Carl Zeiss Meditec, Dublin, CA). *Results*. No significant differences were found between average GCIPL thickness values between preoperative and postoperative analysis. However, statistical significant differences were found in GCIPL thickness at the temporal macular quadrants at six months after surgery. Quality measurement analysis performed by automated segmentation revealed a significant number of segmentation errors. Semimanual segmentation slightly improved the quality of the results. *Conclusion*. SD-OCT analysis of GCIPL thickness found a significant reduction at the temporal macular quadrants at 6 months after Brilliant Blue G-assisted internal limiting membrane peeling for idiopathic macular hole.

1. Introduction

Nowadays, one of the most common surgical procedures for idiopathic macular hole (IMH) management is based on vitrectomy with internal limiting membrane (ILM) peeling [1–3]. Different vital dyes such as indocyanine green (ICG) or Brilliant Blue G (BBG) and other substances such as triamcinolone acetonide (TA) have been used to assist in peeling of the ILM of the neuroretina [4–6]. However, several authors have reported histological and functional damage to the retina after IMH surgery with ICG-assisted ILM peeling [3, 7–10]. In contrast, BBG or TA appears to be safer alternatives for ILM peeling [6, 11, 12].

On the other hand, ILM peeling itself may induce visible changes of the inner retinal surface, although no changes in retinal nerve fiber layer (RNFL) thickness have been detected [13]. However, there is some controversy about the effect that BBG-assisted ILM peeling has on the retinal ganglion cell complex (RGCC) [14, 15]. Moreover, a recent study has suggested that ILM peeling may reduce retinal sensitivity and increase the incidence of microscotomas [16].

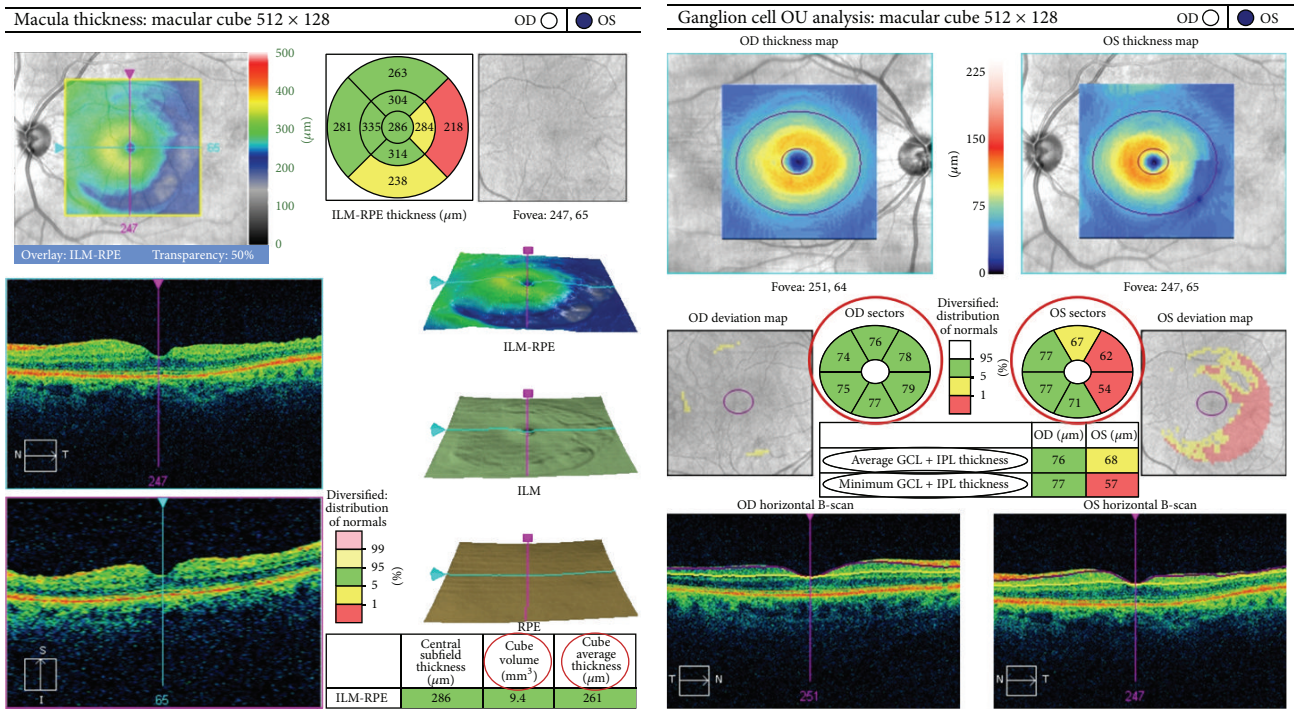

Figure 1: Macular analysis of the left eye and ganglion cell analysis of both eyes of a 78-year-old woman at 6 months after vitrectomy with Brilliant Blue G-assisted internal limiting membrane peeling for idiopathic macular hole. (a) OCT cross-section analysis showing cube volume and cube thickness. (b) Average, minimum, and sectorial macular thickness of the ganglion cell-inner plexiform layer of both eyes. A macular temporal defect may be appreciated in the left eye.

To our knowledge, only a few groups have evaluated the effect of ILM peeling on the RGCC after idiopathic macular hole surgery using the RTVue-100 SD OCT (Optovue, Fremont, CA, USA) with different results [14, 15, 17]. In the current study, we evaluated for the first time the capacity of the new ganglion cell analysis (GCA) software of the Cirrus HD-OCT (Carl Zeiss Meditec, Dublin, CA) to analyze the retinal ganglion cell-inner plexiform layer (GCIPL) after BBG-assisted internal limiting membrane peeling for idiopathic macular hole surgery. Additionally, we evaluated how BBG-assisted ILM peeling affects the macular and average GCIPL thickness at 1 and 6 months after macular hole surgery with this new software.

2. Materials and Methods

This study was a multicenter ($n = 5$), retrospective, and observational study of 32 patients. The institutional review board approval of every center was obtained. All of the patients underwent a vitrectomy associated with BBG-assisted peeling of the retinal ILM as a consequence of an IMH between January 2011 and July 2012. Seven patients were excluded for the following reasons: a history of glaucoma (1), failure to correctly identify the limits of the GCIPL by the ganglion cell analysis software by automated or semimanual segmentation (4), or macular holes greater than the central area of analysis where the GCA software does not measure the GCIPL thickness (2) (Figure 1). Therefore, a total of 25 eyes of 25 patients were included in this study.

Demographic information collected from the clinical chart included patient age, sex, combined cataract surgery, macular hole stage, preoperative best-corrected visual acuity (BCVA), postoperative BCVA, intraocular hypertension after surgery (>25 mmHg), history of glaucoma, and failure to close the macular hole. Best-corrected visual acuity was measured using a decimal visual acuity chart, and the decimal visual acuity was converted to the logarithm of the minimum angle of resolution (logMAR) units for statistical analysis.

Three-dimensional cube OCT data were obtained with the Cirrus HD-OCT device using the Macular Cube 200 × 200 scan protocol. This protocol performs 200 horizontal B-scans comprising 200 A-scans per B-scan over 1024 samples within a cube measuring 6 × 6 × 2 mm. The GCA software (6.0 version) evaluates the thickness of the ganglion cell plus inner plexiform layers. The average, minimum, and sectorial thicknesses of the GCIPL are measured in an elliptical annulus (vertical inner and outer radius of 0.5 mm and 2.0 mm; horizontal inner and outer radius of 0.6 and 2.4 mm, resp.) around the fovea. In order to avoid segmentation errors, OCT measurements with signal strength (SS) below 5 were excluded (0: lowest SS; 10: highest SS).

All OCT images were obtained by experienced clinical technicians. Eyes were dilated with tropicamide 1% and phenylephrine 2.5%. Average GCIPL thickness, macular cube

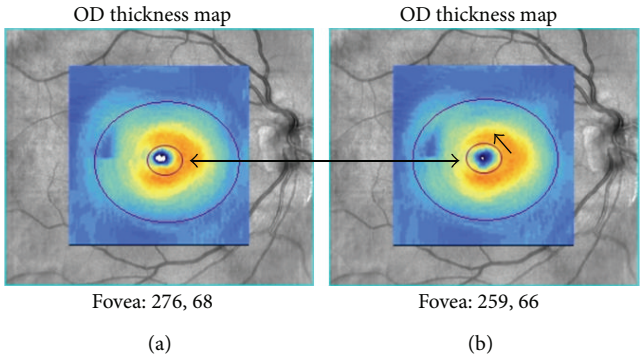

Figure 2: This example shows the relocation of the area of analysis (semimanual segmentation). The center was manually displaced following the direction of the black arrow (b).

average thickness (MCAT), and macular cube volume (MCV) values of the patients included in this study were measured preoperatively, at 1 and at 6 months after macular hole surgery by scanning with the Cirrus HD-OCT system (Carl Zeiss Meditec, Dublin, CA) (Figure 1).

The main outcome measure was the comparison of average GCIPL thickness preoperatively and at 6 months after macular hole surgery with BBG-assisted ILM peeling. Comparison of MCAT and MCV preoperatively and at 6 months after macular hole surgery with ILM peeling was the secondary outcome measures. Moreover, all values were obtained at 1 month after surgery. Average, minimum, and sectorial (superior, inferior, superonasal, inferonasal, superotemporal, and inferotemporal) GCIPL thickness values were obtained and compared in every patient preoperatively and at 1 and 6 months after surgery (Figure 1).

Each GCIPL scan was evaluated in order to identify how many cases had a greater GCIPL thickness after surgery compared to before. This data was studied to evaluate the quality of the measurements, as the real GCIPL thickness should not be higher in the postoperative period.

A comparison between preoperative and postoperative macular GCIPL thickness values was also performed by semimanual segmentation. The Cirrus HD-OCT (Carl Zeiss Meditec, Dublin, CA) GCIPL analysis software is not capable of real manual segmentation of the macular layers, but it does allow relocation of the area of analysis (Figure 2). This procedure was performed in every scan by an experienced clinical technician in order to improve the quality of the measurements by repositioning the area of analysis in the real center of the fovea.

Surgery was performed using a standard 23- or 25-gauge 3-port pars plana vitrectomy. The infusion cannula was placed in the inferotemporal quadrant. If the posterior hyaloid was still attached to the optic disc, its detachment was induced by suction with the vitrectomy probe. A volume of 0.1 mL BBG (Fluoron GmbH, Ludwigsfeld, Germany) at a concentration of 0.25 mg/mL was injected into the vitreous cavity over the posterior pole for 30 seconds. The ILM was grasped at the temporal quadrant and peeled off with forceps

Table 1: Demographic characteristics.

Parameter	Values	%
Sex		
Male	11	44
Female	14	56
Age*	70.48 ± 8.66	
Eye		
Right	13	52
Left	12	48
Macular hole stage		
2	6	24
3	8	32
4	11	44
Visual acuity (log MAR)		
Preoperative*	0.70 ± 0.32	
Postoperative*	0.34 ± 0.32	
Glaucoma		
No	25	100
Yes	0	0
Macular hole closure	25	100

*Mean ± SD.
log MAR: logarithm of the minimum angle of resolution.

in an area of 2-disc diameter around the macular hole. Fluid-air exchange and intraocular gas tamponade with SF6 at 20% were performed. After surgery, patients were asked to remain in a facedown position for at least 50 minutes per hour for four days. In 12 patients, the crystalline lens was removed by phacoemulsification followed by intraocular lens implantation before pars plana vitrectomy. A topical beta blocker (timolol maleate 0.5% BID) was routinely used to prevent postoperative intraocular pressure (IOP) rise.

The differences in the OCT values between the preoperative time and at 1 and at 6 months after surgery were analyzed using the paired t-test. The descriptive statistics are expressed as the means, standard deviations (SDs), and percentages. Visual acuity data were converted to the logarithm of the minimal angle of resolution (logMAR). Statistical analysis was performed using SPSS, version 15.0 (SPSS Inc., Chicago, IL). A P value of ≤ 0.05 was considered significant.

3. Results and Discussion

The study sample was comprised of 25 eyes of 25 participants (mean age 70.48 ± 8.66 years old, range: 49–82). Mean preoperative and postoperative (6 months) BCVA were 0.7 ± 0.32 logMAR units and 0.34 ± 0.32 logMAR units, respectively. The rate of closure of macular holes by OCT evaluation was 100% at 1 and 6 months after surgery. Twelve patients underwent a combined cataract surgery with pars plana vitrectomy. None of the patients had a postoperative retinal detachment. There was no recorded incidence of increased postoperative IOP above 25 mmHg. Demographic data are shown in Table 1.

Average MCV was 10.22 ± 0.81 μm at the preoperative period, 10.03 ± 1.06 μm at 1 month after surgery, and 9.85

Table 2: Comparison between preoperative and postoperative (at 1 month after surgery) macular GCIPL thickness values performed by automated segmentation.

$N = 25$	Preoperative (μm)	SD (μm)	Postoperative (μm)	SD (μm)	Difference (μm)	SD (μm)	P value*
Average GCIPL thickness	60.72	18.20	61.52	17.37	−0.8	0.83	0.865
Minimum GCIPL thickness	33.56	18.20	43.60	23.83	−10.04	−5.63	0.134
GCIPL superior	59.76	26.37	64.04	27.73	−4.28	−1.36	0.531
GCIPL inferior	53.88	23.79	59.56	18.48	−5.68	5.31	0.363
GCIPL superonasal	59.04	24.77	65.64	22.01	−6.6	2.76	0.243
GCIPL superotemporal	69.48	14.87	59.20	20.37	10.28	−5.5	0.076
GCIPL inferonasal	54.48	20.62	62.80	18.90	−8.32	1.72	0.116
GCIPL inferotemporal	67.40	20.55	59.36	22.77	8.04	−2.22	0.176

*Student's t-test.
GCIPL: ganglion cell-inner plexiform layer.
SD: standard deviation.

Table 3: Comparison between preoperative and postoperative (at 1 month after surgery) macular GCIPL thickness values performed by semimanual segmentation.

$N = 25$	Preoperative (μm)	SD (μm)	Postoperative (μm)	SD (μm)	Difference (μm)	SD (μm)	P value*
Average GCIPL thickness	69.23	19.50	65.00	14.80	4.23	4.70	0.466
Minimum GCIPL thickness	49.69	23.29	47.85	23.78	1.85	−0.50	0.832
GCIPL superior	66.31	21.64	63.15	19.27	3.15	2.37	0.610
GCIPL inferior	63.31	22.35	63.54	16.49	−0.23	5.86	0.973
GCIPL superonasal	71.08	25.08	68.69	23.15	2.38	1.93	0.728
GCIPL superotemporal	75.23	14.21	62.08	18.27	13.15	−4.06	0.083
GCIPL inferonasal	67.15	24.13	71.69	17.07	−4.54	7.06	0.303
GCIPL inferotemporal	72.00	19.20	61.46	17.16	10.54	2.03	0.198

*Student's t-test.
GCIPL: ganglion cell-inner plexiform layer.
SD: standard deviation.

± 0.95 μm at 6 months after surgery. Additionally, MCAT was 283.92 ± 21.86 μm at the preoperative period, 279.8 ± 29.23 μm at 1 month after surgery, and 274.64 ± 26.53 μm at 6 months after surgery. Statistically significant differences in the average MCV and MCAT were found at 6 months after surgery ($P = 0.008$ and $P = 0.016$, resp.). In contrast, no differences were found in the average MCV and MCAT at 1 month after surgery ($P = 0.186$ and $P = 0.318$, resp.).

Preoperative and postoperative average GCIPL thickness values obtained by automated segmentation were 60.72 ± 18.20 μm and 61.52 ± 17.37 μm, respectively, with no statistically significant differences between the two groups (Table 2). Similarly, preoperative and postoperative average GCIPL thickness obtained by semimanual segmentation was 69.23 ± 19.50 and 65.00 ± 14.80 μm, respectively, and no statistically significant differences were found either (Table 3). However, automated segmentation analysis showed statistically significant differences in the GCIPL thickness at the superior-temporal quadrant at 6 months after surgery ($P = 0.026$) (Table 4). No differences were found in the comparison of other GCIPL quadrants analyses. In contrast, when the analysis was performed by semimanual segmentation, statistically significant differences were found in the GCIPL thickness at both the superotemporal and inferotemporal quadrants at 6 months after surgery ($P = 0.011$ and $P = 0.013$, resp.) (Table 5).

Quality measurement analysis performed by automated segmentation showed that GCIPL thickness was higher in the postoperative period in around 50% of the scans (Table 6). Therefore, a significant number of segmentation errors can be expected when the automated analysis is performed in patients with macular holes. Similarly, the quality measurement analysis performed by semimanual segmentation revealed only a slight improvement in the GCIPL segmentation (Table 7).

Nowadays, ILM peeling combined with pars plana vitrectomy is considered an effective procedure for IMH surgery [1]. The removal of ILM is associated with better anatomic results and faster visual acuity recovery after surgery [1, 18, 19]. However, some adverse effects have been documented after ILM peeling, which may be associated with the use of vital dyes during surgery [20–23]. Recently, BBG-assisted ILM peeling has been reported to be safer than other dyes [24–26]. Still, a marked decrease of the average RGCC thickness at 6 months after surgery has been recently documented after ICG or BBG-assisted ILM peeling, with no differences

Table 4: Comparison between preoperative and postoperative (at 6 months after surgery) macular GCIPL thickness values performed by automated segmentation.

$N = 25$	Pre-operative (μm)	SD (μm)	Postoperative (6 m) (μm)	SD (μm)	Difference (μm)	SD (μm)	P value*
Average GCIPL thickness	60.72	18.20	61.20	14.71	−0.48	3.49	0.912
Minimum GCIPL thickness	33.56	18.20	44.20	19.38	−10.64	−1.18	0.053
GCIPL superior	59.76	26.37	58.32	19.46	1.44	6.91	0.808
GCIPL inferior	53.88	23.79	60.16	15.07	−6.28	8.72	0.292
GCIPL superonasal	59.04	24.77	64.28	20.28	−5.24	4.49	0.353
GCIPL superotemporal	69.48	14.87	59.52	14.83	9.96	0.04	**0.026**
GCIPL inferonasal	54.48	20.62	64.08	15.56	−9.6	5.06	0.080
GCIPL inferotemporal	67.40	20.55	60.72	17.31	6.68	3.24	0.070

*Student's t-test.
GCIPL: ganglion cell-inner plexiform layer.
SD: standard deviation.

Table 5: Comparison between preoperative and postoperative (at 6 months after surgery) macular GCIPL thickness values performed by semimanual segmentation.

$N = 25$	Preoperative (μm)	SD (μm)	Postoperative (6 m) (μm)	SD (μm)	Difference (μm)	SD (μm)	P value*
Average GCIPL thickness	69.23	19.50	63.77	10.14	5.46	9.36	0.241
Minimum GCIPL thickness	49.69	23.29	45.08	16.94	4.62	6.35	0.499
GCIPL superior	66.31	21.64	60.69	15.80	5.62	5.84	0.292
GCIPL inferior	63.31	22.35	62.31	14.40	1.00	7.95	0.866
GCIPL superonasal	71.08	25.08	67.85	17.23	3.23	7.85	0.590
GCIPL superotemporal	75.23	14.21	60.08	10.70	15.15	3.51	**0.011**
GCIPL inferonasal	67.15	24.13	72.54	11.13	−5.38	13.01	0.313
GCIPL inferotemporal	72.00	19.20	58.62	10.19	13.38	9.01	**0.013**

*Student's t-test.
GCIPL: ganglion cell-inner plexiform layer.
SD: standard deviation.

between both dyes [17]. In contrast, Sevim and Sanisoglu showed no significant decrease of the average, superior, and inferior RGCC thickness after BBG-assisted ILM peeling [14].

The variables generated by the GCC measuring mode of the original software of the RTVue-100 SD OCT (Optovue, Fremont, CA, USA) employed by Baba et al. and Sevim et al. include the average, superior (0–180 degrees), and inferior (180–360 degrees) thickness of the RGCC, which comprises the retinal nerve fiber layer, the ganglion cell layer, and the inner plexiform layer. In contrast, the ganglion cell analysis (GCA) software of the Cirrus HD-OCT (Carl Zeiss Meditec, Dublin, CA) used in this study allows obtaining the GCIPL thickness, and therefore the retinal nerve fiber layer is not included in the measurement. Furthermore, GCA software generates specific variables for each quadrant of the macular area (superior, inferior, superonasal, inferonasal, superotemporal, and inferotemporal), as well as the average and minimum GCIPL thickness. Therefore, a more specific analysis of the inner retinal thickness area may be performed with this software. Actually, we observed no changes in the average GCIPL thickness at 1 and 6 months after surgery (Tables 3–6). However, when the analysis was performed by semimanual segmentation and individual macular quadrants, a focal GCIPL thickness decrease in the superotemporal and inferotemporal macular area was seen at 6 months after surgery (Table 5). Similarly, when the analysis was performed by automated segmentation, a focal GCIPL thickness decrease was observed in the superotemporal macular area.

Based on our results, we hypothesize that as the RNFL is thinner at the temporal area than at the nasal area [27], the ganglion cells may be more exposed to the retinal surface, and consequently to the BBG dye, which could have some toxic effects over these cells. Some in vitro studies have found a significant decrease in cell viability in both retinal pigment epithelial cells and retinal ganglion cells at exposure times to BBG as early as 3 minutes [28–30]. This reduction in cell viability has been attributed to a cytostatic effect [31]. Additionally, the ILM peeling may cause a mechanical damage over the ganglion cell layer, which is "less" protected by the RNFL at the temporal area. On the other hand, ILM was usually grasped and peeled off from the temporal quadrant, which may contribute to the mechanical damage at this area.

Several groups have reported nasal visual defects after ICG-assisted ILM peeling in IMH surgery [8–10, 32]. Some factors that may be responsible for this defect include ICG

Table 6: Quality measurement analysis between the preoperative and postoperative macular GCIPL thickness values performed by automated segmentation.

$N = 25$	Postoperative (1 m)				Postoperative (6 m)			
	GCIPL (< or =)*		GCIPL (>)†		GCIPL (< or =)*		GCIPL (>)†	
Average GCIPL thickness	12	48%	13	52%	11	44%	14	56%
Minimum GCIPL thickness	9	36%	16	64%	9	36%	16	64%
GCIPL superior	11	44%	14	56%	12	48%	13	52%
GCIPL inferior	10	40%	15	60%	10	40%	15	60%
GCIPL superonasal	14	56%	11	44%	12	48%	13	52%
GCIPL superotemporal	15	60%	10	40%	18	72%	7	28%
GCIPL inferonasal	11	44%	14	56%	12	48%	13	52%
GCIPL inferotemporal	15	60%	10	40%	16	64%	9	36%
Average	**12.13**	**49%**	**12.88**	**52%**	**12.5**	**50%**	**12.5**	**50%**

*GCIPL (< or =): number of cases where the ganglion cell-inner plexiform layer thickness is lower than or equal to before surgery.
†GCIPL (>): number of cases where the ganglion cell-inner plexiform layer thickness is higher than before surgery.

Table 7: Quality measurement analysis between the preoperative and postoperative macular GCIPL thickness values performed by semimanual segmentation.

$N = 25$	Postoperative (1 m)				Postoperative (6 m)			
	GCIPL (< or =)*		GCIPL (>)†		GCIPL (< or =)*		GCIPL (>)†	
Average GCIPL thickness	13	52%	12	48%	14	56%	11	44%
Minimum GCIPL thickness	13	52%	12	48%	13	52%	12	48%
GCIPL superior	13	52%	12	48%	15	60%	10	40%
GCIPL inferior	14	56%	11	44%	16	64%	9	36%
GCIPL superonasal	15	60%	10	40%	14	56%	11	44%
GCIPL superotemporal	15	60%	10	40%	17	68%	8	32%
GCIPL inferonasal	12	48%	13	52%	12	48%	13	52%
GCIPL inferotemporal	13	52%	12	48%	16	64%	9	36%
Average	**13.50**	**54%**	**11.50**	**46%**	**14.63**	**59%**	**10.38**	**42%**

*GCIPL (< or =): number of cases where the ganglion cell-inner plexiform layer thickness is lower than or equal to before surgery.
†GCIPL (>): number of cases where the ganglion cell-inner plexiform layer thickness is higher than before surgery.

concentration, time of tissue contact, and ILM mechanical tractions [7]. However, no visual field defects have been found after BBG-assisted ILM removal [33].

The GCC color map provided by the RTVue software may allow identifying specific areas of focal ganglion cell loss. Actually, Baba et al. showed one case of a predominantly temporal GCC loss in the color-coded GCC thickness map reported [17].

On the other hand, we observed a significant decrease in the MCAT and MCV at 6 months after surgery. Some patients presented a preoperative abnormal increase of both parameters, secondary to microcystic edema usually present at the edge of the macular hole [34–36]. Additionally, MCAT and MCV results may be affected significantly by the positioning of the scanning beam in the pupil and the resultant angle of incidence on the retina [37]. In fact, this measurement error may be even more frequent when IMH is present.

The study had some limitations. First, our series of patients is relatively small, in part because the GCA software of the Cirrus HD-OCT has only recently become commercially available. Therefore, future studies should be performed to validate our results. Second, longer observation periods are needed in order to evaluate the GCIPL progress over time. Third, the automatic segmentation performed by the GCA software may be altered in some patients where the macular morphology is distorted due to the IMH (Figure 3). Actually, these measurement errors may be the reason why almost no differences were found in the average GCIPL thickness in our study. In fact, we observed that GCIPL thickness analysis in some macular quadrants was higher after surgery than before surgery, even if the analysis was performed by automated or semimanual segmentation (Tables 6 and 7, resp.). Therefore, additional studies should be performed in order to determine the ability of the Cirrus HD-OCT (Carl Zeiss Meditec, Dublin, CA) to analyze the GCIPL in patients with different macular diseases. Alternatively, a real manual segmentation could be performed by custom OCT analysis software (i.e., OCTOR).

In conclusion, only focal temporal changes in the GCIPL thickness may be appreciated after vitrectomy with BBG-assisted ILM peeling for IMH. Furthermore, the results provided by Cirrus HD-OCT (Carl Zeiss Meditec, Dublin, CA) ganglion analysis software should be carefully evaluated

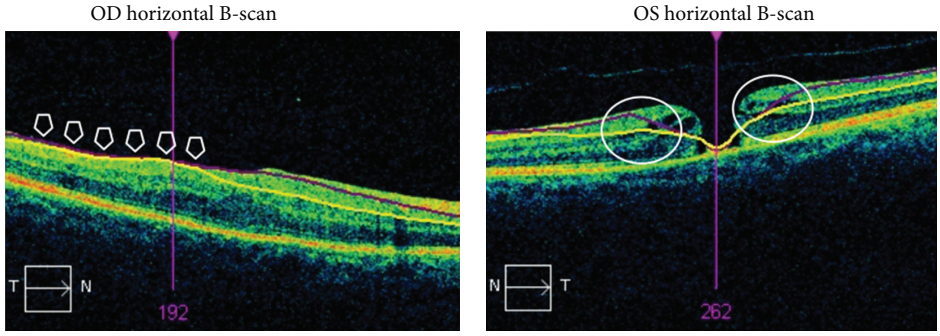

(a) (b)

Figure 3: Examples of scans with incorrect ganglion cell-inner plexiform layer segmentation due to macular morphology distortion. (a) OCT ganglion cell analysis in a patient after idiopathic macular hole surgery. (b) OCT ganglion cell analysis in a patient with an idiopathic macular hole. The arrows show an area where the automated segmentation was incorrectly performed.

in patients with maculopathies where there is a macular morphology distortion. However, semimanual segmentation may slightly help to improve the quality of the GCIPL analysis in these patients.

4. Conclusions

A significant reduction of GCIPL thickness at the temporal macular quadrants was observed by SD-OCT analysis with the new ganglion cell analysis (GCA) software of the Cirrus HD-OCT (Carl Zeiss Meditec, Dublin, CA) at 6 months after vitrectomy with BBG-assisted internal limiting membrane removal for idiopathic macular hole surgery. This reduction detection was higher when the analysis was performed by semimanual segmentation. On the other hand, an increase in the postoperative GCIPL thickness was observed in a significant number of patients, although this increase was less pronounced when the analysis was performed by semimanual segmentation. As we assume that an increase in GCIPL thickness is not expected after surgery, we hypothesize that these values may be artefacts or even a subtle inner retinal edema after ILM peeling, which could be caused by BBG dye. In this study we have evaluated the capacity of the new software of the Cirrus HD-OCT (Carl Zeiss Meditec, Dublin, CA) to analyze changes in the retinal GCIPL after internal limiting membrane peeling for idiopathic macular hole surgery, but further studies should be performed in patients with other frequent macular pathologies. To our knowledge, no study has previously validated this software in macular pathology. Glaucoma specialists must take into consideration this possible bias in GCIPL thickness analysis in patients with vitreomacular surface changes.

Conflict of Interests

The authors report that they have no proprietary or conflict of interests.

Acknowledgments

The authors thank Aurora Alvarez, Miriam Camiña, Diego Ruiz-Casas (M.D.), and Ismael Samhan-Arias for their contribution to the SD-OCT image acquisition and data recollection.

References

[1] H. L. Brooks Jr., "Macular hole surgery with and without internal limiting membrane peeling," *Ophthalmology*, vol. 107, no. 10, pp. 1939–1949, 2000.

[2] C. Haritoglou, C. A. Gass, M. Schaumberger, O. Ehrt, A. Gandorfer, and A. Kampik, "Macular changes after peeling of the internal limiting membrane in macular hole surgery," *American Journal of Ophthalmology*, vol. 132, no. 3, pp. 363–368, 2001.

[3] F. Ando, K. Sasano, N. Ohba, H. Hirose, and O. Yasui, "Anatomic and visual outcomes after indocyanine green-assisted peeling of the retinal internal limiting membrane in idiopathic macular hole surgery," *American Journal of Ophthalmology*, vol. 137, no. 4, pp. 609–614, 2004.

[4] S. E. Burk, A. P. Da Mata, M. E. Snyder, R. H. Rosa Jr., and R. E. Foster, "Indocyanine green-assisted peeling of the retinal internal limiting membrane," *Ophthalmology*, vol. 107, no. 11, pp. 2010–2014, 2000.

[5] H. Enaida, T. Hisatomi, Y. Hata et al., "Brilliant blue G selectively stains the internal limiting membrane/brilliant blue G-assisted membrane peeling," *Retina*, vol. 26, no. 6, pp. 631–636, 2006.

[6] G. K. Shah, B. J. Rosenblatt, K. J. Blinder, M. G. Grand, and M. Smith, "Triamcinolone-assisted internal limiting membrane peeling," *Retina*, vol. 25, no. 8, pp. 972–975, 2005.

[7] A. Gandorfer, C. Haritoglou, C. A. Gass, M. W. Ulbig, and A. Kampik, "Indocyanine green-assisted peeling of the internal limiting membrane may cause retinal damage," *American Journal of Ophthalmology*, vol. 132, no. 3, pp. 431–433, 2001.

[8] C. Haritoglou, A. Gandorfer, C. A. Gass, M. Schaumberger, M. W. Ulbig, and A. Kampik, "Indocyanine green-assisted peeling of the internal limiting membrane in macular hole surgery affects visual outcome: a clinicopathologic correlation,"

American Journal of Ophthalmology, vol. 134, no. 6, pp. 836–841, 2002.

[9] S. Kanda, A. Uemura, T. Yamashita, H. Kita, K. Yamakiri, and T. Sakamoto, "Visual field defects after intravitreous administration of indocyanine green in macular hole surgery," *Archives of Ophthalmology*, vol. 122, no. 10, pp. 1447–1451, 2004.

[10] E. Tsuiki, A. Fujikawa, N. Miyamura, K. Yamada, K. Mishima, and T. Kitaoka, "Visual field defects after macular hole surgery with indocyanine green-assisted internal limiting membrane peeling," *American Journal of Ophthalmology*, vol. 143, no. 4, pp. 704–705, 2007.

[11] M. Remy, S. Thaler, R. G. Schumann et al., "An in vivo evaluation of Brilliant Blue G in animals and humans," *British Journal of Ophthalmology*, vol. 92, no. 8, pp. 1142–1147, 2008.

[12] R. Ejstrup, M. La Cour, S. Heegaard, and J. F. Kiilgaard, "Toxicity profiles of subretinal indocyanine green, Brilliant Blue G, and triamcinolone acetonide: a comparative study," *Graefe's Archive for Clinical and Experimental Ophthalmology*, vol. 250, no. 5, pp. 669–677, 2012.

[13] P. D. Brazitikos, J. M. Katsimpris, E. Tsironi, and S. Androudi, "Retinal nerve fiber layer thickness evaluation after trypan blue-assisted macular surgery," *Retina*, vol. 30, no. 4, pp. 640–647, 2010.

[14] M. S. Sevim and H. Sanisoglu, "Analysis of retinal ganglion cell complex thickness after brilliant blue-assisted vitrectomy for idiopathic macular holes," *Current Eye Research*, vol. 38, no. 1, pp. 180–184, 2013.

[15] T. Baba, S. Yamamoto, R. Kimoto, T. Oshitari, and E. Sato, "Reduction of thickness of ganglion cell complex after internal limiting membrane peeling during vitrectomy for idiopathic macular hole," *Eye*, vol. 26, no. 9, pp. 1173–1180, 2012.

[16] R. Tadayoni, I. Svorenova, A. Erginay, A. Gaudric, and P. Massin, "Decreased retinal sensitivity after internal limiting membrane peeling for macular hole surgery," *British Journal of Ophthalmology*, vol. 96, no. 12, pp. 1513–1516, 2012.

[17] T. Baba, A. Hagiwara, E. Sato, M. Arai, T. Oshitari, and S. Yamamoto, "Comparison of vitrectomy with brilliant blue G or indocyanine green on retinal microstructure and function of eyes with macular hole," *Ophthalmology*, vol. 119, no. 12, pp. 2609–2615, 2012.

[18] C. Eckardt, U. Eckardt, S. Groos, L. Luciano, and E. Reale, "Removal of the internal limiting membrane in macular holes. Clinical and morphological findings," *Ophthalmologe*, vol. 94, no. 8, pp. 545–551, 1997.

[19] T. S. Hassan and G. A. Williams, "Counterpoint: to peel or not to peel: is that the question?" *Ophthalmology*, vol. 109, no. 1, pp. 11–12, 2002.

[20] H. Enaida, T. Sakamoto, T. Hisatomi, Y. Goto, and T. Ishibashi, "Morphological and functional damage of the retina caused by intravitreous indocyanine green in rat eyes," *Graefe's Archive for Clinical and Experimental Ophthalmology*, vol. 240, no. 3, pp. 209–213, 2002.

[21] M. Veckeneer, K. Van Overdam, J. Monzer et al., "Ocular toxicity study of trypan blue injected into the vitreous cavity of rabbit eyes," *Graefe's Archive for Clinical and Experimental Ophthalmology*, vol. 239, no. 9, pp. 698–704, 2001.

[22] R. Narayanan, J. K. Mungcal, M. C. Kenney, G. M. Seigel, and B. D. Kuppermann, "Toxicity of triamcinolone acetonide on retinal neurosensory and pigment epithelial cells," *Investigative Ophthalmology and Visual Science*, vol. 47, no. 2, pp. 722–728, 2006.

[23] S. Ueno, M. Kondo, C. Piao, K. Ikenoya, Y. Miyake, and H. Terasaki, "Selective amplitude reduction of the PhNR after macular hole surgery: ganglion cell damage related to ICG-assisted ILM peeling and gas tamponade," *Investigative Ophthalmology & Visual Science*, vol. 47, no. 8, pp. 3545–3549, 2006.

[24] A. Ueno, T. Hisatomi, H. Enaida et al., "Biocompatibility of brilliant blue G in a rat model of subretinal injection," *Retina*, vol. 27, no. 4, pp. 499–504, 2007.

[25] D. Shukla, J. Kalliath, N. Neelakantan, K. B. Naresh, and K. Ramasamy, "A comparison of brilliant blue g, trypan blue, and indocyanine green dyes to assist internal limiting membrane peeling during macular hole surgery," *Retina*, vol. 31, no. 10, pp. 2021–2025, 2011.

[26] K. Fukuda, F. Shiraga, H. Yamaji et al., "Morphologic and functional advantages of macular hole surgery with Brilliant blue G-assisted internal limiting membrane peeling," *Retina*, vol. 31, no. 8, pp. 1720–1725, 2011.

[27] R. Varma, M. Skaf, and E. Barron, "Retinal nerve fiber layer thickness in normal human eyes," *Ophthalmology*, vol. 103, no. 12, pp. 2114–2119, 1996.

[28] S. Balaiya, V. S. Brar, R. K. Murthy, and K. V. Chalam, "Comparative in vitro safety analysis of dyes for chromovitrectomy: indocyanine green, brilliant blue green, bromophenol blue, and infracyanine green," *Retina*, vol. 31, no. 6, pp. 1128–1136, 2011.

[29] M. Morales, V. Freire, A. Asumendi et al., "Comparative effects of six intraocular vital dyes on retinal pigment epithelial cell," *Investigative Ophthalmology & Visual Science*, vol. 51, no. 11, pp. 6018–6029, 2010.

[30] D. Yuen, J. Gonder, A. Proulx, H. Liu, and C. Hutnik, "Comparison of the in vitro safety of intraocular dyes using two retinal cell lines: a focus on brilliant blue G and indocyanine green," *American Journal of Ophthalmology*, vol. 147, no. 2, pp. 251.e2–259.e2, 2009.

[31] S. Kawahara, Y. Hata, M. Miura et al., "Intracellular events in retinal glial cells exposed to ICG and BBG," *Investigative Ophthalmology and Visual Science*, vol. 48, no. 10, pp. 4426–4432, 2007.

[32] C. A. Gass, C. Haritoglou, M. Schaumberger, and A. Kampik, "Functional outcome of macular hole surgery with and without indocyanine green-assisted peeling of the internal limiting membrane," *Graefe's Archive for Clinical and Experimental Ophthalmology*, vol. 241, no. 9, pp. 716–720, 2003.

[33] P. B. Henrich, C. Haritoglou, P. Meyer et al., "Anatomical and functional outcome in brilliant blue G assisted chromovitrectomy," *Acta Ophthalmologica*, vol. 88, no. 5, pp. 588–593, 2010.

[34] T. M. Aaberg, C. J. Blair, and J. D. M. Gass, "Macular holes," *American Journal of Ophthalmology*, vol. 69, no. 4, pp. 555–562, 1970.

[35] D. R. Guyer, W. R. Green, S. de Bustros, and S. L. Fine, "Histopathologic features of idiopathic macular holes and cysts," *Ophthalmology*, vol. 97, no. 8, pp. 1045–1051, 1990.

[36] M. R. Hee, C. A. Puliafito, C. Wong et al., "Optical coherence tomography of macular holes," *Ophthalmology*, vol. 102, no. 5, pp. 748–756, 1995.

[37] A. Hariri, S. Y. Lee, H. Ruiz-Garcia, M. G. Nittala, F. M. Heussen, and S. R. Sadda, "Effect of angle of incidence on macular thickness and volume measurements obtained by spectral-domain optical coherence tomography," *Investigative Ophthalmology and Visual Science*, vol. 53, no. 9, pp. 5287–5291, 2012.

Hindawi Publishing Corporation
BioMed Research International
Volume 2014, Article ID 769296, 8 pages
http://dx.doi.org/10.1155/2014/769296

Research Article

Comparison of Reaction Response Time between Hand and Foot Controlled Devices in Simulated Microsurgical Testing

Marcel Pfister,[1,2] Jaw-Chyng L. Lue,[1] Francisco R. Stefanini,[1,2,3] Paulo Falabella,[1,2,3] Laurie Dustin,[4] Michael J. Koss,[1,2,5] and Mark S. Humayun[2]

[1] *Doheny Eye Institute, 1450 San Pablo Street, Los Angeles, CA 90033, USA*
[2] *Department of Ophthalmology, Keck School of Medicine, University of Southern California, 1450 San Pablo Street, Los Angeles, CA 90033, USA*
[3] *Department of Ophthalmology and Visual Sciences, Federal University of Sao Paulo (UNIFESP), Rua Botucatu, No. 740, 04023-900 Sao Paulo, SP, Brazil*
[4] *Department of Preventive Medicine, University of Southern California, 1975 Zonal Avenue, Los Angeles, CA 90089, USA*
[5] *Department of Ophthalmology, Ruprecht-Karls-University, Grabengasse 1, 69117 Heidelberg, Germany*

Correspondence should be addressed to Marcel Pfister; 2marcel.pfister@gmx.net

Received 29 March 2014; Revised 1 June 2014; Accepted 7 June 2014; Published 6 July 2014

Academic Editor: Jerzy Nawrocki

Purpose. We hypothesized that reaction times (RTs) for a switch release are faster for hand-controlled than for foot-controlled switches for physiological and anatomical reasons (e.g., nerve conduction speed). The risk of accidental trauma could be reduced if the surgeon reacted quicker and therefore improve the surgical outcome. *Method*. We included 47 medical professionals at USC. Demographics and handedness were recorded. Under a microscope, a simple reaction time test was performed, testing all extremities multiple times in a random order. Additionally, a subjective questionnaire was administered. *Results*. The mean RTs for hands are 318.24 ms ± 51.13 and feet 328.69 ± 48.70. The comparison of hand versus foot showed significant shorter RTs for the hand ($P = 0.025$). Partially significant differences between and within the experience level groups could be demonstrated by level of education (LE) and microscopic surgeries/week (MSW) ($P = 0.57$–0.02). In the subjective questionnaire, 91.5% ($n = 43/47$) of test subjects prefer to use hand controls. *Conclusion*. Our data show that the RT for hands is faster than feet. Similarly the subjective questionnaire showed a greater preference for hand actuation. This data suggest a hand-controlled ophthalmic instrument might have distinct advantages; however, clinical correlation is required.

1. Introduction

Very delicate eye surgeries are usually performed by a surgeon, working through a microscope, who is often required to make quick intraoperative decisions. The surgical management of vitreous and retinal pathologies (e.g., retinal detachment or vitreous bleeding) can include removal of the vitreous, intervention on the retina, or intraocular illumination and magnification. Vitreoretinal surgeries are dynamic and precise maneuvers that require a fast reaction time (RT). The RT represents the time between the initiation of a given event (e.g., intraocular bleeding) and the surgeon's response to that event (e.g., elevation of intraocular pressure) [1]. A short RT might be associated with better outcomes and with the prevention of iatrogenic trauma.

All currently commercially available vitrectomy systems are controlled using a foot-pedal (e.g., Stellaris PC—Bausch & Lomb; Constellation Vision System—Alcon; Eva—DORC; NovitreX—Oertli). When the pedal is depressed, the console machine responds by increasing the vacuum and cut rate at the tip of the vitreous cutter. If the retina is inadvertently sucked into the cutter, the surgeon must react quickly to release the pedal, thereby stopping or reducing the suction force. By doing so, the surgeon can prevent serious complications and damage to the retina, such as retinal detachment, retinal holes, or vitreous hemorrhage. Any of these events can

cause severe long-term retinal tissue damage with a possible need for further surgery or may even result in permanent vision loss. The length of the release time (pedal) plays a key role in the outcome.

Several articles have been published on simple RT tests [2], but only a few studies have measured eye-hand or eye-foot response times [2, 3]. The hypothesis of the present study was that for physiological, anatomical (e.g., nerve-conduction velocity), and ergonomic reasons, the time required to release a switch with the hand is shorter than the time required to release a switch with the foot. If this hypothesis is correct, then the risk of trauma to the eye could, in theory, be reduced if the cut and vacuum rates were controlled by hand and if so, then the results of the surgery might be improved.

Our study was designed to evaluate the RTs of surgeons or future surgeons, testing both the dominant and nondominant hands and feet. To the best of our knowledge, this is the first RT study in which medical professionals were tested while using a microscope. Data analysis included the subjects' age, gender, medical training, frequency of surgery performed (with and without microscope), and participation in extracurricular activities involving a hand switch. In addition, we measured the intrinsic RT for a mechanical switch release. The collected data could reinforce the need for a hand-controlled vitrectomy system.

2. Materials and Methods

A total of 47 volunteers, all medical students and ophthalmic surgeons from the Department of Ophthalmology at the Keck School of Medicine of the University of Southern California, participated in this study. Written informed consent to participate in this study was obtained from all subjects. The protocol was approved by the University of Southern California Health Science Institutional Review Boards (IRB) at IRB Submission Tracking and Review system (iStar) number HS-13-00467. All participants were at least 18 years of age on the day of their participation. Exclusion criteria included active injury affecting any extremity or self-report of an unresolved concussion.

The subjects' age, sex, dominant hand, years of medical training (student-consultant), experience with a surgical microscope, and participation in extracurricular activities involving use of a hand switch (e.g., computer gaming/playing a musical instrument) were recorded. The dominant hand was assessed by the questionnaire. To determine the participants dominant foot, we performed the so-called "Kick-Test" for each participant in order to determine the dominant foot. This information was gathered using an anonymous multiple choice questionnaire completed by the participant directly before the RT testing. Each test subject was assigned to a number for data anonymization.

After the test, participants were asked two subjective questions about the use of hand and foot switches: (1) which extremity did you feel reacted the fastest? and (2) which extremity did you feel the most comfortable using?

3. Test Equipment and Setup

Each test subject was placed in the following setup to mimic a real eye surgical environment. The participant was seated at a table with a preinstalled surgical microscope (Nikon SMZ-645 StereoZoom microscope with adjustable holder from Diagnostic Instrument). To prevent unwanted distraction, the test room was kept quiet, the lights were dimmed, and only the examiners were present [4, 5]. The subject was asked to look into the surgical microscope, under which both a red and a green light emitting diode (LEDs) were placed. The red LED would turn on to indicate that the experiment had started and that the subject should press and hold the switch and wait for the green LED to appear. The green LED would light randomly, between 2 and 15 seconds after the beginning of the test, to prevent predictability. Each of the four extremities of each subject was tested five times. The mean value of these five tests was used as the reaction time of a participant extremity. The order in which the extremities were tested was randomized. Based on previous publications, the cut off for RTs recorded was set to 180 ms (minimum) and 500 ms (maximum) [2, 6].

The interval between the start of the experiment (red LED) and the green LED lit time was pseudorandomly programmed in a CPU board (6 external interrupts control, 40 MHz CPU on R-Engine-A board time counters of 0.6 μs time resolution from Tern Inc.) with a custom C++ program. The RT was defined as the time between the lighting of the green LED and the moment the electrical break of the switch circuit happened. The green LED signal and the electrical break signal were automatically acquired by the programmable board, and the difference was calculated and stored. In the program, a RT longer than 0.5 second was considered abnormal and, therefore, was excluded automatically. Release of the snap switch before the green LED signal was also considered a failed trial.

To accurately evaluate the RT from human test subjects and minimize the machine's RT, we considered the moment of the electrical break of a pressed subminiature snap switch (D2F-FL with lever, Omron Electronics Inc.) as the onset of the human response. The RT of this subminiature snap switch is less than 1 ms. The RT was examined using a high-speed video camera (640 × 512 resolution at 1000 fps, MotionScope M1, RedLake). For hand tests, we used a dummy hand piece mounted with the D2F subminiature snap switch (Figure 1). For foot tests, we used a conventional foot pedal (BL2390, Stellaris PC foot pedal, Bausch & Lomb) with the same D2F subminiature snap switch mounted underneath the foot pedal. The testing with the high-speed camera was performed 10 times for the hand switch and foot switch with the original test equipment and analyzed by J.-C. L.

4. Statistical Methods

The statistical significance for within subject differences in RTs was assessed using paired t-tests. Analysis of variance tests were used to compare RTs between subcategories, adjusting for age and gender. The covariate adjusted means and standard errors are reported in the tables. Trend tests

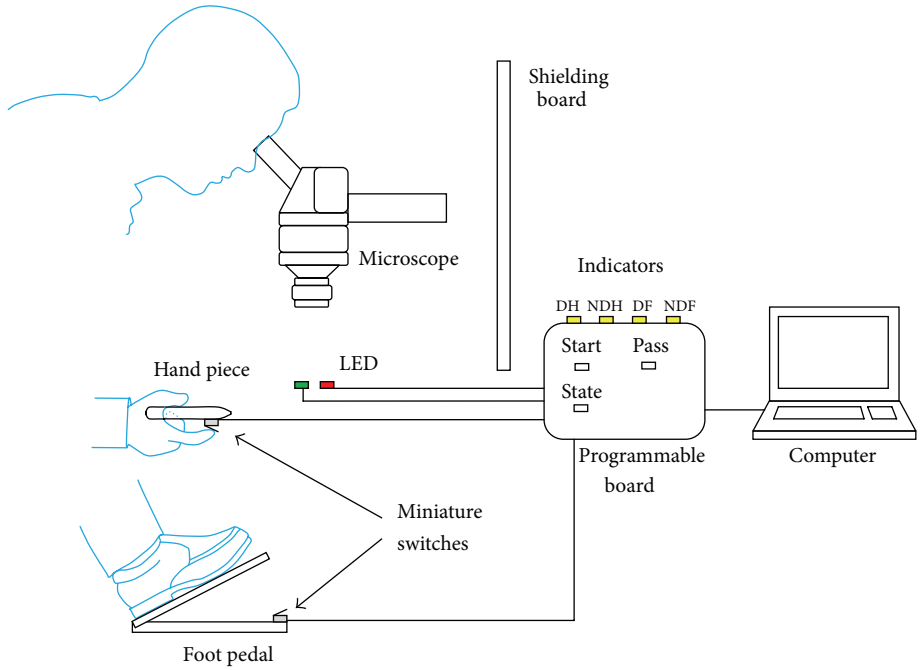

Figure 1: Schematics of systematic setup for the response time experiment.

were also run across ordinal categories. For comparison of RTs by gender, the analysis of covariance was adjusted for age, and the analysis by age group was adjusted for gender. SAS V9.3 programming language (SAS Inst., Cary, NC) was used for all analysis, and the accepted level of significance for all tests was $P < 0.05$.

5. Results

As we tested and compared dominant versus nondominant hands and feet, we could demonstrate significantly faster RTs with the dominant extremity ($P > 0.011$; Tables 1 and 2).

The results of this simple RT test demonstrate significantly faster reaction times of the hands compared to the feet ($P < 0.01$; Table 3).

Male subjects were significantly faster with both hands and feet than were female subjects (Table 4).

The results of the subjective questions were in favor of the handheld instruments.

We could demonstrate a trend toward slower RTs for the hands with increasing age of the subjects. Statistically significant differences of the RTs for the feet could be demonstrated when comparing the different age groups (DF $P = 0.004$; NDF $P = 0.01$), but no statistical trend could be shown (DF $P = 0.68$; NDF $P = 0.51$) (Table 7).

Except for DH and NDH difference across education levels (test for trend $P = 0.03$), no statistical significance and no trend could be demonstrated by analyzing the subjects' different experience levels or number of surgeries performed per week (Tables 8 and 9).

As a variable of daily routines we chose the frequency of computer gaming and home-row typing, based upon statements in the questionnaires. For computer gaming frequency, significance was found for DH-NDH (test for trend $P = 0.01$) and NDF ($P = 0.02$). All other tests were not significant (Tables 10 and 11).

The results of the machine RT testing (hand switch versus foot switch) showed for the mini-joystick an average bouncing time of 8.75 ms ± 1 ms. For the foot pedal, the bouncing time was 64.1 ms, with standard deviation of 24.4 ms.

6. Discussion

We hypothesized that RTs with the hand are shorter than RTs with the foot, which could be demonstrated as a proof of principle with this cohort of medical students, physicians in training, and fully trained specialists. It is, however, important to note that a good surgical result depends on many more factors than RT. The RT of a surgeon is objectively measurable, whereas the essential surgical setting of experience balanced with a well-trained operating room team is at least as important. Since possible variations in the design of new surgical devices may facilitate faster RTs, we wanted to understand how these changes might be reflected among different age groups, genders, and training levels.

Many changes in navigation tools and surgical devices have been introduced over the last few decades. In the early 1990s, the semiautomatic transmission vehicle was introduced in the Formula 1 car racing game. In a sport where high performance is crucial in every aspect, the hand-controlled pedal shift had completely displaced the conventional gearbox with the foot-controlled clutch within just 5 years. Changes can also be seen in aviation. With advancing technology, the fly-by-wire system, a computer-assisted navigation unit, became more and more common in commercial and military airplanes. The centerpiece control

Table 1: Dominant versus nondominant hand (n = 47 subjects); $P < 0.05$ = statistically significant.

	Mean ± SD (ms)	Paired t-test/P value
Dominant Hand (DH)	311.1 ± 51.9	
Nondominant Hand (NDH)	325.4 ± 56.8	
Difference (dominant/nondominant)	−14.3 ± 37.3	**T = −2.63, df = 46 P = 0.011**
Effect size	0.383	

Table 2: Dominant versus nondominant foot (n = 47 subjects); $P < 0.05$ = statistically significant.

	Mean ± SD (ms)	Paired t-test/P value
Dominant foot (DF)	321.5 ± 51.0	
Nondominant foot (NDF)	335.9 ± 53.0	
Difference (dominant/nondominant)	−14.4 ± 36.5	**T = −2.32, df = 46 P = 0.01**
Effect size	0.395	

unit for the pilot is a multifunctional hand-controlled sidestick.

Interestingly, in ocular surgery, a highly delicate and individual medical specialization, some basic handling steps have not changed in decades. The use of foot-pedal controls can be tracked to the time when the suction and ultrasound force for phacoemulsification [7] were introduced in 1967. Foot-pedal control of the cut rate and suction force for pars plana vitrectomy [8] was introduced in 1972. With rapid technological advances, new inventions in robotics and microdevices have become available, providing an opportunity to fundamentally rethink and update surgical systems that were developed in the 1960s and 1970s. This has already happened in fields such as neurosurgery, with the use of live MRI imaging or robot-assisted surgical tools.

To determine if the benefit is dependent on age, sex, experience, or level of education, we created a questionnaire for our participants to analyze if there exists significant differences among subgroups. We could demonstrate that the average RT for hands was significantly faster than the average RT for feet ($P = 0.025$). This reflects our expectation of a shorter nerve-conduction time for the brain-hand combination than for the brain-foot combination because the neural pathway from the brain to the hand is shorter. The dominant hand and the dominant foot, as determined by a kick-test, were significantly faster than the nondominant side (hands $P = 0.01$; feet $P = 0.01$). Also, more than 91% of all participants felt more comfortable with and preferred the hand switch, as they stated in the questionnaire (see Tables 5 and 6).

Consistent with previous simple RT studies, the RTs of male participants were significantly faster than those of female participants with all four extremities. ($P = 0.001$–0.005) [9–11]. Again, it is necessary to mention that a faster RT does not imply a better surgeon or a better surgical outcome. When analyzing the subgroups with regard to their experience level, we found no statistically significant faster RTs in more advanced or better educated participants (Table 8). However, the results showed a close to significant trend toward shorter RTs for the dominant hand. This shows again the complexity of factors that lead to a good surgery, as it might be reasonable to assume that the surgical skills of the more experienced surgeon and the surgical outcomes achieved by this surgeon would be better. With regard to the subjective questions, it is also interesting to note that experienced surgeons (fellows and practitioners), even when they were well trained with the foot switch, stated that they felt faster and more comfortable with the hand switch (87.5% preferred the hand switch) (see Tables 5 and 6). We assume that this is an indicator that the hand is the human's favorite tool and the training effect for other extremities is limited due to physiological conditions (e.g., nerve-conduction velocity).

When we sorted the participants by age, those between 20 and 35 years old had significantly faster RTs with the dominant hand and foot than those who were 44 years of age or older. This finding is also reflected in previous studies that found a lengthening of RTs beginning in the late 20 s [11, 12]. RTs for the feet were especially faster in the younger cohort of this study (Table 7). Based on this finding, we conclude that hand-controlled devices could have a positive effect for older surgeons, even though they are more experienced. Also RTs become more variable in older test subjects [13].

We found no significant difference in RTs to be associated with the frequency with which the participants performed surgery using a surgical microscope (Table 9). This perhaps can be linked to basic shortcomings of the questionnaire used in studies. Although we tried to formulate clear multiple choice questions, the participants' answers remain subjective. Thus, a complete verification of the given answers is impossible.

To get an impression of the individual backgrounds of the participants in our study, we tried to acquire information about the subjects' everyday activities, such as home-row typing, computer gaming, or playing a musical instrument. None of these items showed positive correlations to the RTs.

To further investigate the methodological bias we measured, in addition to the RTs of medical professionals' extremities, the RTs for a miniature hand joystick switch (10 kOhm pot joystick potentiometer, rotation angle: 50°, 254 series, CTS Electronic Components) and a conventional foot switch (BL2390, Stellaris PC foot pedal, Bausch & Lomb). In the conventional foot switch, the effective aspiration range is

Table 3: RTs of hands (average) versus feet (average) ($n = 47$ subjects); $P < 0.05$ = statistically significant.

	Mean ± SD (ms)	Paired t-test/P value
Hands (average of dominant and nondominant hand)	318.2 ± 51.1	
Feet (average of dominant and nondominant foot)	328.7 ± 48.7	
Hands versus feet Difference (hands-feet)	−10.4 ± 30.9	**T = −2.32, df = 46 P = 0.025**
Effect size	0.337	

Table 4: RT analysis of variance of gender (mean ± SE); $P < 0.05$ = statistically significant.

	n	DH (ms)	NDH (ms)	Difference (ms)	DF (ms)	NDF (ms)	Difference (ms)
Female	21	338 ± 10	354 ± 11	−16 ± 8	345 ± 10	360 ± 11	−15 ± 8
Male	26	289 ± 9	302 ± 10	−13 ± 7	302 ± 9	316 ± 10	−14 ± 7
Difference		49	52	3	43	44	1
Effect size		1.068	1.026	0.083	0.938	0.867	0.028
F-test, 1 df		13.31	11.24	0.05	9.10	8.79	0.01
ANOVA P		**<0.001**	**0.002**	0.83	**0.004**	**0.005**	0.93

Table 5: Subjective question 1: percentage of preferred extremity.

Which extremity did you feel reacted the best?			
	Hand	Foot	No difference
All participants $n = 47$	43/47 (91,48%)	2/47 (4,25%)	2/47 (4,25%)
Experience surgeons (fellows/practitioners) $n = 24$	21/24 (87,5%)	1/24 (4,16%)	2/24 (8,33%)

Table 6: Subjective question 2: percentage of preferred extremity.

Which extremity did feel most comfortable using?			
	Hand	Foot	No difference
All participants $n = 47$	43/47 (91,48%)	1/47 (2,12%)	3/47 (6,38%)
Experience surgeons (fellows/practitioners) $n = 24$	21/24 (87,5%)	0/24 (0%)	3/24 (12,5%)

controlled by the pedal's travel distance from the triggering position to the furthest down position. The state-of-the-art machine does provide programming options for users to modify the vacuum levels of the beginning and ending positions across the entire effective travel range. The lowest vacuum that can be programmed at the beginning is zero. In this case, the aspiration at the cutter tip can increase as the user pedal is pressed down further past the triggering position.

A timely response to some medical trauma situations, such as a sudden bleeding in the eye or a clog in a vitreous cutter, requires a prompt cessation of the aspiration power. In the ideal case, assuming the user takes no time to retract the foot, the pedal will still take some time to bounce back to the initial position with zero aspiration. With this time element in mind, we measured the bouncing time of a miniature joystick and a foot pedal. The bouncing time is defined as the traveling time from its far most position to its resting position after the switch is suddenly released. For the mini-joystick, the bouncing time is 3 ms ± 1 ms. If there is a knob with mass of 0.677 g ± 0.001 g for ergonomic purposes, the bouncing time is 8.75 ms ± 1 ms. For the foot pedal, the bouncing time is around 64.1 ms, with standard deviation of 24.4 ms. As a consequence, even in an ideal case in which the user can retract his/her extremity instantly, the machine will still take a certain time to return to zero aspiration. This result strongly suggests that a hand joystick switch is preferred to reduce the RT that can cause unwanted medical trauma.

In our setup, the participants saw a red LED as a sign that the experiment had started. We are aware that this red LED could be interpreted as a warning sign that an event is likely to occur in the near future. It is reported that subjects react faster when they are given a warning indication [14]. However, we do not believe the LED lights provided any additional bias to our results. A number of unintended events/outcomes can occur during ophthalmic surgery (e.g., retinal bleeding, retinal breaks, inadvertent suction of the retina, retinal incarceration, etc.) which require immediate reaction by the surgeon. Therefore, while performing surgical procedures, ophthalmic surgeons are already highly concentrated, focused, and aware of unexpected events that could occur. We also focused on the central visual field with a small LED on which the subjects had to concentrate and to which they had to react. It is known that signals in peripheral visual fields are correlated to slower RTs [14].

Further, the complete release of the switch and the full stop of the cutter that are relevant in vitreoretinal surgery procedures. The variation and dynamic control of the cut rate and vacuum also play a critical role in ophthalmic surgery. Since the hands are a human's most precise tool and since hands have higher tactile acuity than feet, it is likely that the control of the cutter by a hand switch is safer and, therefore, more favorable.

A possible shortcoming of this study was that we tried to simulate a real surgical setting as well as possible, but the test was still performed in an artificial environment. This might

Table 7: RT analysis of variance of age (mean ± SE).

	n	DH (ms)	NDH (ms)	Difference (ms)	DF (ms)	NDF (ms)	Difference (ms)
Age, gender adjusted							
≥20	3	327 ± 26	367 ± 28	−40 ± 22	388 ± 24	408 ± 25	−20 ± 21
21–27	6	285 ± 18	308 ± 20	−23 ± 16	286 ± 17	306 ± 18	−19 ± 15
28–35	22	305 ± 10	322 ± 11	−17 ± 8	324 ± 9	327 ± 9	−3 ± 8
36–43	13	325 ± 12	329 ± 14	−4 ± 11	313 ± 11	347 ± 12	−33±10
44–51	2	341 ± 26	320 ± 35	21 ± 27	353 ± 29	352 ± 31	1 ± 26
>51	1	427	457	−31	424	426	−2
F-test, 5 df		2.34	2.84	0.86	4.13	3.48	1.30
ANOVA P		**0.06**	0.10	0.52	**0.004**	**0.01**	0.28
Test for trend		**0.03**	0.42	0.11	0.68	0.51	0.73

Table 8: RT analysis of variance of education (mean ± SE); $P < 0.05$ = statistically significant.

$P < 0.05$ = statistically significant	n	DH (ms)	NDH (ms)	Difference (ms)	DF (ms)	NDF (ms)	Difference (ms)
Education							
Student	8	328 ± 19	314 ± 22	14 ± 15	335 ± 20	350 ± 22	−16 ± 16
Resident	14	316 ± 12	326 ± 14	−10 ± 10	319 ± 12	333 ± 14	−14 ± 10
Fellow	11	309 ± 14	323 ± 16	−14 ± 11	330 ± 14	331 ± 16	−1 ± 12
Practitioner	13	287 ± 14	322 ± 15	−35 ± 11	299 ± 14	326 ± 15	−26 ± 12
F-test, 3 df		1.07	0.08	1.89	1.11	0.24	0.94
ANOVA P		0.37	0.97	0.15	0.36	0.87	0.43
Test for trend		0.09	0.94	0.03	0.20	0.48	0.53

Table 9: RT analysis of variance of frequency of surgical microscope use (mean ± SE); $P < 0.05$ = statistically significant.

	n	DH (ms)	NDH (ms)	Difference (ms)	DF (ms)	NDF (ms)	Difference (ms)
Use of surgical microscope							
No	9	318 ± 18	328 ± 20	−10 ± 12	346 ± 18	351 ± 19	−4 ± 14
Assisting	7	312 ± 19	313 ± 21	−1 ± 14	322 ± 19	338 ± 20	−16 ± 15
Every month	8	305 ± 17	352 ± 19	−47±12	319 ± 17	334 ± 18	−14 ± 14
Every week	19	315 ± 12	322 ± 13	−7 ± 9	313 ± 12	335 ± 13	−21 ± 10
Every day	4	288 ± 24	305 ± 26	−18 ± 18	308 ± 24	309 ± 26	−1 ± 19
F-test, 4 df		0.36	0.80	2.23	0.58	0.42	0.35
ANOVA P		0.84	0.53	0.08	0.68	0.79	0.85
Test for trend		0.52	0.63	0.92	0.17	0.28	0.76

Table 10: RT analysis of variance of computer gaming (mean ± SE); $P < 0.05$ = statistically significant.

$P < 0.05$ = statistically significant	n	DH (ms)	NDH (ms)	Difference (ms)	DF (ms)	NDF (ms)	Difference (ms)
Computer games							
No	28	313 ± 9	318 ± 10	−5 ± 7	323 ± 9	335 ± 9	−11 ± 7
1x/yr	5	294 ± 21	305 ± 23	−11 ± 16	299 ± 21	311 ± 21	−12 ± 17
1x/month	10	312 ± 15	339 ± 16	−27 ± 11	317 ± 15	331 ± 14	−14 ± 12
1x/week	3	300 ± 27	346 ± 29	−46 ± 21	322 ± 27	350 ± 26	−27 ± 22
Daily	1	379	449	−70	420	495	−75
F-test, 4 df		0.74	1.93	1.72	1.32	3.20	0.64
ANOVA P		0.57	0.13	0.16	0.29	0.02	0.63
Test for trend		0.87	0.06	0.01	0.70	0.26	0.32

Table 11: RT analysis of variance of home row typing (mean ± SE); $P < 0.05$ = statistically significant.

	n	DH (ms)	NDH (ms)	Difference (ms)	DF (ms)	NDF (ms)	Difference (ms)
Typing-home Row							
No	14	297 ± 13	308 ± 15	−11 ± 11	309 ± 14	335 ± 15	−27 ± 11
1x/week	2	299 ± 32	326 ± 37	−27 ± 27	327 ± 34	322 ± 36	5 ± 26
Daily	31	318 ± 9	333 ± 10	−15 ± 7	327 ± 9	337 ± 10	−10 ± 7
F-test, 2 df		0.91	0.86	0.15	0.55	0.08	1.01
ANOVA P		0.41	0.43	0.86	0.58	0.92	0.37
Test for trend		0.20	0.19	0.79	0.30	0.94	0.22

have affected the results of the participants as it is likely that the level of awareness is higher in the operating room when performing actual surgery on a human patient. Furthermore, we used an original foot pedal for vitreoretinal surgery (Bausch & Lomb) and a one pressure-point, no dynamic prototype switch as a hand piece. Based on our findings, we suggest further studies with an advanced hand piece and with more specific questions in the census questionnaire. The use of more subgroups and a larger sample size should also be considered.

In spite of these shortcomings, we believe that we demonstrated objective findings in this study: primarily the superior RT of the hand versus the foot. This finding could be an incentive for a transition in device design by medical companies and could also be the basis for a new approach in education for the next generation of surgeons.

7. Conclusion

This research contributes to our understanding of the average RT of medical professionals (i.e., ophthalmologists at different levels of training) when they are faced with a specific event happening through a surgical microscope. We chose the RT as an easy-to-test objective parameter that might influence the surgical outcome. We could demonstrate that the RT with hands was significantly faster than with the foot. Experience and level of education had no significant influence on the reaction time. Also, advantages of the hand switch can be seen for the handheld mini-joystick as the bouncing time was only 8.75 ms ± 1 ms compared to 64.1 ms ± 24.4 ms for the foot pedal. We feel that our findings can contribute to future approaches in the design of surgical instruments not only in ophthalmology but also in other fields. To improve RTs in the surgical field, hand-controlled devices appear to be desirable. Further studies are needed.

Conflict of Interests

The authors declare that there is no conflict of interests regarding the publication of this paper.

Acknowledgments

The research group is supported by the Dr. Werner Jackstädt-Stiftung, Wuppertal, Germany. The authors also appreciate the programming effort from students Diana Zhou and Jason Chen at the Science High School Advanced Research Program at Doheny Eye Institute and University of Southern California.

References

[1] R. A. Magill, *Motor Learning: Concepts and Applications*, Boston, Mass, USA, McGraw-Hill, 5th edition, 1998.

[2] J. T. Eckner, J. S. Kutcher, and J. K. Richardson, "Pilot evaluation of a novel clinical test of reaction time in National Collegiate Athletic Association Division I football players," *Journal of Athletic Training*, vol. 45, no. 4, pp. 327–332, 2010.

[3] R. Montés-Micó, I. Bueno, J. Candel, and A. M. Pons, "Eye-hand and eye-foot visual reaction times of young soccer players," *Optometry*, vol. 71, no. 12, pp. 775–780, 2000.

[4] D. E. Broadbent, *Decision and Stress*, Academic Press, London, UK, 1971.

[5] M. Trimmel and G. Poelzl, "Impact of background noise on reaction time and brain DC potential changes of VDT-based spatial attention," *Ergonomics*, vol. 49, no. 2, pp. 202–208, 2006.

[6] C. A. Kushida, J. Dorrian, N. L. Rogers, and D. F. Dinges, "Sleep deprivation: clinical issues, pharmacology and sleep loss effects," in *Psychomotor Vigilance Performance: Neurocognitive Assay Sensitive to Sleep Loss*, pp. 39–70, Marcel Dekker, New York, NY, USA, 2005.

[7] C. D. Kelman, "Phaco-emulsification and aspiration. A new technique of cataract removal A preliminary report," *American Journal of Ophthalmology*, vol. 64, no. 1, pp. 23–35, 1967.

[8] R. Machemer, H. Buettner, E. W. Norton, and J. M. Parel, "Vitrectomy: a pars plana approach," *Transactions—American Academy of Ophthalmology and Otolaryngology*, vol. 75, no. 4, pp. 813–820, 1971.

[9] C. E. Noble, B. L. Baker, and T. A. Jones, "Age and sex parameters in psychomotor learning," *Perceptual and Motor Skills*, vol. 19, no. 3, pp. 935–945, 1964.

[10] J. J. Adam, F. G. W. C. Paas, M. J. Buekers, I. J. Wuyts, W. A. C. Spijkers, and P. Wallmeyer, "Gender differences in choice reaction time: Evidence for differential strategies," *Ergonomics*, vol. 42, no. 2, pp. 327–335, 1999.

[11] G. Der and I. J. Deary, "Age and sex differences in reaction time in adulthood: Results from the United Kingdom health and lifestyle survey," *Psychology and Aging*, vol. 21, no. 1, pp. 62–73, 2006.

[12] C. W. Luchies, J. Schiffman, L. G. Richards, M. R. Thompson, D. Bazuin, and A. J. DeYoung, "Effects of age, step direction, and reaction condition on the ability to step quickly," *Journals of Gerontology A: Biological Sciences and Medical Sciences*, vol. 57, no. 4, pp. M246–M249, 2002.

[13] D. F. Hultsch, S. W. S. MacDonald, and R. A. Dixon, "Variability in reaction time performance of younger and older adults," *Journals of Gerontology B: Psychological Sciences and Social Sciences*, vol. 57, no. 2, pp. P101–P115, 2002.

[14] J. T. Brebner and A. T. Welford, "Introduction: an historical background sketch," in *Reaction Times*, pp. 1–23, Academic Press, New York, NY, USA, 1980.

Hindawi Publishing Corporation
BioMed Research International
Volume 2014, Article ID 246096, 11 pages
http://dx.doi.org/10.1155/2014/246096

Research Article

Advance in ERG Analysis: From Peak Time and Amplitude to Frequency, Power, and Energy

Mathieu Gauvin,[1] Jean-Marc Lina,[2,3] and Pierre Lachapelle[1]

[1] *Department of Ophthalmology & Neurology-Neurosurgery, Montreal Children's Hospital Research Institute, McGill University, 2300 Tupper Street, Montreal, QC, Canada H3H 1P3*
[2] *Département de Génie Électrique, École de Technologie Supérieure, Montréal, QC, Canada*
[3] *Centre de Recherches Mathématiques, Montréal, QC, Canada*

Correspondence should be addressed to Pierre Lachapelle; pierre.lachapelle@mcgill.ca

Received 10 April 2014; Accepted 30 May 2014; Published 1 July 2014

Academic Editor: Jerzy Nawrocki

Purpose. To compare time domain (TD: peak time and amplitude) analysis of the human photopic electroretinogram (ERG) with measures obtained in the frequency domain (Fourier analysis: FA) and in the time-frequency domain (continuous (CWT) and discrete (DWT) wavelet transforms). *Methods*. Normal ERGs ($n = 40$) were analyzed using traditional peak time and amplitude measurements of the a- and b-waves in the TD and descriptors extracted from FA, CWT, and DWT. Selected descriptors were also compared in their ability to monitor the long-term consequences of disease process. *Results*. Each method extracted relevant information but had distinct limitations (i.e., temporal and frequency resolutions). The DWT offered the best compromise by allowing us to extract more relevant descriptors of the ERG signal at the cost of lesser temporal and frequency resolutions. Follow-ups of disease progression were more prolonged with the DWT (max 29 years compared to 13 with TD). *Conclusions*. Standardized time domain analysis of retinal function should be complemented with advanced DWT descriptors of the ERG. This method should allow more sensitive/specific quantifications of ERG responses, facilitate follow-up of disease progression, and identify diagnostically significant changes of ERG waveforms that are not resolved when the analysis is only limited to time domain measurements.

1. Introduction

The electroretinogram (ERG) identifies the electrical signal that is generated by the retina in response to a light stimulus. It is the first biopotential ever recorded from a human subject, namely, by Dewar in 1877 [1]. However, despite significant (r)evolution in the recording technologies (essentially from the string galvanometer to the digital amplifier and supporting computer software) and, consequently, the significantly enhanced quality of the ERG signal thus obtained, analysis of the ERG remains for the most part limited to amplitude and peak time measurements of its major components, namely, the a- and b-waves. This is at least what is recommended in the ERG standard of the International Society for Clinical Electrophysiology of Vision (ISCEV) [2]. The a- and b-waves of the ERG are said to reflect the activity generated by the photoreceptors and the bipolar-Müller cell complex, respectively [3–5]. These components are usually referred to as the slow waves of the ERG. Also identified in the ERG signal are the small, high-frequency, oscillations that are often seen riding on the ascending limb of the b-wave [6, 7]. These components, referred to as oscillatory potentials (OPs), are most probably generated by the retinal cells of the inner retina (i.e., bipolar, amacrine, or horizontal cells) although their exact origin remains debated [8, 9]. The OPs appear to be major contributors to the shaping of the ERG waveform [10] and there is an abundant literature attesting to the clinical value of including the OPs when analyzing pathological ERGs [6, 11, 12]. Unfortunately, in order to optimize the visualization of the OPs one must modify the recording bandwidth of the ERG from a broadband (e.g., 1–1000 Hz) to a narrower band (e.g., 100–1000 Hz) that removes the low-frequency components of the ERG (i.e., a- and b-waves) and consequently selectively enhances the high-frequency components (i.e., OPs) [2]. However, when doing so one must always keep in mind the possibility of introducing artifactual

components (such as ringing artifacts and phase lags) to the ERG thus obtained.

It is clear from the above that the ERG waveform results from the amalgamation of several frequency components. Is it possible to monitor the frequency composition of the ERG signal without altering the signal as it is done with the bandwidth restriction approach? Would the use of such an approach significantly improve analysis of the ERG beyond what is accomplished when using time and amplitude measures of the ERG only? Although advanced analytical approaches are now frequently used when studying biopotentials, such as the electroencephalogram [13], the electrocardiogram [14], and the electromyogram [15], to date they have only been sporadically applied to the ERG [8, 16, 17]. The purpose of this study was therefore to compare peak time and amplitude measurements of human photopic ERGs with measures obtained in the frequency domain using the Fourier analysis as well as in the time-frequency domain using the continuous (CWT) and discrete (DWT) wavelet transforms. For the sake of brevity, our study was limited to the photopic ERG only.

2. Materials and Methods

Normal photopic ERGs were obtained from 40 healthy subjects (26 females and 14 males, average age 29.9 ± 8.4 years) using a protocol that was approved by the Institutional Review Board of the Montreal Children's Hospital and in accordance with the Declaration of Helsinki.

According to a previously published method of ours, the ERGs were recorded with both eyes dilated (tropicamide 1%) using an active electrode (DTL fiber electrode) placed in the inferior conjunctival bag, with reference and ground electrodes pasted at the external canthi and forehead, respectively [18–21]. The ERGs were evoked to flashes of white light (flash duration: 20 μs; interstimulus interval: 1.5 s; and average of at least 10 flashes per recording) of 0.64 log cd·s·m^{-2} in intensity that were delivered against a rod desensitizing background light of 30 cd·m^{-2} (measured using a research radiometer IL1700; International Light, Newburyport, MA, USA). ERG waves from both eyes were averaged to yield a single waveform of 150 ms in length (sampling rate: 3413.33 Hz) that included a prestimulus baseline of 20 ms.

2.1. ERG Analysis. The amplitude of the a-wave was measured from the prestimulus baseline to the most negative trough of the ERG, while the amplitude of the b-wave was measured from the trough of the a-wave to the most positive peak of the ERG that followed the a-wave [2]. Peak times were measured from flash onset to the peak of the a- and b-waves [2]. Given that these measures of the ERG are taken in the time domain, they will be referred to as time domain (TD) measurements.

Frequency domain analysis (or Fourier analysis (FA)) of the ERG was carried out using the fast Fourier transform (FFT) algorithm implemented in MATLAB R2013b (Mathworks, Natick, MA, USA) as follows:

$$X(k) = \sum_{t=0}^{N-1} x(t)\, e^{-i(2\pi/N)tk}, \quad k = 0, 1, \ldots, N-1, \qquad (1)$$

where $X(k)$ represents the FFT coefficients, $x(t)$ denotes the raw ERG time-series, and N denotes the number of data points in $x(t)$. Each FFT coefficient weighs the energetic contribution of a single frequency component to the signal so that a frequency spectrum can be illustrated by tracing $X(k)$. Considering the size (512 data points) and sampling frequency (3413.33 Hz) of our ERG waveforms, we were able to compute the FFT coefficients for frequencies ranging between 0 and 1706.66 Hz in increments of 6.66 Hz (i.e., frequency resolution). However, given the limitation imposed by our recording bandwidth (1–1000 Hz) we limited our analysis to frequencies ranging between 0 and 300 Hz to safely avoid artifactual contamination (such as that predicted by the Nyquist-Shannon sampling theorem [22]).

In order to localize the energy content of the ERG in both time and frequency we computed, using MATLAB, the continuous wavelet transform (CWT) of selected ERGs as follows:

$$\mathrm{CWT}(a,b) = \frac{1}{\sqrt{a}} \int_{-\infty}^{+\infty} x(t)\, \psi^* \left(\frac{t-b}{a} \right) dt, \qquad (2)$$

where $\mathrm{CWT}(a,b)$ represents the wavelet coefficients localized at scales a (frequency) and moments b (time), $x(t)$ denotes the unprocessed ERG time-series, and ψ^* denotes the complex conjugate of the Morse wavelet [23], which was chosen for its good frequency resolution [24]. To illustrate the time-frequency scalogram of the CWT, we took the absolute value of $\mathrm{CWT}(a,b)$ and normalized it to its maximal value so that the time-frequency scalograms of the ERG are shown as colored two-dimensional plots of $\mathrm{CWT}(a,b)$ in which minimum energy values are displayed in blue and maximal values in red.

Use of the CWT approach allowed us to analyse the ERG, continuously, at every possible scale a and translation b. This approach, however, requires extensive computation time and also yields a lot of redundant information (i.e., since each coefficient has similar neighboring values) that will remain unused in the set of coefficients $\mathrm{CWT}(a,b)$ [25]. Interestingly, if the scale and translation parameters of the wavelet are taken at discrete values, we then obtain a discrete wavelet transform (DWT), where the scales a and translations b are based on powers of two (i.e., $a_j = 2^j$, $b_{j,k} = k2^j$) so that (2) can be discretized as follows:

$$\mathrm{DWT}(j,k) = \int_{-\infty}^{+\infty} x(t)\, 2^{-j/2} \psi\left(2^{-j}t - k\right) dt, \qquad (3)$$

where $\mathrm{DWT}(j,k)$ represents the wavelet coefficients localized at discrete scales j (frequency) and discrete moments k (time), $x(t)$ designates the raw ERG time-series, and ψ designates the Haar wavelet [25]. $\mathrm{DWT}(j,k)$ was computed using the fast wavelet transform algorithm of Mallat [25, 26] implemented in MATLAB. We chose the Haar wavelet, for its simplicity (i.e., simplest wavelet available) and its orthonormal basis, which allows the wavelet coefficients $\mathrm{DWT}(j,k)$ to be reconstructed accurately and efficiently without any loss of information (using the inverse DWT) even if all the redundant information contained in the CWT is discarded [25, 27]. Similar to the CWT scalograms, the most prominent

Table 1: Normative data (mean ± standard deviation (SD) and coefficient of variation (CV, in bold)) obtained for each parameter (time, frequency, amplitude, power, and energy) assessed using the different analytical approaches compared in this study (time domain, frequency domain, and continuous and discrete time-frequency domain). The time domain allows timing and amplitude quantification of two major components (i.e., the a- and b-waves). The frequency domain identifies the frequency and power of three major components (probably associated with the a- and b-waves and OPs). The continuous time-frequency domain allows timing, frequency, and energy measurements of three main components (probably associated with the a- and b-waves and OPs). Finally, with the discrete time-frequency domain, the components are identified in predetermined temporal windows (i.e., intervals) and frequency bands (i.e., instead of precise timing and frequency) and allow more components to be identified and the a- and b-wave can be quantified independently (i.e., in contrast to the frequency domain or continuous time-frequency domain in which the a- and b-waves formed a single low-frequency component).

	Time domain (peak time and amplitude)			
	Time (ms)	Frequency (Hz)	Amplitude (μV)	Origin
Main component 1	13.53 ± 1.55 **(11)**	n/a	32.21 ± 5.11 **(16)**	a-wave
Main component 2	30.98 ± 1.33 **(4)**	n/a	104.81 ± 18.66 **(18)**	b-wave
	Frequency domain (Fourier analysis)			
	Time (ms)	Frequency (Hz)	Power (μW/Hz)	Probable origin
Main component 1	n/a	28.81 ± 7.17 **(29)**	10.46 ± 2.15 **(21)**	a- and b-waves
Main component 2	n/a	75.38 ± 7.69 **(10)**	3.43 ± 0.89 **(26)**	OPs
Main component 3	n/a	146.00 ± 13.31 **(9)**	1.88 ± 0.43 **(23)**	OPs
	Time-frequency domain (continuous wavelet transform)			
	Time (ms)	Frequency (Hz)	Energy (μV·s)	Probable origin
Main component 1	31.04 ± 0.89 **(3)**	29.70 ± 5.71 **(19)**	202.8 ± 21.08 **(10)**	a- and b-waves
Main component 2	32.04 ± 2.22 **(7)**	73.81 ± 6.28 **(9)**	111.57 ± 23.17 **(21)**	OPs
Main component 3	29.81 ± 1.96 **(7)**	150.28 ± 11.57 **(8)**	69.29 ± 16.79 **(24)**	OPs
	Time-frequency domain (discrete wavelet transform)			
	Time interval (ms)	Frequency band (Hz)	Energy (μV·s)	Probable origin
Main component 1	−20 to 17.5	20 ± 6.6	78.08 ± 10.66 **(14)**	a-wave
Main component 2	17.5 to 55	20 ± 6.6	214.46 ± 19.02 **(9)**	b-wave
Main component 3	0 to 17.5	40 ± 13.3	100.79 ± 9.39 **(9)**	a-wave
Main component 4	17.5 to 55	40 ± 13.3	228.41 ± 28.05 **(12)**	b-wave
Main component 5	8.125 to 55	80 ± 26.6	145.83 ± 21.75 **(15)**	OPs
Main component 6	17.5 to 40.35	160 ± 53.3	80.81 ± 12.48 **(15)**	OPs

energy component of the DWT scalogram will appear as a deep dark red (high energy) rectangle in the region of the DWT scalogram where it is located (i.e., located in time and frequency), and, conversely, the absence of any component at given locations will appear as deep dark blue (no energy) rectangles.

2.2. Statistical Analyses. Mean value, standard deviation (SD), and coefficient of variation (CV) were computed for all ERG parameters that were identified using the different analytical approach. Z-scores were used to evaluate the significance of selected descriptor changes. All tests were set to a level of significance of 5%.

3. Results

3.1. Time and Amplitude Measurements in the Time Domain. As reported in Table 1, time domain analysis allowed the identification of two major ERG components, one peaking at 13.53 ± 1.55 ms (mean ± SD obtained in our 40 subjects) with an amplitude of 32.21 ± 5.11 μV (identified as the a-wave at Figure 1(a)) and another one which peaks at 30.98 ± 1.33 ms with an amplitude of 104.81 ± 18.66 μV (identified as the b-wave at Figure 1(a)).

3.2. Fourier Analyses (FA). The frequency components contributing to the genesis of the ERG can be identified using the FA, such as that obtained with the FFT. This is best exemplified in Figure 1 and Table 1, where three major frequency components are identified in the normal ERGs. As shown with the black arrows, the low-frequency components of the ERG (presumably a- and b-waves) usually formed a smooth peak of large magnitude, culminating at 28.8 ± 5.7 Hz (i.e., mean ± SD obtained from our 40 subjects) on the frequency spectrum. However, in some instances, two distinct peaks could be identified (see double black arrows in panels (a) and (d)). In the later cases, only the peak of highest magnitude was considered for further analysis. In contrast, the higher frequency components of the ERG (probably the OPs) usually formed two distinct peaks (see grey arrows) of low magnitude located at 75 ± 7.7 Hz and 146 ± 13.3 Hz, respectively. However, given that FA only looks at the frequency content of the ERG without taking into consideration if those frequencies are time-locked or not to the stimulus, its use can lead to erroneous interpretations of the ERG. This is best illustrated with the ERGs shown in Figures 1(c) and 1(d) where the noise contaminants (such as 60 Hz in Figure 1(c)) appear to contribute more to the making of the ERG than the retinal evoked components themselves.

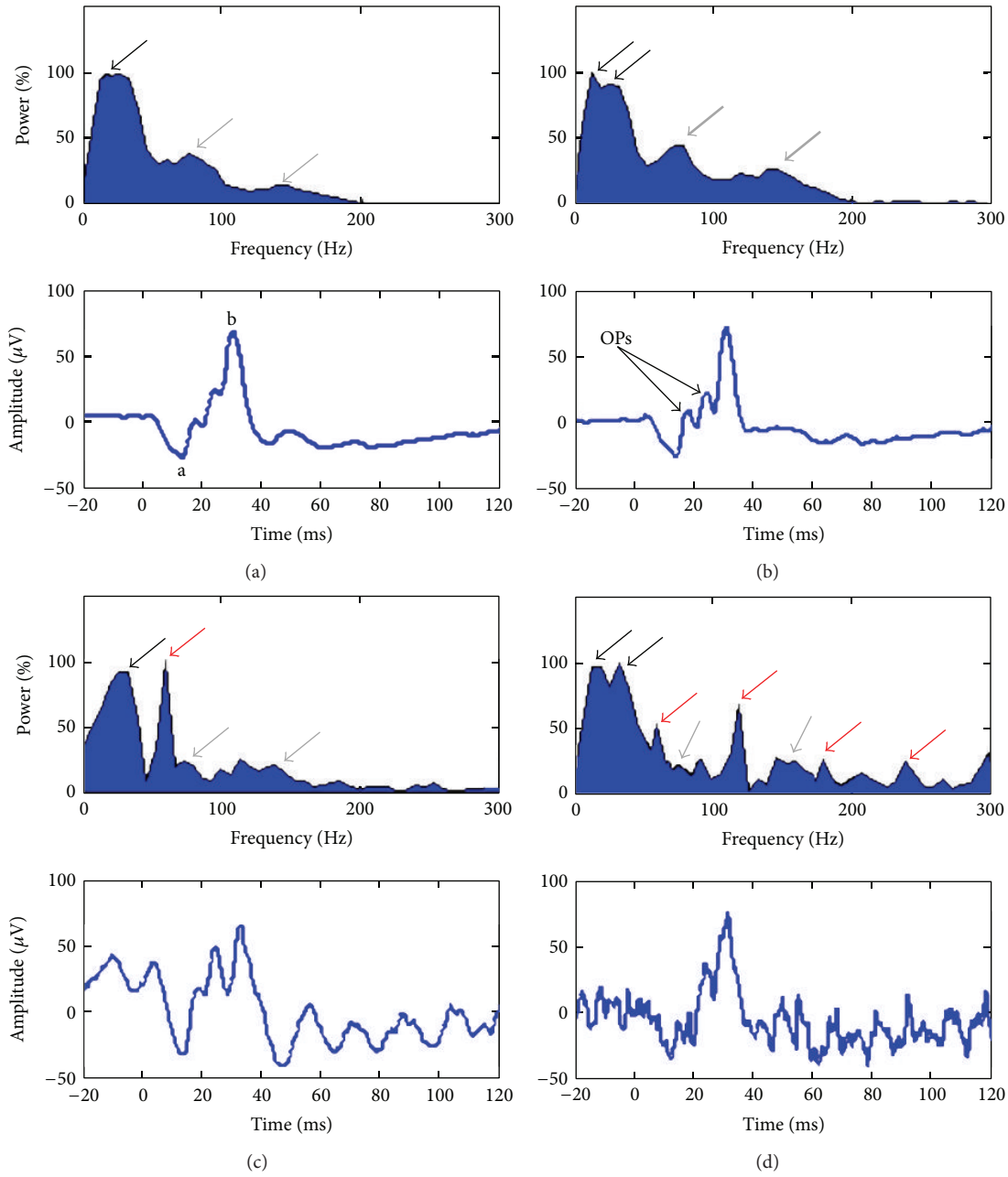

Figure 1: Fourier analysis (FA) of 4 normal ERGs. The frequency spectrums are shown as normalized power spectrum, in percentage, where the spectrums are normalized to their maximal value. The associated ERGs are shown at the bottom of each spectrum. The a-wave, b-wave, and OPs are indicated as "a," "b," and "OPs," respectively. (a) FA of a composite ERG, averaged from 40 subjects, showing the 3 typical frequency components that contribute to the ERG (~30 Hz: a- and b-waves contribution, black arrow; ~75 Hz and ~150 Hz: oscillatory potentials (OPs) contribution, gray arrows). (b) FA of an ERG showing enhanced OPs (increased ~75 Hz and ~150 Hz component contribution; thick gray arrows). (c) FA of a typical contaminated ERG showing the 3 standard ERG components (see arrows, same color-coding as previous panels) and a sharp, noise-related, maximal component at 60 Hz (60-cycle line interference contribution, red arrow). This sharp noise component seems to disturb the identification of the OPs component located at ~75 Hz. (d) FA of another contaminated ERG showing the 3 characteristic frequency components (see arrows, same color-coding as previous panels) of the ERG and 4 interference-related components at 60, 120, 180, and 240 Hz, respectively (60-cycle harmonics contribution, red arrows). These noise components seem to complicate the identification of the two typical OPs components located at ~75 Hz and ~150 Hz.

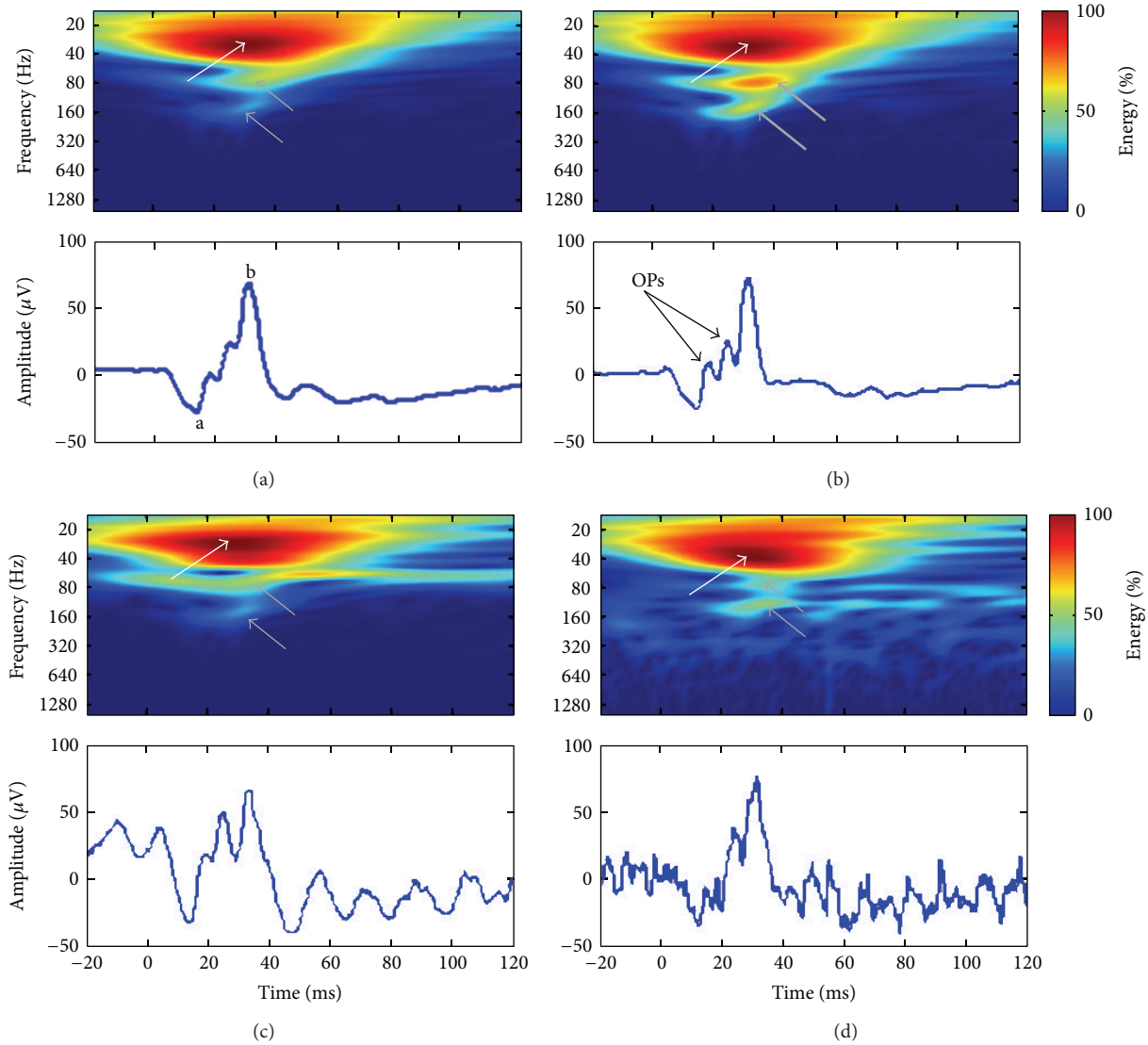

Figure 2: Continuous wavelet transform (CWT) analysis of the ERGs that were shown at Figure 1. All scalograms were normalized to their maximal energy values, and the color-coding (see colorbar) indicates low (blue), moderate (green), and high (red) energy values. The associated ERGs are shown at the bottom of each scalogram. The a-wave, b-wave, and oscillatory potentials are indicated as "a," "b," and "OPs," respectively. (a) CWT of the composite ERG showing the energy (as per colorbar) and the temporal location of the 3 typical frequency components that were previously identified in the Fourier domain (~30 Hz: a- and b-waves contribution, white arrow; ~75 Hz and ~150 Hz: oscillatory potentials (OPs) contribution, gray arrows). (b) CWT of the ERG that had enhanced OPs [increased ~75 Hz and ~150 Hz energy; thick gray arrows]. (c) CWT of the contaminated ERG showing the 3 standard components (see arrows, same color-coding as previous panels) and a strip of moderate energy localized at 60 Hz for the whole duration of the signal (60-cycle interference contribution). (d) CWT of the second contaminated ERG also evidencing the 3 characteristic frequency components of the ERG and several transient, interference-related, patches of energy (60-cycle harmonics contribution).

These limitations of FA can be overcome by adding a temporal resolution to the frequency domain.

3.3. Continuous Wavelet Transform (CWT) Analyses. As shown in Figure 2, use of the CWT approach allowed us to more precisely localize (in both time and frequency, as reported in Table 1) the abovementioned frequency components of the ERG signal and even in the presence of significant noise contaminants (as seen in panels (c) and (d)). In each scalogram, the a- and b-waves formed a cluster of hot (dark red) coefficients (see white arrows) centered at 29.7 ± 5.7 Hz (i.e., mean ± SD obtained in our 40 subjects) and peaking at 31.0 ± 0.9 ms (i.e., time-locked to the peak time of the ERG b-wave). Similarly, the OPs formed two distinct clusters (see grey arrows) centered at 73.8 ± 7.7 Hz and 150.3 ± 11.6 Hz and peaking at 32 ± 2.2 ms and 29.8 ± 1.9 ms, respectively. As shown in the scalogram of panels C and D, the high- (i.e., OPs) and low-frequency (i.e., corresponding to the a- and b-waves) components continued to remain the major light-evoked (i.e., time-locked to the stimulus) components of

the ERG response in spite of significant noise contamination. The latter contrasts with results obtained using the FA where one cannot dissociate evoked from nonevoked frequency components (compare results shown in Figures 2(c) and 2(d) with corresponding FA results shown in Figures 1(c) and 1(d)).

In each scalogram of Figure 2, the value of the coefficients that identified the hot clusters pertaining to the a- and b-waves or OPs was centered on a section of the clusters where all coefficients had the same value (i.e., equipotential regions). This attribute of the CWT will generate redundant information (i.e., similar or equal coefficient values) that will complicate the accurate identification of the time-frequency coordinates (i.e., ill-posed coordinates) of the ERG components, by introducing an uncertainty factor. For example, given that the red clusters of Figure 2 extend over a large area of the scalograms, this prevents an accurate quantification of the a-wave energy, which is most probably hidden by the higher energy b-wave. These limitations can be overcome if we impose a discretization over the possible frequencies and times at which the information is computed.

3.4. Discrete Wavelet Transform (DWT) Analysis. As illustrated in Figure 3, the DWT scalograms decomposed the signals into seven contiguous frequency bands (20, 40, 80, 160, 320, 640, and 1280 Hz), each including a range of frequencies (reported in Table 1) around their respective central frequency (CF). For example, the 20 Hz band quantified the energy oscillating between 13.33 and 26.66 Hz (i.e., $20 \pm 20/3$, that is, $CF \pm CF/3$). Use of this expansion simplifies the choice of relevant coefficients (i.e., seen as rectangles of different sizes in the scalograms of Figure 3) that may be used as energy descriptors of the ERG.

3.4.1. Identification of DWT Descriptors. As seen with the DWT scalograms of Figure 3, the major frequency components are confined to the time-frequency region that is surrounded by white borders and where six major components can be identified (i.e., rectangles of various colors shown in panel (a) and magnified in panel (b)) and thus quantified (as reported in Table 1). The DWT also removed the redundancy so that the b-wave energy, quantified with the 20b and 40b descriptors (panel (b)), is now represented by two rectangles (i.e., identified as 20b and 40b) confined to an area of the scalogram that is limited to the vicinity of the b-wave peak rather than spread across most of the CWT scalogram. This allowed the quantification of two descriptors, time-locked to the a-wave, which we identified as 20a and 40a. The 20a and 40a were of lower energy compared to the 20b or 40b (see Table 1), indicating that, as expected, the b-wave energy is greater than that of the a-wave. Finally, the high-frequency components, indicated as 80ops and 160ops, were also easily identified (i.e., maximal value in the 80 and 160 Hz bands, resp.).

3.4.2. Improvement of ERG Segregation Using the DWT. As indicated above, the a- and b-wave components were seen on both the 20 Hz (20a and 20b descriptors) and 40 Hz bands (40a and 40b descriptors). These descriptors can be used to segregate ERGs of different morphologies. This is better illustrated in Figure 3(c), where two ERGs of distinct morphologies were similar ($P > 0.05$) in terms of a- and b-wave peak time and amplitude but were significantly different ($P < 0.05$) on the basis of their DWT b-wave descriptors (20b and 40b). In one example, the ascending limb of the b-wave has a sharp morphology (blue tracing) and showed a lower 20b descriptor ($P < 0.05$), compared to the broader ascending limb of the b-wave (compare first half of ascension of tracing in red) which disclosed an attenuated 40b parameter ($P < 0.05$). Similarly, we were also able to segregate ERGs that differed in OPs prominence (such as what is shown in Figure 3(d)). Although these ERGs were indistinguishable ($P > 0.05$) on the basis of peak time and amplitude measurements of the a- and b-waves, they were significantly different ($P < 0.05$) on the basis of their 80ops and 160ops energy content which were higher (blue tracing) or lower (red tracing) compared to average.

3.5. Applications of Refined Analytical Approach to Clinical ERGs. In Figure 4(a) the ERG waveforms obtained from a patient diagnosed with retinitis pigmentosa (RP) that was followed up for more than 30 years are illustrated. As shown, the low amplitude (and low signal-to-noise ratio or low SNR) of these pathological ERGs, especially those obtained later in the disease process (tracings 23 and 29), seriously compromises an accurate measurement of these waveforms. This is best exemplified in Figure 4(c), where an accurate measurement of the b-wave amplitude could only be achieved for ERGs obtained within the first 13 years, due to the highly contaminated ERGs recorded subsequently. However, use of the DWT still permitted the extraction of b-wave descriptors (i.e., 20b and 40b) as shown in the scalograms of Figure 4(b) and therefore allowed us to monitor progression of the disease process for an additional period of 16 years, as shown in Figure 4(d). Furthermore, as revealed in Figure 4(d), both eyes followed the same degeneration pattern, which appeared to follow an exponential decay function that correlated well with that which characterized (using b-wave amplitude measures) the first 13 years. Interestingly, the use of the inverse DWT of the low-frequency bands (i.e., 20 and 40 Hz bands) allowed us to reconstruct noise-free ERGs (Figure 4(e)), that were nearly identical in both eyes, as it was also the case for the ERGs (measurable, high SNR) recorded in earlier exams (tracings 0, 1, 3, and 9 of Figure 4(a)). The validation of this denoising approach (i.e., inverse DWT) is further demonstrated in Figure 5, where we reconstructed the 20 consecutive single-flash recordings obtained from a RP patient that were used to generate the average waveform. As shown, the 20 denoised single-flash waveforms (red tracings) are nearly identical (mean (±SD) Pearson coefficients = 0.92 ± 0.02) to the averaged response (i.e., blue tracing obtained by averaging the 20 consecutive noisy responses (gray traces)). In contrast, the mean Pearson coefficients obtained between the single sweeps and the averaged response were of 0.52 ± 0.03.

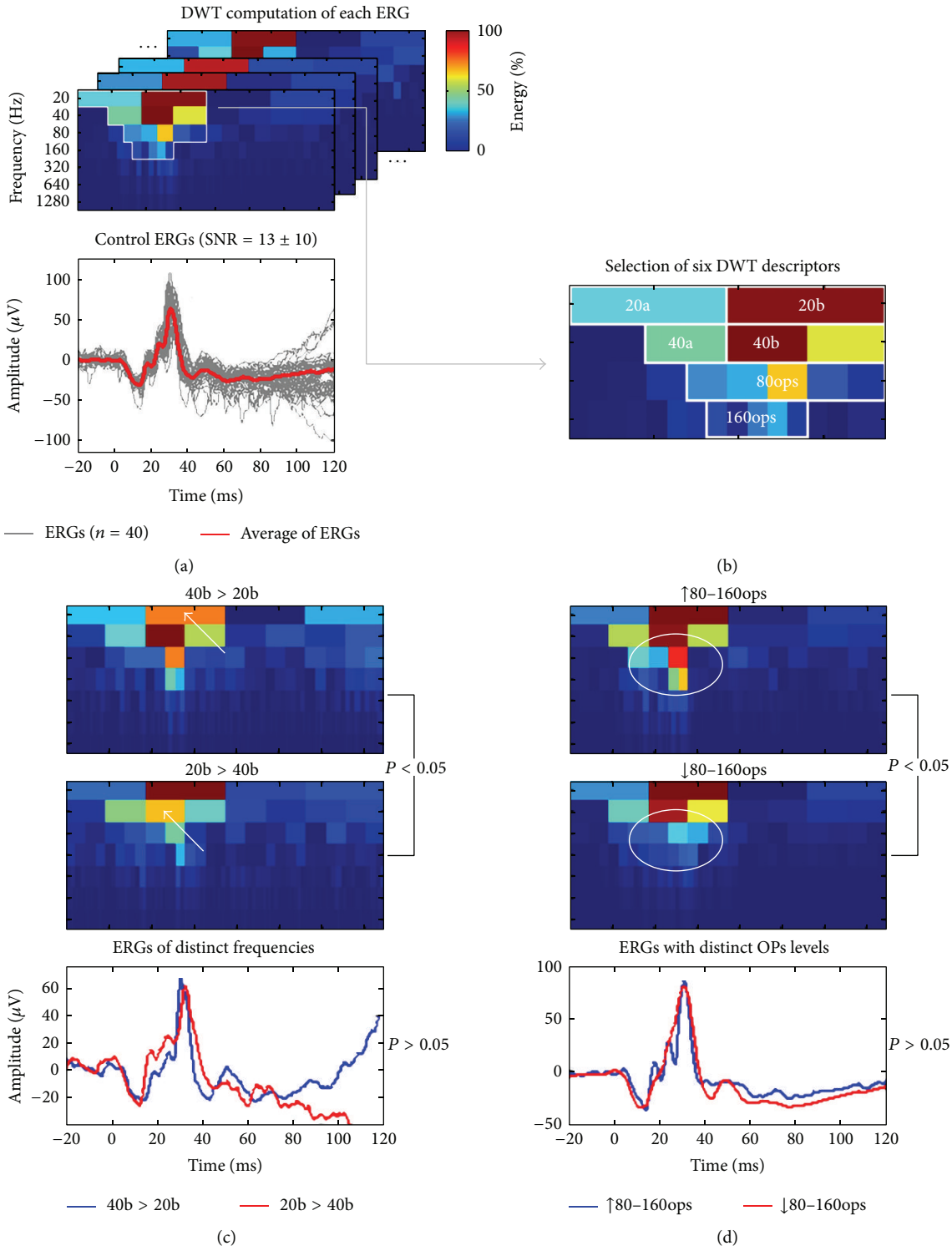

FIGURE 3: Analysis method and classification improvement of normal ERGs using the discrete wavelet transform (DWT). (a) We computed the DWT of 40 normal ERGs with various signal-to-noise ratios (SNR = 13 ± 10, gray traces; averaged response: red trace) and extracted, in each scalogram, descriptors (see panel (b)) localized inside the region of maximal energy (delimited by white borders). (b) Magnification of the averaged ERG (red trace at panel (a)) scalogram that shows where we identified six novel DWT descriptors of the ERGs (20a and 40a: a-wave energy; 20b and 40b: b-wave energy; and 80ops and 160ops: oscillatory potentials (OPs) energy). ((c) and (d)) The DWT descriptors were used to segregate ERGs of distinct morphologies, that had similar ($P > 0.05$) a- and b-wave amplitudes and peak times but significantly ($P < 0.05$) smaller 20b or 40b descriptors (panel (c), white arrows) or significantly larger or smaller 80ops and 160ops descriptors in the DWT scalograms (panel (d), white circles).

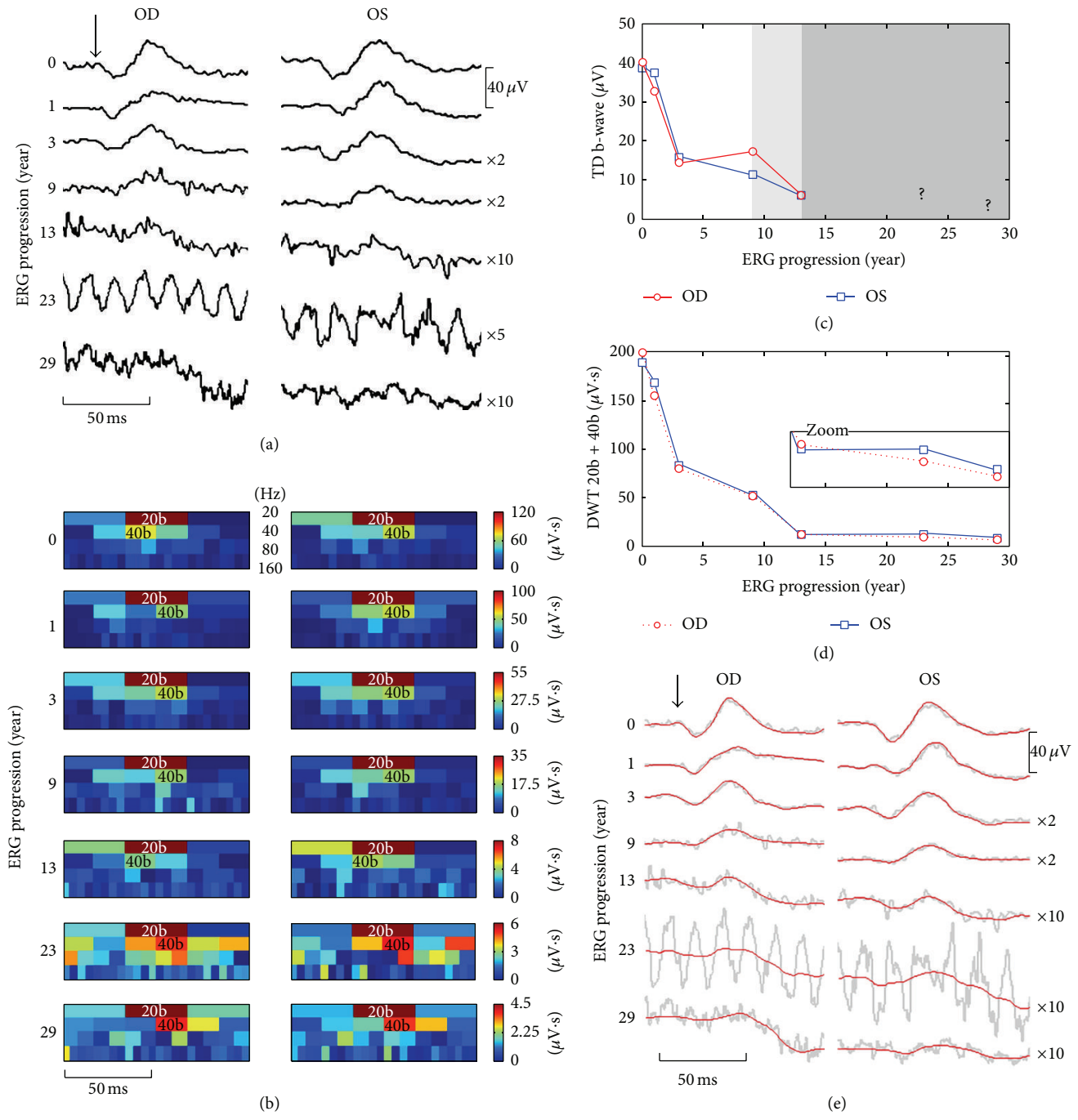

Figure 4: (a) ERG traces (averaged from up to 100 responses) obtained at seven time points in the right (OD) eye and left (OS) eye of a male patient affected with retinitis pigmentosa (both eyes presented with nonrecordable scotopic ERGs, constricted visual fields, pigmentary deposits, and decreased visual acuity) in a time span of 3 decades. The horizontal (time) and vertical (voltage) scale bars apply to both eyes and some traces have been magnified (×2, ×5, or ×10 times) for visualization purposes. The flash onset is indicated by the black vertical arrow. ERG progression is shown in years since the first visit on the left-hand side. (b) Scalograms computed for each pathological ERG waveform (presented in the same order than in panel (a)) in which we quantified the 20b and 40b descriptors. Note that, in some scalograms, the position of the 40b descriptors was delayed (i.e., delayed latency of the b-wave) compared to normals (see Figure 3) and the 40b descriptors were always more severely attenuated than the 20b. (c) Progression of the TD b-wave amplitudes from both eyes. Because of the noise contaminants the 4th and 5th ERG were imprecisely measured (indicated by the lighter gray background on the graph), while the last two ERGs were nonmeasurable, thus preventing the quantification of disease progression from that point (indicated by the darker gray background). (d) Using the DWT descriptors of the b-wave (20b + 40b) allowed us to monitor the disease progression more precisely and for the whole time span (additional 16 years of monitoring: see zoomed box). (e) Using the inverse DWT, we reconstructed the low-frequency bands (i.e., 20 and 40 Hz bands), obtaining the biological denoised responses which are shown, in red, on top of the unprocessed gray tracings.

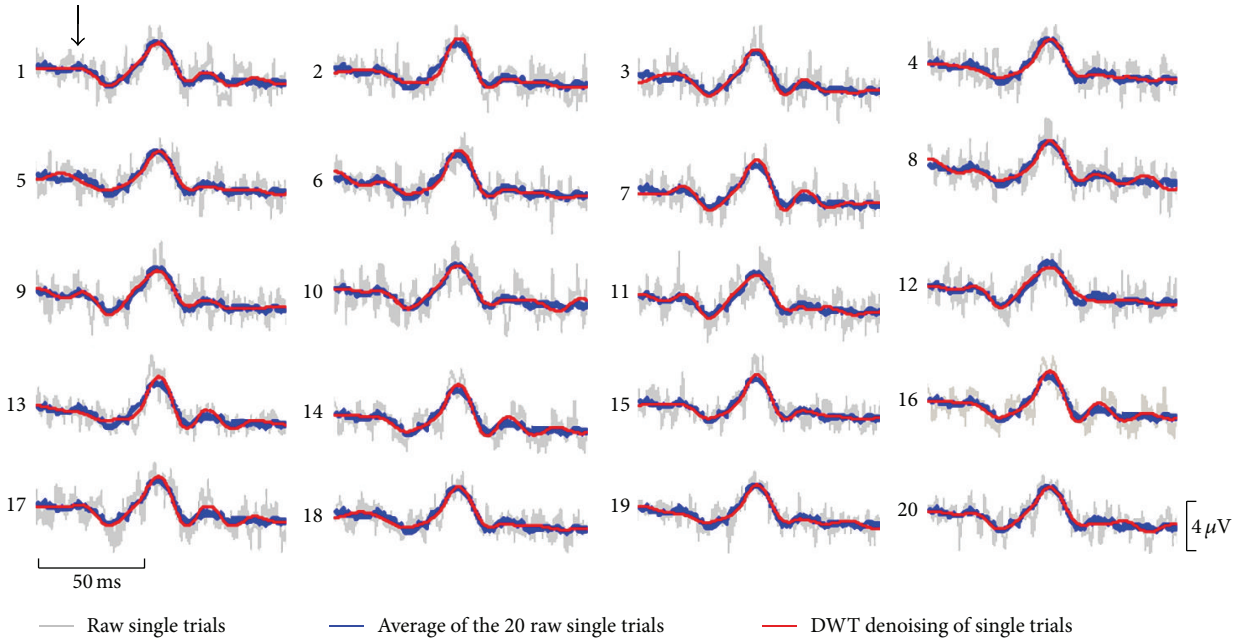

Figure 5: 20 consecutive single-flash ERG responses (gray traces) obtained from a patient affected with retinitis pigmentosa. The average of these 20 raw ERG responses canceled the uncorrelated noise to yield the blue tracing (overlaid on top of each single-flash response). DWT denoising of the individual noisy single-flash responses reveals denoised biological responses, which are shown as red traces. All red traces are nearly identical (shape and amplitude) to the trace obtained from the average (i.e., blue traces) of the 20 noisy responses, thus validating this denoising approach. The horizontal (time) and vertical (voltage) scale bars apply to each trace. The flash onset is indicated by the black vertical arrow.

4. Discussion

To date, analysis of the ERG relies mostly on time domain (TD) measurements (peak time and amplitude) of its two major components, namely, the a- and b-waves. However, as shown with the examples illustrated in Figures 4 and 5 and as previously suggested [28–31], TD measurements are subjected to noise contamination. These contaminants can arise from numerous factors such as the subject (e.g., eye blinks, head/eye movements, etc.), external sources (e.g., mechanical vibrations, electromagnetic coupling with the 50/60 Hz power lines, computer monitors, electrical lighting, etc.), and, if the data is digitized, the digitization process itself (e.g., digitization artifacts, aliasing, etc.). Therefore, limiting the ERG analysis to TD measures only could jeopardize the detection of subtle functional changes.

4.1. From Fourier to Wavelets. FA methods, such as the one presented in Figure 1 (i.e., FFT), performed well in identifying the three major frequency components of the normal photopic ERG response. However, when a noise contaminant was distributed over the entire ERG response, the resulting frequency-power distribution was misleading (as shown in Figures 1(c) and 1(d)). This is due to the fact that the FA assumes that all the frequency components that compose a signal are periodic and, consequently, ignores the possibility that some frequencies could be found at precise poststimulus time locations only. This explains why the amplitude of a component can be over- or underestimated when relying solely on FA analysis. In other words, while Fourier analyses are well-suited to identify the frequency components that compose the ERG signal, they are of no use to determine their respective magnitude and temporal location within the signal. Such information is of crucial importance if one wishes to define the signal with all its subtleties. This can be accomplished with a time-frequency domain analysis of the ERG.

Use of the CWT (Figure 2) approach allowed us to clearly identify the temporal as well as the frequency coordinates of the three major frequency components of the ERG, thus remedying the FA limitations alluded to above. We have shown that, with the CWT scalograms, each of these components was time-locked to the largest wave of the ERG (i.e., the b-wave). Furthermore, compared to corresponding FA estimates, their respective weights (i.e., relative energy levels) were also more accurately determined, even in noisy ERG recordings.

4.2. The DWT: An Optimal Compromise. Interestingly, it seems, from FA and CWT analyses, that the components of the ERG cannot be associated with single frequency values but rather to a range of values. For example, in the FA power spectrums of Figure 1, each component had a broad Gaussian-like distribution (i.e., suggestive of a band of frequencies) rather than a sharp peak (i.e., suggestive of a single frequency) as it would be the case for a pure sinusoid. Similar broad distributions of individual frequency components were also observed in the CWT of the same ERG signals (see Figure 2), the major difference being that the magnitude of these frequency components can now be time-correlated to

specific events of the ERG signal. Consequently, since these components contain a band of frequencies rather than a single frequency, analysis of the ERG at different frequency bands using the DWT scalogram (rather than at each possible frequency with the CWT) offers a simplified scheme (exempt of redundancy) to identify relevant ERG descriptors (see Figures 3(a) and 3(b)).

In the DWT scalograms the a- and b-waves were characterized by distinct components located in the 20 Hz (20a and 20b descriptors) and 40 Hz (40a and 40b descriptors) bands. It was difficult to accurately determine these distinct frequency components using the CWT, although in the FA some ERGs did show both the 20 and 40 Hz components (i.e., identified as double-peaks in Figures 1(b) and 1(d)). Furthermore, quantifying the ERG waveforms using the DWT augmented the specificity (i.e., ability to discriminate between distinct ERG morphologies, as shown in Figures 3(c) and 3(d)) and sensitivity (i.e., reduced the variability, as shown by the CV reported in Table 1) of the measures obtained.

Finally, at the end-stage of severe degenerative retinopathies (such as RP), nearly extinguished ERGs (e.g., low-SNR, such as the one shown in Figures 4(a) and 5) are often the last measurable signs of functional vision [32]. As shown in Figure 4, extracting relevant ERG descriptors from these residual ERGs using a TD approach (e.g., peak time and amplitude measures) becomes nearly impossible as the SNR decreases. Use of the DWT permitted the quantification of such responses, thus extending the length of the follow-up period of disease progression by an additional 16 years. This allowed us to demonstrate the exponential decay known to characterize the long-term course of the cone ERG amplitude in patients affected with RP [33]. Furthermore, use of the inverse DWT of selected frequency bands allowed us to reconstruct noise-free ERG waveform thus confirming the presence of a residual biological response in signals that were reported as nonmeasurable using the TD approach. The validation of this DWT-denoising approach was demonstrated in Figure 5, where each of the 20 denoised ERGs was highly similar to the averaged response (obtained by averaging the 20 consecutive responses).

4.3. Limitations of the Study. In this study we limited the TD approach to its most widespread descriptors (i.e., amplitude and peak time of the a- and b-waves), but other unusual descriptors (e.g., area-under-the-curve of the a- or b-wave, time to reach a certain percentage of the a- or b-wave amplitudes, steepness of the rising or descending flank of the b-wave, filtered OPs measurements, etc. [6, 31, 34]) could also be of use to identify subtle morphological changes, albeit similarly sensitive to noise contaminant errors.

5. Conclusions

In this paper, we have presented a brief overview of the different analytical approaches that can be used to quantify the ERG waveform. As long as the response remains measurable, the traditional measurements of the a- and b-waves can be used to monitor the peak time and the amplitude of the ERG signal. However, these measurements only look at the ERG signal as a whole, instead of looking at the different frequency components (possibly of distinct cellular origin) separately. The discrete wavelet transform offers the possibility to extract more components of the ERG signal, even in very poor SNR responses. Standardized time domain analysis of retinal function should thus be complemented with advanced DWT descriptors of the ERG. The latter should allow more sensitive/specific quantifications of ERG responses, facilitate follow-up of disease progression, and identify diagnostically significant changes of ERG waveforms that are not resolved when the analysis is only limited to time domain measurements, thus bringing the analysis and interpretation of the ERG signal in the 21st century, as it is already the case with other biopotentials such as the electroencephalogram and electrocardiogram.

Conflict of Interests

The authors of the paper (Mathieu Gauvin, Jean-Marc Lina, and Pierre Lachapelle) do not have any financial disclosure or conflict of interests to report.

Acknowledgment

This study was funded by Grants-in-aid from the Canadian Institutes for Health Research (MOP-126082) and the Vision Health Research Network of the Fonds de Recherche du Québec-Santé.

References

[1] A. F. de Rouck, "History of the electroretinography," in *Principles and Practice of Clinical Electrophysiology of Vision*, J. R. Heckenlively and G. B. Arden, Eds., pp. 139–185, The Mit Press, London, UK, 2006.

[2] M. F. Marmor, A. B. Fulton, G. E. Holder, Y. Miyake, M. Brigell, and M. Bach, "ISCEV Standard for full-field clinical electroretinography (2008 update)," *Documenta Ophthalmologica*, vol. 118, no. 1, pp. 69–77, 2009.

[3] P. A. Sieving, K. Murayama, and F. Naarendorp, "Push-pull model of the primate photopic electroretinogram: a role for hyperpolarizing neurons in shaping the b-wave," *Visual Neuroscience*, vol. 11, no. 3, pp. 519–532, 1994.

[4] D. C. Hood and D. G. Birch, "Human cone receptor activity: the leading edge of the a-wave and models of receptor activity," *Visual neuroscience*, vol. 10, no. 5, pp. 857–871, 1993.

[5] R. F. Miller and J. E. Dowling, "Intracellular responses of the Müller (glial) cells of mudpuppy retina: their relation to b-wave of the electroretinogram," *Journal of Neurophysiology*, vol. 33, no. 3, pp. 323–341, 1970.

[6] P. Lachapelle, "The human suprathreshold photopic oscillatory potentials: method of analysis and clinical application," *Documenta Ophthalmologica*, vol. 88, no. 1, pp. 1–25, 1994.

[7] L. Wachtmeister, "Oscillatory potentials in the retina: what do they reveal," *Progress in Retinal and Eye Research*, vol. 17, no. 4, pp. 485–521, 1998.

[8] W. Zhou, N. Rangaswamy, P. Ktonas, and L. J. Frishman, "Oscillatory potentials of the slow-sequence multifocal ERG in primates extracted using the Matching Pursuit method," *Vision Research*, vol. 47, no. 15, pp. 2021–2036, 2007.

[9] H. Heynen, L. Wachtmeister, and D. van Norren, "Origin of the oscillatory potentials in the primate retina," *Vision Research*, vol. 25, no. 10, pp. 1365–1373, 1985.

[10] P. Lachapelle, "Oscillatory potentials as predictors to amplitude and peak time of the photopic b-wave of the human electroretinogram," *Documenta Ophthalmologica*, vol. 75, no. 1, pp. 73–82, 1990.

[11] P. Lachapelle, S. Rousseau, M. Mckerral et al., "Evidence supportive of a functional discrimination between photopic oscillatory potentials as revealed with cone and rod mediated retinopathies," *Documenta Ophthalmologica*, vol. 95, no. 1, pp. 35–54, 1998.

[12] L. Wachtmeister, "Basic research and clinical aspects of the oscillatory potentials of the electroretinogram," *Documenta Ophthalmologica*, vol. 66, no. 3, pp. 187–194, 1987.

[13] K. Gadhoumi, J. Lina, and J. Gotman, "Discriminating preictal and interictal states in patients with temporal lobe epilepsy using wavelet analysis of intracerebral EEG," *Clinical Neurophysiology*, vol. 123, no. 10, pp. 1906–1916, 2012.

[14] P. S. Addison, "Wavelet transforms and the ECG: a review," *Physiological Measurement*, vol. 26, no. 5, pp. R155–R199, 2005.

[15] A. Phinyomark, C. Limsakul, and P. Phukpattaranont, "Application of wavelet analysis in EMG feature extraction for pattern classification," *Measurement Science Review*, vol. 11, no. 2, pp. 45–52, 2011.

[16] J. D. Forte, B. V. Bui, and A. J. Vingrys, "Wavelet analysis reveals dynamics of rat oscillatory potentials," *Journal of Neuroscience Methods*, vol. 169, no. 1, pp. 191–200, 2008.

[17] J. M. Miguel-Jiménez, L. Boquete, S. Ortega, J. M. Rodríguez-Ascariz, and R. Blanco, "Glaucoma detection by wavelet-based analysis of the global flash multifocal electroretinogram," *Medical Engineering and Physics*, vol. 32, no. 6, pp. 617–622, 2010.

[18] M. Rufiange, S. Rousseau, O. Dembinska, and P. Lachapelle, "Cone-dominated ERG luminance-response function: the Photopic Hill revisited," *Documenta Ophthalmologica*, vol. 104, no. 3, pp. 231–248, 2002.

[19] M. Rufiange, J. Dassa, O. Dembinska et al., "The photopic ERG luminance-response function (photopic hill): method of analysis and clinical application," *Vision Research*, vol. 43, no. 12, pp. 1405–1412, 2003.

[20] M. Rufiange, M. Dumont, and P. Lachapelle, "Modulation of the human photopic ERG luminance-response function with the use of chromatic stimuli," *Vision Research*, vol. 45, no. 17, pp. 2321–2330, 2005.

[21] M. Garon, M. Rufiange, R. Hamilton, D. L. McCulloch, and P. Lachapelle, "Asymmetrical growth of the photopic hill during the light adaptation effect," *Documenta Ophthalmologica*, vol. 121, no. 3, pp. 177–187, 2010.

[22] H. Nyquist, "Certain topics in telegraph transmission theory," *Proceedings of the IEEE*, vol. 90, no. 2, pp. 280–305, 2002.

[23] J. M. Lilly and S. C. Olhede, "On the analytic wavelet transform," *IEEE Transactions on Information Theory*, vol. 56, no. 8, pp. 4135–4156, 2010.

[24] G. A. Worrell, K. Jerbi, K. Kobayashi, J. M. Lina, R. Zelmann, and M. Le Van Quyen, "Recording and analysis techniques for high-frequency oscillations," *Progress in Neurobiology*, vol. 98, no. 3, pp. 265–278, 2012.

[25] S. G. Mallat, *A Wavelet Tour of Signal Processing: The Sparse Way*, Academic Press, Houston, Tex, USA, 3rd edition, 2009.

[26] J. Buckheit, S. Chen, D. Donoho, and I. Johnstone, *About WaveLab*, Stanford University Press, Stanford, Calif, USA, 1995.

[27] S. G. Mallat, "Theory for multiresolution signal decomposition: the wavelet representation," *IEEE Transactions on Pattern Analysis and Machine Intelligence*, vol. 11, no. 7, pp. 674–693, 1989.

[28] M. Bock, M. Andrassi, L. Belitsky, and B. Lorenz, "A comparison of two multifocal ERG systems," *Documenta Ophthalmologica*, vol. 97, no. 2, pp. 157–178, 1998.

[29] M. Gur and Y. Zeevi, "Frequency-domain analysis of the human electroretinogram," *Journal of the Optical Society of America*, vol. 70, no. 1, pp. 53–59, 1980.

[30] A. C. Fisher, R. P. Hagan, and M. C. Brown, "Automatic positioning of cursors in the transient pattern electroretinogram (PERG) with very poor SNR using an Expert System," *Documenta Ophthalmologica*, vol. 115, no. 2, pp. 61–68, 2007.

[31] H. Jägle, J. Heine, and A. Kurtenbach, "L: M-cone ratio estimates of the outer and inner retina and its impact on sex differences in ERG amplitudes," *Documenta Ophthalmologica*, vol. 113, no. 3, pp. 105–113, 2006.

[32] E. Rispoli, A. Iannaccone, and E. M. Vingolo, "Low-noise electroretinogram recording techniques in retinitis pigmentosa," *Documenta Ophthalmologica*, vol. 88, no. 1, pp. 27–37, 1994.

[33] E. L. Berson, "Long-term visual prognoses in patients with retinitis pigmentosa: the Ludwig von Sallmann lecture," *Experimental Eye Research*, vol. 85, no. 1, pp. 7–14, 2007.

[34] J. J. vos Hzn., M. A. J. M. Coemans, and J. F. W. Nuboer, "No evidence for polarization sensitivity in the pigeon," *The Journal of Experimental Biology*, vol. 198, part 2, pp. 325–335, 1995.

Hindawi Publishing Corporation
BioMed Research International
Volume 2014, Article ID 613434, 6 pages
http://dx.doi.org/10.1155/2014/613434

Research Article

The Outcomes of Primary Scleral Buckling during Repair of Posterior Segment Open-Globe Injuries

Dan Cohen,[1] Jaime Levy,[2] Tova Lifshitz,[2] Nadav Belfair,[2] Itamar Klemperer,[2] Noam Yanculovich,[2] and Boris Knyazer[2]

[1] *Joyce and Irving Goldman Medical School, Faculty of Health Sciences, Ben-Gurion University of the Negev, 84101 Be'er-Sheva, Israel*
[2] *Department of Ophthalmology, Soroka University Medical Center, Faculty of Health Sciences, Ben-Gurion University of the Negev, P.O. Box 151, 84101 Be'er-Sheva, Israel*

Correspondence should be addressed to Boris Knyazer; knyazer@bgu.ac.il

Received 27 February 2014; Accepted 30 May 2014; Published 22 June 2014

Academic Editor: Jerzy Nawrocki

Objective. To compare visual outcomes of eyes which underwent primary scleral buckling (PSB) treatment during posterior segment open-globe injury (OGI) repair with eyes not treated with PSB. *Methods*. We retrospectively reviewed 38 eyes which underwent a posterior segment OGI repair with no preoperative evidence of retinal detachment (RD) at Soroka University Medical Center (1995–2010). 19 (50%) underwent scleral repair alone (control group) and the other 19 eyes were treated with PSB also (PSB group). We compared visual outcomes in these two groups and rates of subsequent postoperative complications. *Results*. Baseline characteristics of the groups were similar. Compared with the control group, the PSB group had statistically significant lower rates of proliferative vitreoretinopathy (PVR) (5.3% versus 38.4%, $P < 0.05$) and a trend towards lower rates of RD (15.8% versus 41.1%, $P = 0.1$). PSB group eyes had a statistically significant improvement of their best distance visual acuity (BDVA) with lower means of final BDVA-grade ($P < 0.05$) and logMAR vision ($P < 0.05$). Eyes in the control group had no improvement in these parameters. *Conclusion*. PSB procedure during posterior segment OGI repair may decrease the risk of subsequent retinal complications and improve final visual outcome.

1. Introduction

Ocular trauma is a common cause of visual impairment and loss in working age patients [1]. In industrialized nations, eye injury has become the most frequent reason for hospitalization of ophthalmologic patients [2]. In the USA alone, there are approximately 2.4 million eye injuries each year, and more than 40,000 result in permanent visual impairment [3]. *Open-globe injuries* (OGIs), defined as injuries that include a full-thickness defect in the cornea and or sclera [4], have a reported incidence of between 2 and 6 per 100,000 persons per year [2, 5, 6]. The estimated global incidence rate of OGI is 3.5 cases per 100,000 persons per year, leading to approximately 203,000 OGIs per year worldwide [3].

The OGI classification system [4] has identified important prognostic factors for OGIs and hence classifies them based on the zone of injury, mechanism of injury, the presenting visual acuity, and the presence of a relative afferent pupillary defect (RAPD). Another useful system, the ocular trauma scoring (OTS) system [7], is used to classify ocular trauma and to predict the visual outcome of the injured eye, using parameters of presenting visual acuity, mechanism of injury, presence of endophthalmitis, retinal detachment (RD), and RAPD [7].

While *visual outcomes* of eyes with all-types OGIs may vary from full recovery to complete blindness, it is well recognized that posterior segment (zone II and III injuries) OGIs harbor a worse prognosis [8]. Moreover, these injuries, and particularly zone III injuries (which sometimes involve the macula and optic nerve), frequently correlate with a poor *anatomical outcome* [8–12] despite extensive advances in imaging, instrumentation, materials, and surgical procedures over the decades [8].

The growing understanding that the development of RD in posterior segment OGI might initiate an anatomical destructive series [10, 11, 13–18] has raised the interest in

methods that may prevent the development of RD in these injured eyes [19]. *Primary scleral buckling* (PSB) of any posterior segment OGI, that is, supporting the retina and vitreous base with an encircling scleral buckle at the time of the primary repair, is one suggested method. Besides the fact that PSB at the time of initial surgery is technically easier than scleral buckling done afterwards, this procedure has the potential to reduce the rates of vitreoretinal traction and of subsequent development of retinal tears and detachment.

Several studies examined the role of scleral buckling in the management of ocular trauma. Some showed that prophylactic scleral buckling at the time of vitrectomy for posterior segment trauma was associated with better outcomes [8–11]. In two retrospective studies [15, 16], PSB at the time of posterior segment open-globe repair was associated with an improved visual and anatomical outcome. However, this surgical procedure is still controversial [19]; therefore we have designed this study to clarify its possible benefits.

2. Methods

In this retrospective study we identified and analyzed eyes suffering OGI and underwent primary scleral repair alone or with PSB between 1995 and 2010 at Soroka University Medical Center. The local Ethics Committee at our institution approved this study.

Eyes which had an injury limited to zone I only, less than 3 months of follow-up, evidence of RD (per fundus examination or ultrasonography or at the time of the primary surgery), evidence of endophthalmitis, and eyes whose best distance visual acuity (BDVA) data was missing at the presentation or at the end of the follow-up period were excluded from the study. All included eyes were categorized into two groups according to their PSB status (PSB group and control group).

The chart of each patient was reviewed and evaluated to determine demographic features (age and sex), interval time between trauma and surgery, mechanism of injury, zone of injury, initial BDVA-grade, initial logarithm of the minimal angle of resolution (logMAR) vision score, and a calculated OTS score. Mechanism of injury was classified according to the Birmingham Eye Trauma Terminology [20] as rupture or laceration, and lacerations were classified as penetration, perforation, or IOFB. Zone of injury was defined as zone II or zone III according to the Ocular Trauma Classification Group [4]. The initial Snellen-BDVA was derived from visual tests performed at the time of the patient's admission to our institution. Visual acuity was assessed using a Snellen acuity chart for distance or Jaeger card for near vision. When possible, testing was performed with a pinhole. For eyes without formed vision, the acuity was determined as count fingers (CF), hand motion (HM), light perception (LP), or no light perception (NLP) if the patient was unable to see a bright light source such as the light from an indirect ophthalmoscope. The best assessed visual acuity in these tests was documented as the BDVA. BDVA-grade was divided into five categories according to the Snellen-BDVA, grade 1: 6/6–6/12; grade 2: 6/15–6/36; grade 3: 6/60–CF; grade 4: HM and LP; and grade 5: NLP. The logMAR vision score was calculated by obtaining the logarithm of the reciprocal of the Snellen-BDVA for vision better than or equal to 6/60. Otherwise, the following conversion was used: FC = 1.6, HM = 2.0, LP = 2.5, and NLP = 3.0 logMAR units. OTS score was calculated according to the calculation system that was developed by Kuhn et al. [7].

The outcomes evaluated in this study were final BDVA-grade, final logMAR vision score, rates of RD, rates of proliferative vitreoretinopathy (PVR), rates of ocular hypertension, and number of subsequent surgeries. The data regarding the outcomes was obtained from the outpatient record of each patient at his latest follow-up visit in our institution, with all included patients having minimum of 3 months of follow-up. BDVA-grade was determined and logMAR vision score was calculated the way it was described above for the initial data. Data regarding number of subsequent surgeries was collected as an ordinal parameter divided into one surgery, two surgeries, or multiple (three or more) subsequent surgeries during follow-up period. The development of a postoperative RD and PVR was noted for each patient.

All operations in our institute were performed by two well experienced retinal surgeons (Itamar Klemperer and Nadav Belfair) with similar surgical approaches. After detailed examination and exploration of the eyes, primary scleral wound repair was performed in the operating room with nonabsorbable suture such as 8-0 nylon. Cases of vitreous incarceration were treated by scissors or with vitrectomy till complete release of vitreal remnants. Afterwards, in PSB group eyes, an encircling 3.5 to 4.0 mm solid silicone exoplant was placed with four scleral fixation sutures in the middle of each oblique quadrant. Finally, patients received broad spectrum intravenous antibiotics for at least 72 hours after surgery.

2.1. Statistical Analysis. Statistical analysis was carried out using SPSS for Windows (version 19.0.0, SPSS Inc., Chicago, IL, USA). When comparing the baseline characteristics and the outcomes between the two groups, continuous and ordinal variables were analyzed using Mann-Whitney test, and binary variables were analyzed using χ^2 trend test or Fisher's exact test. When comparing between the final and the initial BDVA within each group, analysis was done using Wilcoxon signed-rank test. A P value of 0.05 or less was accepted as statistical significance.

3. Results

Basic data was collected for 85 patients with OGI, of whom 47 were excluded, with the main reasons for exclusion being injuries limited to zone I and lack of recorded data. Full data was obtained for 38 patients with posterior segment OGI who underwent primary scleral repair at Soroka University Medical Center and had no evidence of RD at their presentation on fundus examination, ultrasonography, nor on the surgery itself. Of the 38 patients' eyes, 19 eyes (50%) underwent PSB during the primary scleral repair (PSB group), and 19 eyes (50%) underwent the repair alone (control group).

Table 1: Baseline demographic and clinical characteristics of PSB and control patients.

	PSB group $n = 19$	Control group $n = 19$	P values
Male	16 (84.2%)	18 (94.7%)	0.60
Mean age (yr)	34.53 ± 15.45	36.84 ± 15.75	0.58
Mean lag time between trauma and surgery (hr)	12.53 ± 8.48	12.80 ± 7.21	0.65
Rupture	7 (36.8%)	7 (36.8%)	1.00
Laceration	12 (63.2%)	12 (63.2%)	1.00
Penetration	2 (10.5%)	6 (31.6%)	0.23
Perforation	0 (0%)	2 (10.5%)	0.49
IOFB	10 (52.6%)	6 (31.6%)	0.19
Zone II	5 (26.3%)	6 (31.6%)	0.72
Zone III	14 (73.7%)	13 (68.4%)	0.72
Mean initial BDVA-grade	2.95 ± 1.13	2.84 ± 1.54	0.78
Mean initial logMAR vision score	1.44 ± 0.85	1.39 ± 1.15	0.77
Mean OTS score	2.68 ± 0.82	2.68 ± 1.37	0.90

PSB: primary scleral buckling; IOFB: intraocular foreign body; BDVA: best distance visual acuity; OTS: ocular trauma score; logMAR: logarithm of the minimal angle of resolution.
Continuous and ordinal variables were analyzed using Mann-Whitney test. Binary variables were analyzed using χ^2 trend test or Fisher's exact test.

Table 2: Outcomes for PSB and control patients.

	PSB group $n = 19$	Control group $n = 19$	P values
Mean follow-up (mo)	20.47 ± 14.93	16.00 ± 13.01	0.33
Mean final BDVA-grade	2.37 ± 1.07	2.89 ± 1.45	0.22
Mean final logMAR vision score	1.10 ± 0.73	1.38 ± 0.98	0.36
RD	3 (15.8%)	7 (41.1%)	0.14
PVR	1 (5.3%)	5 (38.4%)	0.03
Ocular hypertension	0 (0%)	1 (5.8%)	0.47
Subsequent surgeries	2.11 ± 0.88	1.95 ± 0.97	0.60

PSB: primary scleral buckling; BDVA: best distance visual acuity; logMAR: logarithm of the minimal angle of resolution; RD: retinal detachment; PVR: proliferative vitreoretinopathy.
Continuous and ordinal variables were analyzed using Mann-Whitney test. Binary variables were analyzed using χ^2 trend test or Fisher's exact test.

Baseline demographic and clinical characteristics of the patients were compared and are presented in Table 1. No statistically significant differences were found. All the eyes underwent the repair less than 24 hours from the injury, with a similar interval time period between the trauma and the surgery ($P = 0.65$, Table 1). All patients were treated with systemic and topical antibiotics, and they all underwent brain and orbits computed tomography scans to exclude intracranial and intraorbital pathology.

Visual and anatomic outcomes in the two groups are presented in Table 2. The mean follow-up for the PSB group was 20.5 months and for the control group it was 16 months, so that time between initial surgery and most recent BDVA assessment was equivalent in the two groups ($P = 0.33$). Compared with the control group, eyes with PSB had statistically significant lower rates of PVR (5.3% versus 38.4%, $P = 0.03$). The PSB group had also lower rates of RD (15.8% versus 41.1%), but this difference did not reach statistical significance ($P = 0.1$). Although not statistically significant, the analysis also suggested a trend toward improved visual outcome in the PSB group. Eyes in the PSB group had a lower mean final BDVA-grade (2.37 versus 2.89, $P = 0.2$) and a lower mean logMAR score vision (1.10 versus 1.38, $P = 0.3$). The number of the subsequent surgeries was similar between the groups ($P = 0.6$). At the end of the follow-up period, no patient suffered from phthysis of the injured eye, nor sympathetic ophthalmia. No cases presented with posttraumatic endophthalmitis.

Another analysis we made was comparison between the final BDVA and the initial BDVA within each group. This analysis revealed that eyes in the PSB group had a statistically significant improvement in their BDVA while the eyes in the control group had no change in their BDVA. Comparing the final and the initial BDVA-grade in the PSB

Table 3: Comparison between the final and the initial BDVA-grade in the PSB group (n = 19). P value = 0.02.

Final BDVA-grade (mean: 2.37)	**5**					
	4		1		1*	1
	3			3*	3	
	2			4	1	
	1	3*	1	1		
		1	**2**	**3**	**4**	**5**
		Initial BDVA-grade (mean: 2.95)				

PSB: primary scleral buckling; BDVA: best distance visual acuity. Analysis was done using Wilcoxon signed-rank test.

Table 4: Comparison between the final and the initial BDVA-grade in the control group (n = 19). P value = 0.96.

Final BDVA-grade (mean: 2.89)	**5**					2*
	4	1	1	1	2*	2
	3			1*	1	
	2	1	1*	1		
	1	3*	2			
		1	**2**	**3**	**4**	**5**
		Initial BDVA-grade (mean: 2.84)				

PSB: primary scleral buckling; BDVA: best distance visual acuity. Analysis was done using Wilcoxon signed-rank test.

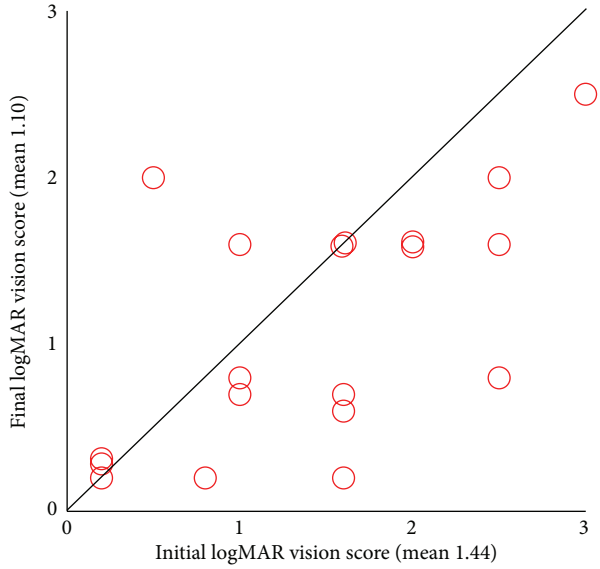

Figure 1: Distribution of final logMAR vision score in correspondence with the initial one in the PSB group (n = 19). P value = 0.04. PSB: primary scleral buckling; logMAR: logarithm of the minimal angle of resolution. Analysis was done using Wilcoxon signed-rank test.

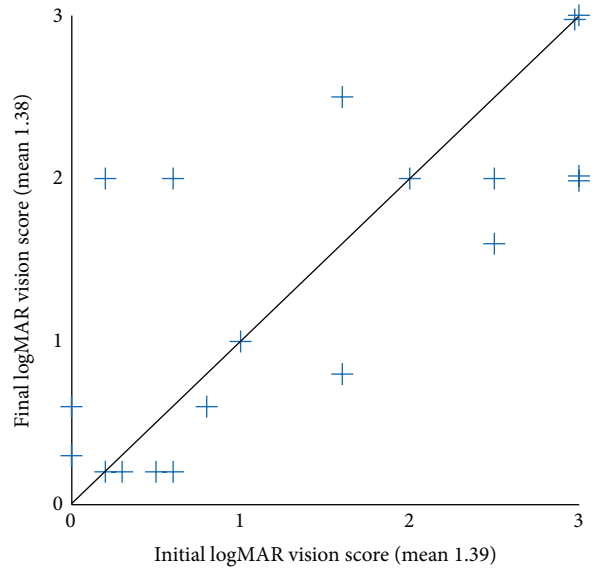

Figure 2: Distribution of final logMAR vision score in correspondence with the initial one in the control group (n = 19). P value = 0.73. LogMAR: logarithm of the minimal angle of resolution. Analysis was done using Wilcoxon signed-rank test.

group (Table 3) showed statistically significant improvement of 0.58 steps in the mean BDVA-grade of these eyes, from mean initial BDVA-grade of 2.95 to final BDVA-grade of 2.37 (P = 0.02), with only 1 of the 19 eyes having deteriorated final BDVA-grade. LogMAR vision score analysis of the PSB group eyes (Figure 1) showed again a statistically significant improvement, from initial mean score of 1.44 to a final mean score of 1.10 (P = 0.04). The same statistical analysis for the control group eyes found no improvement of their BDVA. Comparison between the final and the initial visual parameters showed statistical similarity for both BDVA-grade (P = 0.96, Table 4) and logMAR vision score (P = 0.73, Figure 2), as is also indicated with a fairly even distribution above and beneath the line in Table 4 and in Figure 2.

4. Discussion

Posterior segment OGIs are associated with poor visual and anatomical outcomes [8–12]. A series of anatomical events following an OGI has been described in animal models [13] and appears to follow an analogous series in humans. This series begins with the development of retinal breaks or rhegmatogenous detachment which tend to occur weeks to months following the injury. A subsequent PVR might evolve with the formation of a fibrocellular membrane and a possible further traction [14]. Theoretically, prevention of RD formation in an open-globe injured eye may halt that anatomical course and improve its prognosis. PSB procedure may offer such prevention but still is not considered a consensus [19] and lacks an evidence-based benefit.

In this study, we compared two groups of eyes with posterior segment OGIs which had no evidence of RD at their presentation and underwent their initial surgery at Soroka University Medical Center, Be'er-Sheva, Israel, between 1995 and 2010. The PSB group underwent PSB in addition to their primary scleral repair, and the control group underwent posterior segment open-globe repair alone.

In our study, 41.1% of the eyes in the control group developed RD after the initial open-globe repair, whereas

only 15.8% of the eyes in the PSB group developed a RD. The rate of RD in our control group eyes is comparable to the rate reported in the ophthalmologic literature for all-OGI eyes (40–57%) [10, 11, 15–17], and the rate of RD in our PSB group is lower than this reported rate. RD rate in our PSB group is comparable to that reported in the PSB group of the matched study published by Arroyo et al. (26%) [16]. Such trend is also seen in the analysis of PVR development in our study, which occurs in 10–45% of injured eyes according to previous literature [17, 18]. In our study, the control group had a PVR rate of 38.4% (within the reported range), whereas the PSB group had PVR rate of 5.3% only.

Comparing the outcomes between the PSB and the control groups after average follow-up greater than 18 months, our findings suggest that the addition of PSB at the time of the initial surgery decreases the incidence of subsequent PVR ($P < 0.05$) and may decrease the rates of subsequent RD ($P = 0.14$). Moreover, it may improve the final BDVA of these injured eyes ($P = 0.22$ for final BDVA-grade, and $P = 0.36$ for final logMAR vision). These findings suit the assumption that PSB procedure may improve anatomical and visual outcomes.

Another finding of our study can be derived from comparison of initial to final BDVA within each group. It can be concluded that the addition of PSB improves BDVA while having the repair alone does not change BDVA. This finding can be also derived from the results reported by Arroyo et al. [16] although it was not analyzed statistically there.

Comparison of baseline characteristics between both groups in the study found no statistically significant differences (Table 1). However, one nonsignificant difference strengthens our conclusions regarding the advantages of PSB procedure. The PSB group had worse initial BDVA. Given that poor initial BDVA predicts poor prognosis in OGI cases, one could predict that the PSB group would have worse visual outcome. However, our results showed that PSB group eyes had actually better visual outcome.

Our study has still some limitations. First, this study is a retrospective study which is weaker than a prospective one. Furthermore, the study did not include a case-case matching since an attempt we made to match the eyes according to their baseline injury characters ended with a very low number of couples and a very low potential statistical power. Secondly, owing to limited patient documentation, the two groups could not be compared at few baseline parameters (such as presence of RAPD, choroidal detachment, vitreous haemorrhage, cataract, length of laceration, etc.). Thirdly, this study has finally included relatively few eyes, hence low statistical power. Only one difference between the groups (in PVR) reached statistical significance.

5. Conclusion

Our study suggests that adding PSB procedure during posterior segment OGI repair in eyes without evidence of RD at the presentation decreases the risk of subsequent PVR, may decrease subsequent RD, and may improve BDVA when compared to repair alone. In addition, final BDVA is improved compared to the initial BDVA when PSB is added, while it may not change when having the repair alone. These results suggest that PSB in these eyes may have the potential to alter the expected anatomic consequences of their eye injury and hence may improve their overall outcome. Given the high incidence of ocular trauma in the working age population and its poor prognosis, a larger retrospective study, a meta-analysis, or a randomized clinical trial is warranted to more definitively examine the role of PSB.

Disclosure

This study was performed in partial fulfillment of the M.D. thesis requirements of author Dan Cohen, and its main results were presented in the annual conference of the Israel Ophthalmology Society (ILOS), May 2013.

Conflict of Interests

The authors declare that there is no conflict of interests regarding the publication of this paper. None of the authors has any financial interest in the products used in this study.

References

[1] L. M. Parver, A. L. Dannenberg, B. Blacklow, C. J. Fowler, R. J. Brechner, and J. M. Tielsch, "Characteristics and causes of penetrating eye injuries reported to the National Eye Trauma System Registry, 1985–91," *Public Health Reports*, vol. 108, no. 5, pp. 625–632, 1993.

[2] J. M. Tielsch, L. Parver, and B. Shankar, "Time trends in the incidence of hospitalized ocular trauma," *Archives of Ophthalmology*, vol. 107, no. 4, pp. 519–523, 1989.

[3] G. W. Schmidt, A. T. Broman, H. B. Hindman, and M. P. Grant, "Vision survival after open globe injury predicted by classification and regression tree analysis," *Ophthalmology*, vol. 115, no. 1, pp. 202–209, 2008.

[4] D. J. Pieramici, P. Sternberg Jr., T. M. Aaberg Sr. et al., "A system for classifying mechanical injuries of the eye (globe)," *American Journal of Ophthalmology*, vol. 123, no. 6, pp. 820–831, 1997.

[5] T. A. Karlson and B. E. K. Klein, "The incidence of acute hospital-treated eye injuries," *Archives of Ophthalmology*, vol. 104, no. 10, pp. 1473–1476, 1986.

[6] S. Blomdahl and S. Norell, "Perforating eye injury in the Stockholm population. An epidemiological study," *Acta Ophthalmologica*, vol. 62, no. 3, pp. 378–390, 1984.

[7] F. Kuhn, R. Maisiak, L. Mann, V. Mester, R. Morris, and C. D. Witherspoon, "The ocular trauma score (OTS)," *Ophthalmology Clinics of North America*, vol. 15, no. 2, pp. 163–165, 2002.

[8] D. J. Pieramici, M. W. MacCumber, M. U. Humayun, M. J. Marsh, and J. De Juan E., "Open-globe injury: update on types of injuries and visual results," *Ophthalmology*, vol. 103, no. 11, pp. 1798–1803, 1996.

[9] D. G. Fuller and W. L. Hutton, "Prediction of postoperative vision in eyes with severe trauma," *Retina*, vol. 10, supplement 1, pp. S20–S34, 1990.

[10] G. S. Brinton, T. M. Aaberg, F. H. Reeser, T. M. Topping, and G. W. Abrams, "Surgical results in ocular trauma involving the posterior segment," *American Journal of Ophthalmology*, vol. 93, no. 3, pp. 271–278, 1982.

[11] W. L. Hutton and D. G. Fuller, "Factors influencing final visual results in severely injured eyes," *American Journal of Ophthalmology*, vol. 97, no. 6, pp. 715–722, 1984.

[12] B. Knyazer, J. Levy, S. Rosen, N. Belfair, I. Klemperer, and T. Lifshitz, "Prognostic factors in posterior open globe injuries (zone-III injuries)," *Clinical and Experimental Ophthalmology*, vol. 36, no. 9, pp. 836–841, 2008.

[13] P. E. Cleary and S. J. Ryan, "Method of production and natural history of experimental posterior penetrating eye injury in the rhesus monkey," *American Journal of Ophthalmology*, vol. 88, no. 2, pp. 212–220, 1979.

[14] P. K. Leaver, "Proliferative vitreoretinopathy," *The British Journal of Ophthalmology*, vol. 79, no. 10, pp. 871–872, 1995.

[15] T. W. Stone, N. Siddiqui, J. G. Arroyo, B. W. McCuen II, and E. A. Postel, "Primary scleral buckling in open-globe injury involving the posterior segment," *Ophthalmology*, vol. 107, no. 10, pp. 1923–1926, 2000.

[16] J. G. Arroyo, E. A. Postel, T. Stone, B. W. McCuen, and K. M. Egan, "A matched study of primary scleral buckle placement during repair of posterior segment open globe injuries," *British Journal of Ophthalmology*, vol. 87, no. 1, pp. 75–78, 2003.

[17] L. Wickham, W. Xing, C. Bunce, and P. Sullivan, "Outcomes of surgery for posterior segment intraocular foreign bodies—a retrospective review of 17 years of clinical experience," *Graefe's Archive for Clinical and Experimental Ophthalmology*, vol. 244, no. 12, pp. 1620–1626, 2006.

[18] D. G. Charteris, C. S. Sethi, G. P. Lewis, and S. K. Fisher, "Proliferative vitreoretinopathy—developments in adjunctive treatment and retinal pathology," *Eye*, vol. 16, no. 4, pp. 369–374, 2002.

[19] R. A. Mittra and W. F. Mieler, "Controversies in the management of open-globe injuries involving the posterior segment," *Survey of Ophthalmology*, vol. 44, no. 3, pp. 215–225, 1999.

[20] F. Kuhn, R. Morris, and C. D. Witherspoon, "Birmingham Eye Trauma Terminology (BETT): terminology and classification of mechanical eye injuries," *Ophthalmology Clinics of North America*, vol. 15, no. 2, pp. 139–143, 2002.

Hindawi Publishing Corporation
BioMed Research International
Volume 2014, Article ID 639160, 7 pages
http://dx.doi.org/10.1155/2014/639160

Research Article

Correlation of Choroidal Thickness and Volume Measurements with Axial Length and Age Using Swept Source Optical Coherence Tomography and Optical Low-Coherence Reflectometry

Janusz Michalewski, Zofia Michalewska, Zofia Nawrocka, Maciej Bednarski, and Jerzy Nawrocki

Ophthalmic Clinic Jasne Blonia, ul. Rojna 90, 91-162 Lodz, Poland

Correspondence should be addressed to Zofia Michalewska; zosia_n@yahoo.com

Received 26 February 2014; Accepted 20 May 2014; Published 12 June 2014

Academic Editor: Ron Adelman

Purpose. To report choroidal thickness and volume in healthy eyes using swept source optical coherence tomography (SS-OCT). *Methods*. A prospective observational study of 122 patients examined with swept source OCT (DRI-OCT, Topcon, Japan). In each eye, we performed 256 horizontal scans, 12 mm in length and centered on the fovea. We calculated choroidal thickness manually with a built-in caliper and automatically using DRI-OCT mapping software. Choroidal volume was also automatically calculated. We measured axial length with optical low-coherence reflectometry (Lenstar LS 900, Haag-Streit, Switzerland). *Results*. The choroid has focally increased thickness under the fovea. Choroid was thinnest in the outer nasal quadrant. In stepwise regression analysis, age was estimated as the most significant factor correlating with decreased choroidal thickness ($F = 23.146$, $P < 0.001$) followed by axial length ($F = 4.902$, $P = 0.03$). Refractive error was not statistically significant ($F = 1.16$, $P = 0.28$). *Conclusions*. SS-OCT is the first commercially available system that can automatically create choroidal thickness and volume maps. Choroidal thickness is increased at the fovea and is thinnest nasally. Age and axial length are critical for the estimation of choroidal thickness and volume. Choroidal measurements derived from SS-OCT images have potential value for objectively documenting disease-related choroidal thickness abnormalities and monitoring progressive changes over time.

1. Introduction

The choroid is a vascular layer that supplies the retina with oxygen and nutrition. Until recently, the only diagnostic tool for visualization of choroid was indocyanine angiography. This is an invasive intervention and can only present blood flow and not histological sections. Optical coherence tomography (OCT) devices were primarily designed to visualize the retina and did not reveal structures lying beneath the retinal pigment epithelium due to light scattering on choroidal vasculature. The function of the choroid is associated with many diseases affecting the retina. Thus, imaging and quantitative assessment of choroidal tissue may be of value for the diagnosis of many retinal and choroidal diseases. Spaide et al., using spectral domain OCT (SD-OCT), (Spectralis OCT Heidelberg Engineering, Heidelberg, Germany), was the first to present that SD-OCT may enable the creation of an inverted image when the device is moved closer to the eye. Since SD-OCT has the highest sensitivity near to zero-delay and sensitivity decreases for larger delays, by inverting the OCT image, the choroid is closer to the zero-delay line, providing enhanced sensitivity and increased imaging depth. The device was called EDI-OCT (enhanced depth OCT) [1]. Other authors have confirmed this observation using other commercially available SD-OCT devices [2]. The inverted image in SD-OCT enables measurement of the choroid at several points. However, the system cannot create 3-dimensional choroid maps as the choroidoscleral boundary may not be detected in all cases due to scattering and low penetration through the RPE, which is influenced by the wavelength

used. Some authors attempted to measure choroidal thickness and volume after manual choroidal segmentation [3]. This is perhaps too time-consuming and too complicated for everyday ophthalmic practice. The ability to create choroidal maps, with repeatability similar to the way current SD-OCT devices enable the creation of retina maps, could enable us to precisely determine the mean choroidal thickness in healthy subjects and possibly add information to the pathogenesis and course of various retinal diseases. To produce repeatable choroidal maps, we need exact delineation of the outer choroidal layer, which may be obtained by using a longer light wavelength [4].

The commercially available swept source OCT (SS-OCT; DRI-OCT, Topcon, Japan) uses a longer wavelength than SD-OCT (1050 nm versus 840 nm). Longer wavelengths overcome much of the scattering of light on choroidal vasculature, thus it enables a more exact visualization of the choroid. The purpose of the current study was to determine choroidal thickness and volume in healthy subjects with a commercially available SS-OCT device, furthermore, to correlate the results with age, refractive error, and axial length measured with optical low-coherence reflectometry.

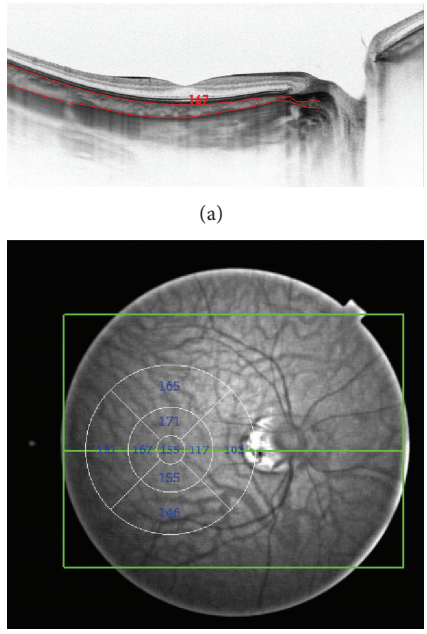

(a)

(b)

Figure 1: (a) Swept source OCT in a healthy volunteer. The red horizontal lines were drawn automatically at the inner and outer choroidal boundaries. The vertical line was drawn manually, to measure central choroidal thickness. (b) Swept source OCT fundus view. The circle and numbers are drawn automatically and represent automated thickness and volume measurements, which were performed in 9 segments according to early treatment diabetic retinopathy study.

2. Material and Methods

We included into this prospective study 122 eyes of 122 healthy volunteers with no visual symptoms or history of ocular disease. The Institutional Ethics Committee Board approved the design of the study. The study is also in adherence with the Declaration of Helsinki. All patients had a comprehensive ophthalmic examination. We carried out OCT imaging using the first commercially available SS-OCT device (DRI-OCT, Topcon, Japan) with a wavelength of 1024 nm and used optical low-coherence reflectometry to measure axial length by optical biometry (Lenstar LS 900, Haag-Streit, Switzerland). Axial length measurement is reportedly very precise with this device, as it is based on a similar mechanism to time domain OCT [5]. We measured spherical equivalent refractive error with an Auto Refractometer (NIDEK Co., Ltd., Japan).

Only patients with no abnormalities both in ophthalmic examination and in SS-OCT were included in the current analysis. Patients with a high refractive error were also included. To exclude diurnal variations all examinations were performed at the same time (3–6 pm). It was estimated in earlier studies that axial length is stable during this time period, lower than that at noon and higher than that in the evening [6].

In all cases, two experienced examiners performed two scanning protocols. First, for manual estimation of choroidal thickness we took a single line scan with a resolution of 3 μm, built from 1024 A-scans with a length of 12 mm. Second, we carried out a 3-dimensional scanning protocol with 3 μm axial resolution and a speed of 100,000 A-scans per second. In this protocol, 256 B-scans were taken on an area of 12×9 μm.

We took manual choroidal thickness measurements between the line representing retinal pigment epithelium, the outer most hyperreflective retinal layer, and the line representing lamina suprachoroidea, the outer hyperreflective line of the choroid. The caliper used for manual segmentation was included in the software. Black on white images were analyzed to exactly spot the outer choroidoscleral boundary (Figure 1(a)).

We utilized the built-in choroidal segmentation tool to automatically define the outer border of the choroid and measured choroidal thickness between the lines indicating retinal pigment epithelium and the choroidoscleral boundary (lamina suprachoroidea) [7]. Choroidal thickness and volume were automatically calculated using the built-in software (Figure 1). We calculated numeric averages of the measurements for each of the 9 map sectors defined by the early treatment diabetic retinopathy study (ETDRS) [8]. The inner and outer rings with diameters of 3 mm and 6 mm, respectively, were segmented into 4 quadrants. Mean choroidal thickness at the fovea was defined as the average thickness in the central 1000 μm diameter of the early treatment diabetic retinopathy study layout (Figure 1(b)).

Using linear regression analysis and stepwise multiple regression analysis, we investigated the relationship between foveal choroidal thickness and age, sex, spherical equivalent of the refractive error, and axial length. ANOVA on ranks test was performed to compare choroidal thickness and volume in different quadrants. We performed statistical analysis with commercially available software (SigmaStat 3.5 for Windows).

Table 1: Choroidal thickness measurement.

	All (μm) (mean age 43.2 years)	Emmetropia (mean age 44.7 years)	All myopic eyes (mean age 41.4 years)	High myopia (>6 Dptr) (mean age 42.6 years)	Hyperopia (mean age 56.9 years)
Fovea manually determined	259	326	231	187	312
Fovea automatically determined (1000 μm diameter)	221	259	208	172	234.7
			Inner ring (3 mm diameter)		
Superior	220	268	204	176	221
Inferior	214	252	200	159	233
Temporal	217	251	204	170	231
Nasal	202	240	188	157	221
			Outer ring (6 mm diameter)		
Superior	231	280	211	176	265
Inferior	210	236	188	157	257
Temporal	216	247	204	174	228
Nasal	182	226	165	140	212

3. Results

The current study included 122 eyes of 122 healthy volunteers. Their mean age was 43 years (15–79 years, SD: 17 years); 52 subjects were male and 70 were female. Spherical equivalents varied from −22 diopter to +6 diopter. 27 eyes were emmetropic, 85 eyes were myopic (44 had high myopia: considered as spherical equivalent >6 D), and 10 eyes were hyperopic. The mean axial length measured with optical low-coherence reflectometry was 25.07 mm (21.33 mm–31.04 mm; SD: 2.19 mm).

3.1. Choroidal Thickness. Table 1 shows the mean choroidal thicknesses by sector.

Fovea thickness measured manually was significantly thicker than when measured automatically ($P = 0.04$), which may be explained by the fact that the manual measurement is a focal measurement and that the automatic measurement measures the mean thickness in a circle with a diameter of 1000 μm. In eyes with high myopia the automatic and manual measurements did not differ ($P = 0.42$), which may be explained by the lack of focal central increased choroidal thickness in high myopia.

Focal measurements of foveal choroidal thickness were significantly thicker than when automatically measured in all quadrants ($P < 0.001$). Automatically measured foveal choroidal thickness did not significantly differ from any quadrant in the inner ring (inferior quadrant: $P = 0.4$, superior quadrant $P = 0.8$, nasal quadrant: $P = 0.08$, and temporal quadrant $P = 0.59$) but it was significantly thicker than the nasal quadrant in the outer ring (inferior quadrant $P = 0.2$, superior quadrant $P = 0.3$, nasal quadrant: $P < 0.001$, and temporal quadrant $P = 0.57$). Also in the inner ring the choroid was not statistically different on any side of the fovea (nasal versus temporal: $P = 0.727$; inferior versus superior: $P = 0.293$). In the outer ring, the choroid nasal to the fovea was thinner than inferior to the fovea ($P = 0.034$), superior to the fovea ($P < 0.001$), and on the temporal side ($P < 0.001$).

3.2. Choroidal Volume. Choroidal volumes in the outer temporal, superior, and inferior quadrant are bigger than in the outer nasal quadrant ($P < 0.001$). Table 2 shows the mean choroidal volume by sector.

Central choroidal volume was significantly smaller than in all quadrants of the inner and outer rings ($P < 0.001$). However, choroidal volume in different ETDRS subfields is measured from different geometrical figures. Choroidal volume in the fovea is the volume of a cylinder with an upper and lower diameter of 1000 μm and the height of the cylinder is the foveal choroidal thickness ($V = \pi r^2 h$; V—cylinder volume, r—radius, and h—height). Choroidal volumes in the inner and outer quadrants are volumes of irregular geometrical figures with base diameters bigger than the foveal, which explains why the choroidal volume values in all subfields are bigger than in the center and that they should not be compared directly. What we can separately compare are the values in the inner circle and the values in the outer circle. In the inner circle no statistical difference was observed between particular subfields (Kruskal-Wallis one-way analysis of variance on ranks; $P = 0.2$, $H = 4.071$). In the outer circle the nasal subfield had significantly lower volume than all other subfields (Tukey's test, $P < 0.05$).

3.3. Adequacy of the Automated Segmentation. In all cases the examiner was able to estimate the outer choroidal boundary. However in 16% of cases a discrepancy existed between the examiners estimation and the automated measurement. In those cases the automatically drawn lines were manually corrected by the examiners.

Table 2: Choroidal volume measurement.

	All (μm^3) (mean age 43.2 years)	Emmetropia (mean age 44.7 years)	All myopic eyes (mean age 41.4 years)	High myopia (>6 Dptr) (mean age 42.6 years)	Hyperopia (mean age 56.9 years)
Fovea automatically determined (1000 μm^3 diameter)	0.17	0.2	0.16	0.13	0.18
		Inner ring (3 mm diameter)			
Superior	0.46	0.4	0.48	0.59	0.35
Inferior	0.34	0.4	0.31	0.25	0.37
Temporal	0.34	0.37	0.32	0.26	0.36
Nasal	0.31	0.4	0.29	0.24	0.35
		Outer ring (6 mm diameter)			
Superior	1.2	1.47	1.12	0.94	1.4
Inferior	1.1	1.24	1.06	0.86	1.36
Temporal	1.1	1.3	1.0	0.91	1.2
Nasal	0.9	1.17	0.87	0.75	1.1

3.4. Relation to Sex, Age, Refractive Error, and Axial Length. Sex was not found to significantly influence choroidal thickness in the whole group ($P = 0.47$).

Age was found to be negatively correlated with central choroidal thickness (both when automatically measured and manually measured; $P < 0.001$) and with central choroidal volume ($P < 0.001$). Regression analysis revealed that choroidal thickness decreases 1.289 μm each year $R^2 = 0.08$ (Figure 2).

Choroidal thickness and volume are also negatively statistically significant dependent on the refractive error ($P < 0.001$). Regression analysis showed that choroidal thickness decreases 12.7 μm with each diopter ($R^2 = 0.25$).

Axial length measured with low-coherence reflectometry was also found to be negatively correlated with choroidal thickness and volume ($P < 0.001$). Regression analysis shows that choroidal thickness decreases 28 μm with each mm of axial length ($R^2 = 0.3$) (Figure 3).

We also performed stepwise multiple regression analysis to calculate which of the factors, age, axial length and refractive error, are associated the most with choroidal thickness. Age was estimated as the most significant factor ($F = 23.146$, $P < 0.001$) followed by axial length ($F = 4.902$, $P = 0.03$). Refractive error showed no significant association with choroidal thickness in multiple regression analysis ($F = 1.16$, $P = 0.28$).

Stepwise regression analysis also revealed that foveal choroidal volume can be predicted from a linear combination of two independent variables among the above mentioned factors: age ($F = 22.711$, $P < 0.001$) and axial length ($F = 39.366$, $P < 0.001$). Refractive error was not estimated as an independent factor in the stepwise regression analysis ($F = 2.952$, $P = 0.08$).

4. Discussion

The Topcon DRI-OCT machine we used was the first commercially available device of its kind. It enables automatic creation of choroidal volume and thickness maps. To date (PubMed Medline) this study involves the largest patient population examined, in which automatically measured choroidal thickness and volume are correlated with sex, age, refractive error, and axial length, not only in normal subjects but also in high myopia and hyperopia (from −22 diopter to +6 diopter).

Stepwise multiple regression analysis confirmed that choroidal thickness and volume, measured with a commercially available SS-OCT device, correlate with two independent variables, axial length, measured with optical low-coherence reflectometry, and age. The choroid both is the thinnest and has the smallest volume nasally. The focal increase of choroidal thickness at the fovea may be explained by increased metabolism.

EDI-OCT was earlier used to measure choroidal thickness. It has the highest sensitivity near to zero-delay and that sensitivity decreases for larger delays; an inversion of the OCT image was proposed, to move the zero-delay line closer to the choroid, providing enhanced sensitivity and increased imaging depth. Choroidal thickness can then be assessed with point-to-point manual caliper measurement taken on a single line scan, which is limited to the subfovea [9–11]. Some authors have suggested using the 6-line scanning protocol to obtain more information [12]. Volume measurement is obtained from compilation of a series of B-scans. To enable automated volume measurement the resolution of borders of the measured area must be clearly visible and distinguishable in all cases. Even if SD-OCT is able to provide retina volume measurements, no commercially available device is able to create choroidal thickness and volume maps. This is probably due to the fact that choroidoscleral boundary is not perfectly visible in all cases. As swept source OCT devices employ a longer light wavelength (1050 nm versus 840 nm in SD-OCT) they overcome much of the scattering of light on choroidal vasculature. SS-OCT obtains time-encoded information by sweeping a narrow-bandwidth laser through a broad optical spectrum. The backscattered intensity is detected with

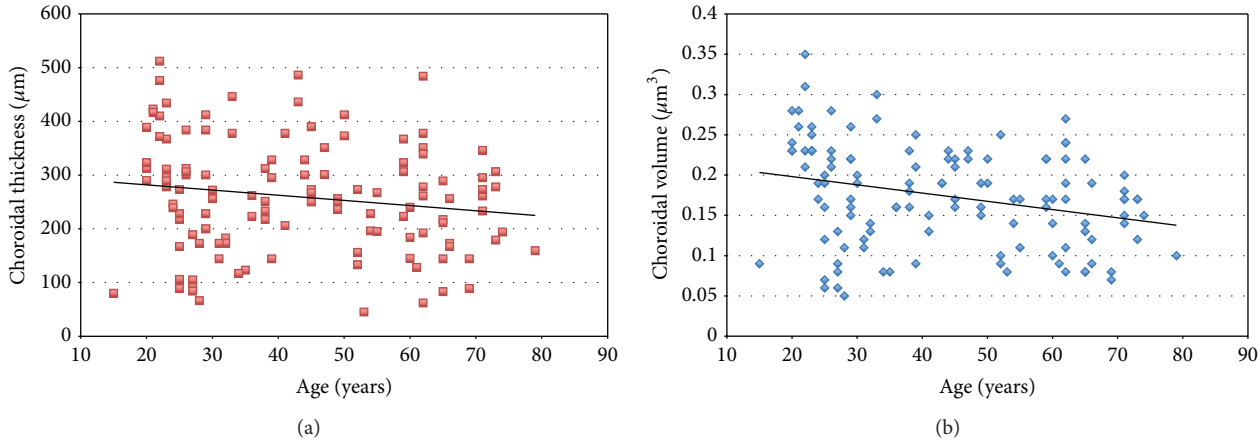

FIGURE 2: Choroidal thickness (a) and volume (b) correlate negatively with age ($P < 0.001$).

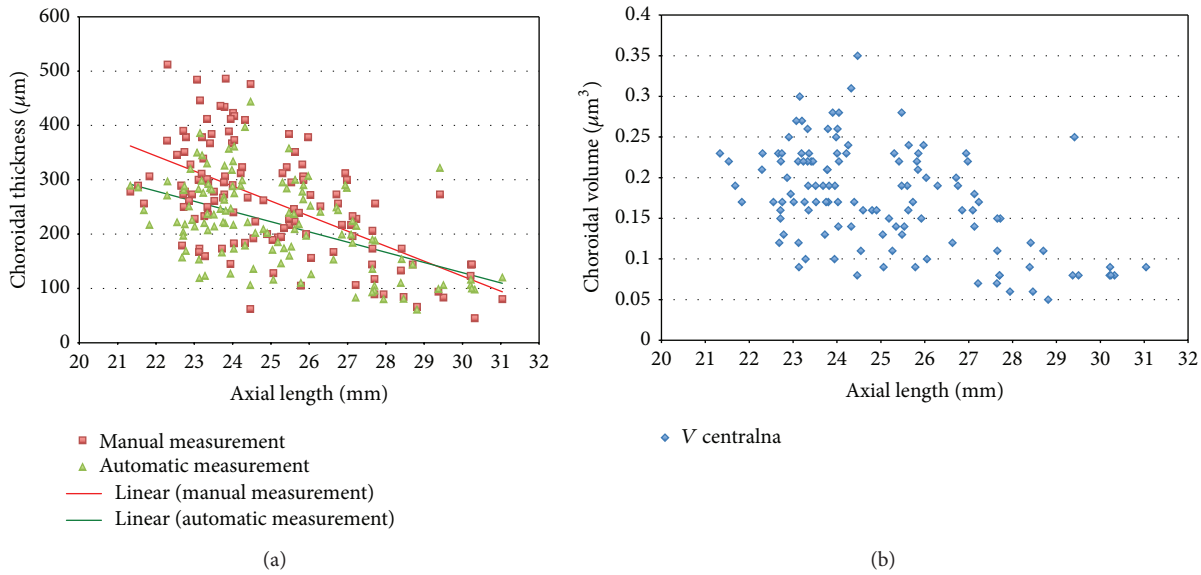

FIGURE 3: Choroidal thickness (a) and volume (b) correlate negatively with axial length ($P < 0.001$).

a photodetector and not with the spectrometers and CCD cameras used in SD-OCT devices. CCD cameras have a finite pixel size and thus there is a drop-off in signal with depth. Using photodetectors instead has led to a further increase in the potential resolution (1 μm). The scan speed in swept-source instruments is twice that of SD-OCT devices (100,000 A-scans/sec compared to 50,000 A-scans/sec.). This enables faster acquisition of B-scans and a more accurate 3-dimensional image of the retina and choroid. It was earlier confirmed that despite the different wavelengths choroidal measurements performed with EDI-SOCT and SS-OCT are highly comparable [13].

This paper is the first to present automatic choroid thickness and volume measurements performed with a commercially available SS-OCT device in a wide range of patients in regard to age (15–79 years) and refractive error (−22 diopter to +6 diopter). The possibility of obtaining choroidal volume scans was presented before [14].

At 221 μm the mean subfoveal choroidal thickness we measured with SS-OCT is lower than that previously reported in SD-OCT studies (272 μm–354 μm) and is lower than the results obtained with the prototype version of SS-OCT performed on Japanese subjects (354 μm) [14].

However, the mean focal subfoveal choroidal thickness (choroidal thickness at the foveola) measured manually was 259 μm, which is more comparable to the previous results mentioned above. The different results may be due to differences in how the measurements are taken. With the earlier SD-OCT machines and the SS-OCT prototype, choroidal thickness measurement is possible only manually at certain spots whereas we were additionally able to measure the mean subfoveal choroidal thickness in all 9 map sectors as defined by ETDRS. Thus, automatic foveal choroidal thickness measurement corresponds to an area with a diameter of 1000 μm, centered on the foveola. The results we obtained may indicate that any increase in choroidal thickness is only focal and that

thickness decreases with the distance from the foveola. Additionally in our group many myopic subjects were included. Another explanation may be that the difference is due to incorrect measurement by the automated software.

Our study confirms earlier SD-OCT and prototype SS-OCT reports that the choroid is thinnest on the nasal side of the fovea. Automatic measurement in certain sectors additionally enabled us to determine that this decrease reaches statistical significance about 1.5 mm from the foveola.

Moreover, this paper is the first to present quantitative measurement of choroidal volume. We succeeded in confirming that choroidal volume is lowest on the nasal side of the fovea, with statistical significance about 1.5 mm from the foveola. Choroidal volume in different ETDRS subfields is measured from different geometrical figures, thus central volume cannot be compared with volumes in the outer and inner rings. Choroidal volume in the fovea is the volume of a cylinder with an upper and lower diameter of 1000 μm and the height of the cylinder is the foveal choroidal thickness ($V = \pi r^2 h$; V—cylinder volume, r—radius, and h—height). Choroidal volumes in the inner and outer quadrants are volumes of irregular geometrical figures with base diameters bigger than the foveal, which explains why the choroidal volume values in all subfields are bigger than in the center. Our SS-OCT study presents a mean subfoveal choroidal volume of 0.17 mm^3, which is lower than in the earlier SD-OCT studies by Shin et al., who reported 0.24 mm^3 [12].

Using multiple regression analysis, we demonstrated that choroidal thickness independently correlates with age and axial length. Correlation between choroidal thickness and age is well established. Autopsy studies have reported a 1.1 μm decrease per year, previous SD-OCT studies have suggested 0.9 μm–1.54 μm per year, and early SS-OCT studies performed with a prototype device reported that the mean decrease is about 14 μm every 10 years [13–17]. Our study presents a yearly mean decrease of 1.289 μm. Our figure may be affected by the R^2 measurements in our study being as low as 0.08 which, in itself, confirms the great interindividual variability also reported by Ikuno et al. [15]. In our study for example, three 20-year-old patients had an axial length of 24 mm yet their central choroidal thickness varied from 288 μm to 361 μm. Ruiz-Moreno et al. on the other hand reported no differences in choroidal thickness between pediatric and older populations [18]. It may require further studies to determine which other factors are responsible for intraindividual changes in choroidal thickness. It may vary with race or other genetic predispositions or other unknown factors.

Regression analysis also revealed that choroidal thickness decreases 18.7 μm with every decrease of 1 diopter ($R^2 = 0.2$). This is more than what Ikuno et al. proposed (9.3 μm per diopter) perhaps because their analysis only included healthy subjects without high myopia whilst our group analyzed a wider spectrum of refractive errors (from −22 to +6 diopter).

Multivariate analysis by Ikuno et al. suggested that refractive error also independently correlates with choroidal thickness whereas we found no correlation. Again, this may be because Ikuno et al. included a low spectrum of axial lengths and refractive errors in their study and we investigated individuals from high myopia to hyperopia [15].

To conclude with, SS-OCT enables automatic creation of choroidal thickness and volume maps.

This study presents that choroid is at its thinnest nasally, about 1.5 mm from the fovea. Choroidal volume is also lowest on the nasal side.

Multivariate analysis confirmed that choroidal thickness independently decreases with increasing age and higher axial length.

Conflict of Interests

The authors declare that there is no conflict of interests regarding the publication of this paper.

References

[1] R. F. Spaide, H. Koizumi, and M. C. Pozonni, "Enhanced depth imaging spectral-domain optical coherence tomography," *The American Journal of Ophthalmology*, vol. 146, no. 4, pp. 496–500, 2008.

[2] V. Manjunath, M. Taha, J. G. Fujimoto, and J. S. Duker, "Choroidal thickness in normal eyes measured using cirrus HD optical coherence tomography," *The American Journal of Ophthalmology*, vol. 150, no. 3, pp. 325–329, 2010.

[3] G. Barteselli, J. Chhablani, S. El-Emam et al., "Choroidal volume variations with age, axial length, and sex in healthy subjects: a three-dimensional analysis," *Ophthalmology*, vol. 119, no. 12, pp. 2572–2578, 2012.

[4] Z. Michalewska, J. Michalewski, and J. Nawrocki, "New OCT technologies take imaging deeper and wider," *Retinal Physycian*, vol. 10, pp. 42–48, 2013.

[5] M. P. Holzer, M. Mamusa, and G. U. Auffarth, "Accuracy of a new partial coherence interferometry analyser for biometric measurements," *The British Journal of Ophthalmology*, vol. 93, no. 6, pp. 807–810, 2009.

[6] R. Chakraborty, S. A. Read, and M. J. Collins, "Diurnal variations in axial length, choroidal thickness, intraocular pressure, and ocular biometrics," *Investigative Ophthalmology and Visual Science*, vol. 52, no. 8, pp. 5121–5129, 2011.

[7] J. Michalewski, J. Nawrocki, Z. Nawrocka, K. Dulczewska-Cichecka, and J. Nawrocki, "Lamina suprachoroidea and suprachoroidal space delineating the outermargin of the choroid in swept-source OCT," *Retina*. In press.

[8] Early Treatment Diabetic Retinopathy Study Research Group, "ETDRS report number 7: early treatment diabetic retinopathy study design and baseline patient characteristics," *Ophthalmology*, vol. 98, supplement 5, pp. 741–756, 1991.

[9] E. A. McCourt, B. C. Cadena, C. J. Barnett, A. P. Ciardella, N. Mandava, and M. Y. Kahook, "Measurement of subfoveal choroidal thickness using spectral domain optical coherence tomography," *Ophthalmic Surgery, Lasers & Imaging*, vol. 41, no. 6, pp. S28–S33, 2010.

[10] Y. Imamura, T. Fujiwara, R. Margolis, and R. F. Spaide, "Enhanced depth imaging optical coherence tomography of the choroid in central serous chorioretinopathy," *Retina*, vol. 29, no. 10, pp. 1469–1473, 2009.

[11] T. Fujiwara, Y. Imamura, R. Margolis, J. S. Slakter, and R. F. Spaide, "Enhanced depth imaging optical coherence tomography of the choroid in highly myopic eyes," *The American Journal of Ophthalmology*, vol. 148, no. 3, pp. 445–450, 2009.

[12] J. W. Shin, Y. U. Shin, and B. R. Lee, "Choroidal thickness and volume mapping by a six radial scan protocol on spectral-domain optical coherence tomography," *Ophthalmology*, vol. 119, no. 5, pp. 1017–1023, 2012.

[13] Y. Ikuno, I. Maruko, Y. Yasuno et al., "Reproducibility of retinal and choroidal thickness measurements in enhanced depth imaging and high-penetration optical coherence tomography," *Investigative Ophthalmology and Visual Science*, vol. 52, no. 8, pp. 5536–5540, 2011.

[14] M. Hirata, A. Tsujikawa, A. Matsumoto et al., "Macular choroidal thickness and volume in normal subjects measured by swept-source optical coherence tomography," *Investigative Ophthalmology and Visual Science*, vol. 52, no. 8, pp. 4971–4978, 2011.

[15] Y. Ikuno, K. Kawaguchi, T. Nouchi, and Y. Yasuno, "Choroidal thickness in healthy Japanese subjects," *Investigative Ophthalmology and Visual Science*, vol. 51, no. 4, pp. 2173–2176, 2010.

[16] R. S. Ramrattan, T. L. van der Schaft, C. M. Mooy, W. C. de Bruijn, P. G. Mulder, and P. T. de Jong, "Morphometric analysis of Bruch's membrane, the choriocapillaris, and the choroid in aging," *Investigative Ophthalmology and Visual Science*, vol. 35, no. 6, pp. 2857–2864, 1994.

[17] R. Margolis and R. F. Spaide, "A pilot study of enhanced depth imaging optical coherence tomography of the choroid in normal eyes," *The American Journal of Ophthalmology*, vol. 147, no. 5, pp. 811–815, 2009.

[18] J. M. Ruiz-Moreno, I. Flores-Moreno, F. Lugo, J. Ruiz-Medrano, J. A. Montero, and M. Akiba, "Macular choroidal thickness in normal pediatric population measured by swept-source optical coherence tomography," *Investigative Ophthalmology and Visual Science*, vol. 54, no. 1, pp. 353–359, 2013.

Hindawi Publishing Corporation
BioMed Research International
Volume 2014, Article ID 492679, 10 pages
http://dx.doi.org/10.1155/2014/492679

Research Article

Comprehensive Detection, Grading, and Growth Behavior Evaluation of Subthreshold and Low Intensity Photocoagulation Lesions by Optical Coherence Tomographic and Infrared Image Analysis

Stefan Koinzer,[1] Amke Caliebe,[2] Lea Portz,[1] Mark Saeger,[1] Yoko Miura,[3] Kerstin Schlott,[3] Ralf Brinkmann,[3] and Johann Roider[1]

[1] *Department of Ophthalmology, University of Kiel, House 25, Arnold-Heller-Straße 3, 24105 Kiel, Germany*
[2] *Institute of Medical Informatics and Statistics, University of Kiel, House 31, Arnold-Heller-Straße 3, 24105 Kiel, Germany*
[3] *Institute of Biomedical Optics, University of Lübeck, Peter-Monnik-Weg 4, 23562 Lübeck, Germany*

Correspondence should be addressed to Stefan Koinzer; koinzer@auge.uni-kiel.de

Received 4 February 2014; Accepted 11 March 2014; Published 12 May 2014

Academic Editor: Jerzy Nawrocki

Purpose. To correlate the long-term clinical effect of photocoagulation lesions after 6 months, as measured by their retinal damage size, to exposure parameters. We used optical coherence tomographic (OCT)-based lesion classes in order to detect and assess clinically invisible and mild lesions. *Methods*. In this prospective study, 488 photocoagulation lesions were imaged in 20 patients. We varied irradiation diameters (100/300 μm), exposure-times (20–200 ms), and power. Intensities were classified in OCT images after one hour, and we evaluated OCT and infrared (IR) images over six months after exposure. *Results*. For six consecutive OCT-based lesion classes, the following parameters increased with the class: ophthalmoscopic, OCT and IR visibility rate, fundus and OCT diameter, and IR area, but not irradiation power. OCT diameters correlated with exposure-time, irradiation diameter, and OCT class. OCT classes discriminated the largest bandwidth of OCT diameters. *Conclusion*. OCT classes represent objective and valid endpoints of photocoagulation intensity even for "subthreshold" intensities. They are suitable to calculate the treated retinal area. As the area is critical for treatment efficacy, OCT classes are useful to define treatment intensity, calculate necessary lesion numbers, and universally categorize lesions in clinical studies.

1. Introduction

Retinal photocoagulation is inexpensive and easy-to-administer, and the treatment requires only limited repetition and follow-up. It remains the basic therapy for peripheral retinal ischemia and an adjunctive therapy for diabetic macular edema [1]. On the other hand, it is a tissue destructive procedure [2]. Side-effects include acute pain, scotomas, reduced colour vision, decreased night vision, and uncontrolled atrophic scarring [3, 4]. Much effort has been undertaken to reduce lesion intensities [5–9], and pilot studies have collected evidence that "subthreshold" laser treatment can be effective [10–15].

Current concepts of "subthreshold" photocoagulation suffer from dissatisfactory endpoint definitions and from poorly reproducible lesion evaluations. Previous studies have used a variety of criteria to define lesion intensity, such as ophthalmoscopic invisibility [16], fluorescein angiographic (FLA) leakage [6, 11], optoacoustics [17], power titration according to reference lesions [18–20], long-term autofluorescence (AF) imaging [16], and others. We believe that modern optical coherence tomography (OCT) has the capacity to improve lesion definition significantly, as it represents a very sensitive method to detect and subclassify even lesions that remain ophthalmoscopically invisible [21, 22]. An OCT-based classifier may discern two to three subvisible lesion

classes and three to four visible lesion classes as we have shown previously [23].

The present study applies the OCT-based classifier in order to anticipate the area of retina that will ultimately be destroyed by a lesion. Photocoagulation efficacy depends on the totally coagulated area [24], and increased numbers of softer lesions are required for the same clinical effect [14]. Reduced intensity of every single lesion, in order to reduce side-effects like scotoma formation or pain, is invariably accompanied by a reduction of the treated area of retina. A suggested algorithm to calculate the affected retinal area for different intensity lesions used an ophthalmoscopic lesion classifier (moderate, light, barely visible), which is observer- and time-dependent [24]. Therefore, this study examines parameters which are on one hand detectable during or shortly after treatment, more reliable, and more sensitive than ophthalmoscopic lesion evaluation and which are on the other hand correlated with the long-term lesion size.

2. Methods

2.1. Clinical Study. Photocoagulation lesions were examined in a noninterventional, prospective clinical trial on 20 patients receiving photocoagulation for retinal vein occlusion (3/20), occlusive vasculitis (1/20), and diabetic retinopathy (16/20). Some of the latter were additionally treated focally for diabetic maculopathy (4/16). The study was reviewed and approved by the Institutional Ethics Committee at the University of Kiel (application no. A 105/10) and was carried out in accordance with the contents of the declaration of Helsinki. All treatment indications followed the treatment guidelines of the German ophthalmological society [25, 26].

We chose a study area of $15^\circ \times 20^\circ$ of untreated peripheral retina. This area was imaged by colour fundus images (Zeiss FF450 plus fundus camera, Carl Zeiss Meditec AG, Jena, Germany), AF, infrared (IR), and spectral domain—OCT images (HRA + OCT Spectralis, Heidelberg Engineering, Heidelberg, Germany) before treatment and one hour, one month, three months and six months thereafter. All study lesions were placed within that area. OCT scans of the study area were acquired in 30 μm steps and averaged from 20 individual sweeps. Using the follow-up function (AutoRescan), we traced the lesions through all consecutive OCT series.

We used spot diameters of 100 or 300 μm and exposure-times of 20, 50, or 200 ms. Threshold powers were titrated outside the study area. As the visibility threshold of 100 μm lesions was exceeded with 200 ms exposure-time even at the lowest possible power setting of the photocoagulator (50 mW), we added an additional group of 100 μm, 100 ms lesions. In the study area, we applied rows of five lesions, starting at threshold power and increasing power lesionwise in step widths as provided by the laser device, a modified Zeiss VISULAS VITE 532 nm *continuous wave* laser (50–200 mW: 10 mW-steps, 200–500 mW: 20 mW-steps, > 500 mW: 50 mW-steps). In separate rows of lesions, power was decreased from the threshold in the same manner. Each patient received 20–50 study lesions. 562 study lesions were applied altogether, and 488 of these fell into the areas scanned by OCT. Outside the study area, patients received photocoagulation therapy according to the guidelines.

2.2. OCT Cross-Sectional Evaluation. All lesions that could be identified in OCT were mounted in a composite of five images (pretreatment, one hour, one month, three months, and six months). These were arranged in groups with common diameter—exposure-time settings. Within each group, we looked for morphological attributes and ordered the lesions in subgroups with increasing intensity. This led to six consecutive and universal classes of detectable OCT morphologies, irrespective of exposure-time and diameter, as published before [23] and reviewed in Figure 2, top lines.

2.3. Photocoagulation Lesion Size Measurements. The greatest linear diameters (GLD) of the lesions were measured in the OCT software. Measurements were carried out in the 1 μm : 1 μm depiction, which we scaled up to 800% magnification. We measured the lesion size at the level of photoreceptor inner segments (IS) or, in class 2 lesions, at the outer nuclear layer (ONL).

Lesion areas were assessed in colour fundus images taken 1 hour after the end of the treatment and IR images taken 1, 3, and 6 months after the treatment. All lesions were contoured manually in image editing software (Gimp 2). All marked lesions' pixel sizes were semiautomatically measured by ImageJ software, and the pixel and real areas were calculated. The scaling factors were retrieved from the camera and OCT manufacturers' softwares. Every lesion was measured by three independent observers. A lesion was considered visible if at least two observers recognized it, and the mean diameter was used for evaluation, but out-of-range values were excluded as described elsewhere [17].

In fundus colour images, we included the bright necrotic lesion core and the greyish denaturation zone into the measurements. An additional halo, which may develop around intense burns, was considered a secondary effect and excluded from the measurements, because it is strongly time-dependent, and exclusion of these halos results in diameter measurements equal to histological damage diameters [27, 28]. In IR images, all reflectivity alterations—bright or dark—that differed from the pretreatment image were included in the lesions size measurement. IR images were evaluated by three independent observers as well.

2.4. Statistics. The analyses of the development of GLD and lesion area for different time points were performed by an ANOVA with repeated measurements with and without interaction. Influence variables were observation time (within subject) and exposure-time and irradiation diameter and OCT class (between subjects). Lesions with no measurable GLD or area values (0-values), respectively, were excluded from these analyses.

All performed tests were two-sided. P values below 0.05 were considered statistically significant. All statistical analyses were carried out with SPSS software, version 20.

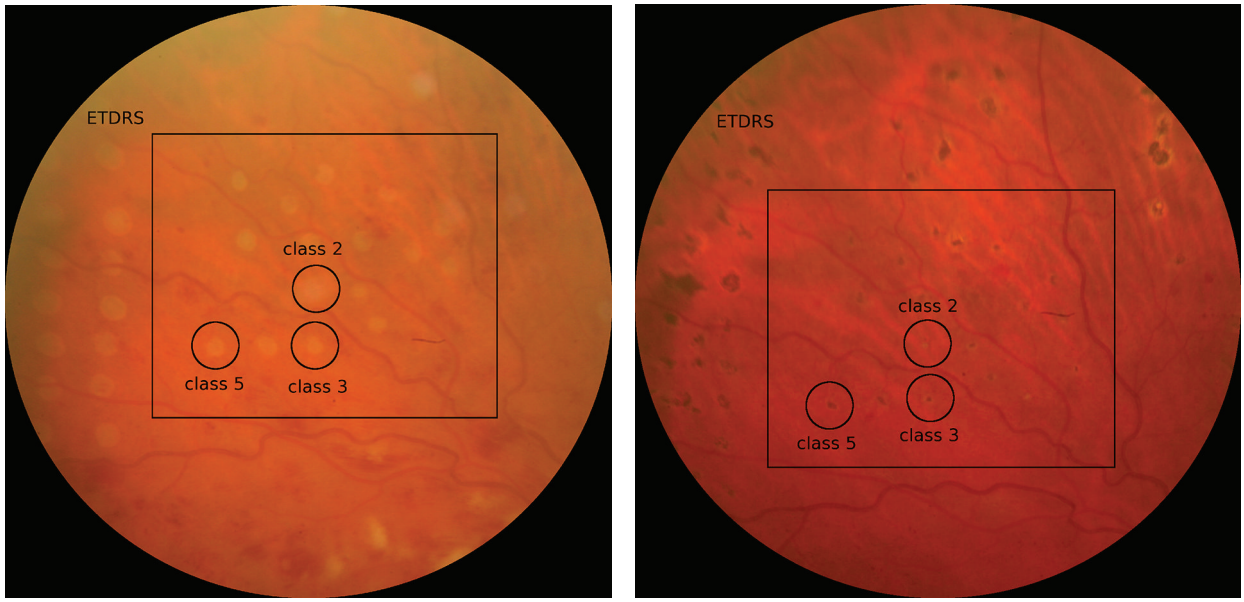

(a) (b)

Figure 1: (a) and (b) show colour fundus images of the same study eye taken one hour after the treatment (a) and 6 months after the treatment (b). Examples of study lesions are marked for OCT classes 2, 3, and 5 lesions. The same lesions are displayed in Figures 2 and 3, classes 2, 3, and 5. The class 2 lesion is invisible after 1 hour, but an optical reflex blurs the location. The classes 3 and 5 lesions are visible in (a) and (b). In the periphery of the fundus, we placed standard panretinal lesions (300 μm, 30 ms, moderate grey).

3. Results

3.1. Clinical Evaluation of Study Lesions (Figure 1). Figure 1 shows fundus images of a typical study area of retina, which contains 4 rows with 5 lesions each, not all of which are visible. Compared to the standard panretinal lesions (300 μm, 30 ms) in the periphery, study lesions were soft, as is demonstrated in Figure 1 at the examples of classes 2, 3, and 5 lesions. The difference is already detectable in 1 hour colour fundus images but becomes more obvious in the 6 months image.

3.2. OCT Classification and Qualitative Analysis (Figure 2). Figure 2 reviews characteristics of the OCT lesion classification in the top rows. The definition of those previously published OCT lesion classes [23] is summarized as follows. Class zero is undetectable. Class one is invisible one hour post-treatment, but detectable at least in OCT images after 1 week. Class two is barely visible in the outer nuclear layer (ONL) after one hour, and class three is clearly visible with an inner segment (IS)—outer segment (OS) junction line interruption after one hour. Class four shows a thinned RPE/Bruch's membrane (BM) complex and RPE elevations at the lesion border. Class five has thinned RPE in the centre and is surrounded by a ring of detached or excavated RPE. Class six has a bright spot in the centre of the dark column in the ONL. The OCT classifier is useful to discern photocoagulation intensity objectively and very accurately.

The lower lines of the composite in Figure 2 show how lesions developed over 6 months in OCT images and give the OCT GLD measurements for each example at all 4 posttreatment time points. We imaged 488 lesions total with OCT. The qualitative OCT analysis of lesion morphologies after one, three, and six months showed that the extent of retinal damage, which includes axial and horizontal extension of OCT alteration, increases with increasing classes and tends to decrease over time.

3.3. Qualitative Analysis of Clinical Lesion Appearance (Figure 3). Figure 3 complements Figure 2 by showing additional data (power, exposure-time, and peak end temperature) and clinical images for the same lesions and at the same time points (fundus colour images and AF and IR images) as Figure 2. Damage areas as measured in colour images (1 hour) or IR images (1–6 months) are indicated as well. Increasing lesion classes show increasing damage areas.

Very mild lesions become apparent in fundus colour images after one hour but are undetectable in the corresponding IR or AF images. Later, mild lesions may vice versa be detectable only in IR and AF images. The comparison of IR and AF images reveals that both show exactly the same discoloration pattern and are, in this clinical context, equivalent. Due to better image quality and availability in some patients, we chose to evaluate IR images to assess lesion areas in this study.

3.4. Sensitivity of Lesion Detection in Fundus Colour (1 Hour), OCT (1 Month), and IR Images (6 Months, Figure 4). Figure 4 shows percentages of lesion visibilities for the different OCT classes in different examination methods. Classes 1 and 2 lesions were rarely ophthalmoscopically visible after 1 hour. There is a clear correlation of lesion class and visibility. The

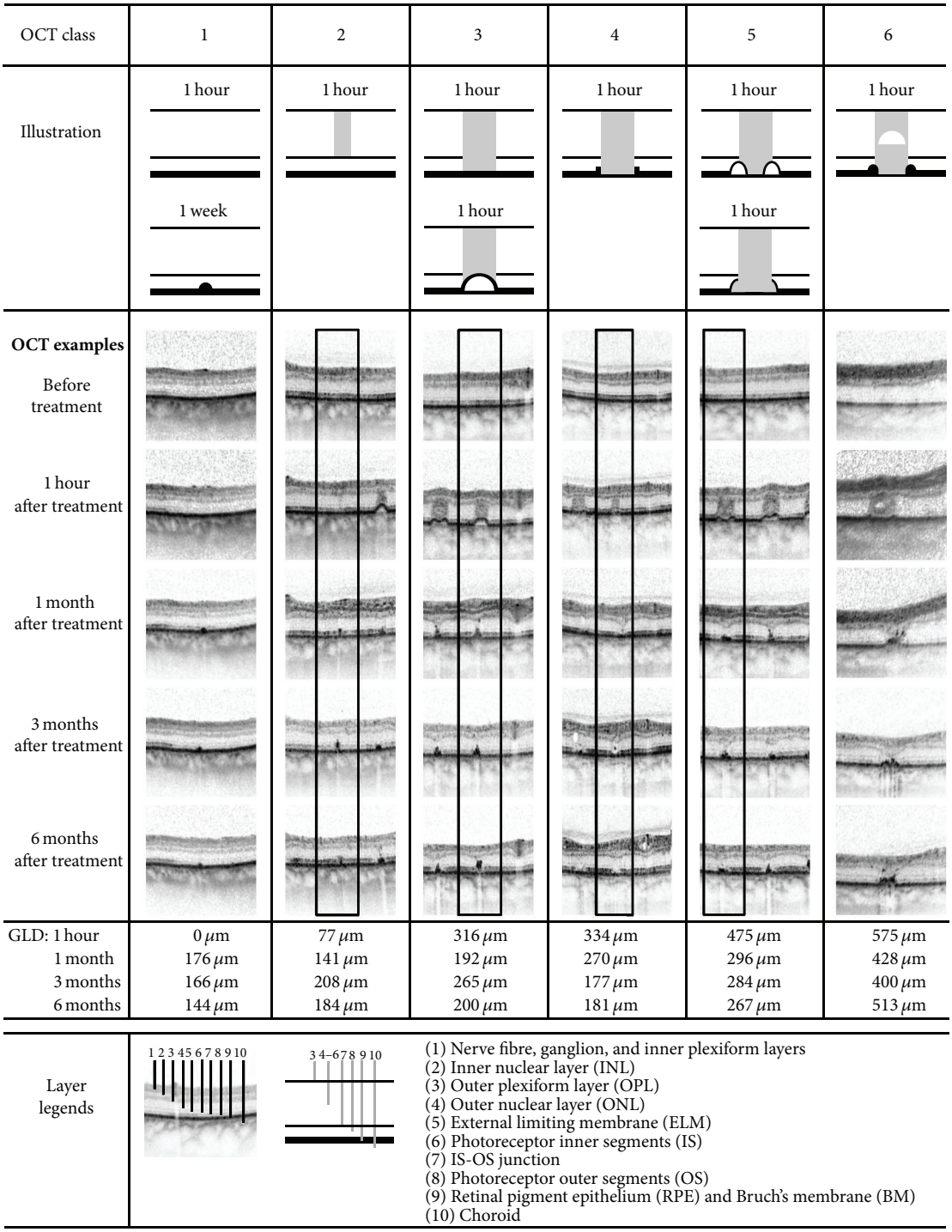

Figure 2: showing representative lesions for 6 consecutive, OCT-based damage classes as defined in a former study [23]. Illustrations of each class are shown at the top of the columns and below representative OCT images taken before the treatment and 1 hour, 1 month, 3 months, and 6 months after the treatment. Classes 3 and 5 may have different OCT appearances, depending on irradiation diameter and exposure-time. All images in a column show the same fundus lesion during follow-up. If an OCT image series shows more than one lesion, a black box demarcates the lesion of interest. At the bottom, the corresponding greatest linear diameters (GLD) are given for all time points, and below that the legend and abbreviations are defined. Physical parameters and clinical images of the same set of lesions are shown in Figure 3.

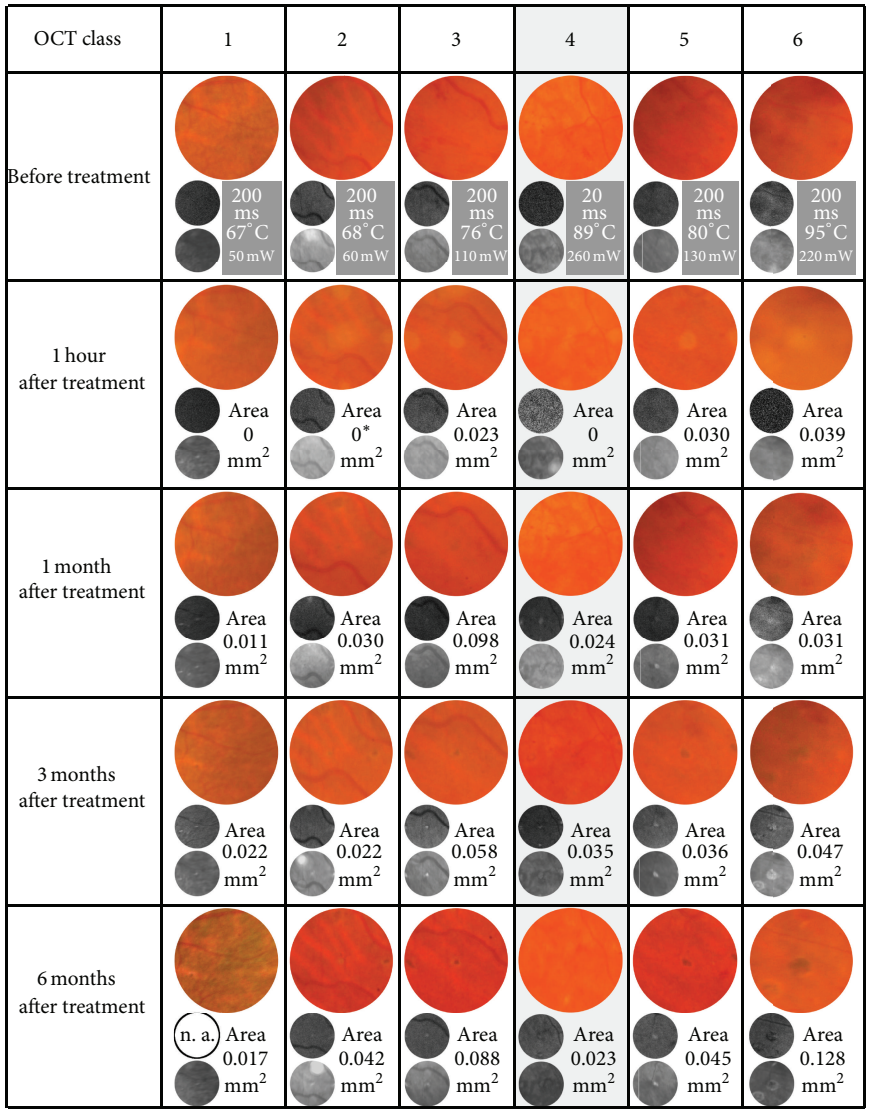

Figure 3: showing the clinical appearance of the lesions from Figure 2 at identical time points (before the treatment, 1 hour, 1 month, and 3 and 6 months after the treatment). Columns compare images of the same lesion over time, and rows compare lesions of different OCT classes at identical time points. Every cell in the composite figure contains a fundus colour image (top), an AF image (middle), and an IR image (bottom). The lesions are centred in all single images. In the top row, we show for each lesion the parameters exposure-time in ms, peak end temperature at the level of the RPE in °C, and power in mW. In the second row (1 hour), the lesion area as measured in the colour image is given in mm^2, and in all consecutive rows (1–6 months), the lesion area as measured in IR images is given in mm^2. The irradiated area of 300 μm lesions is 0.071 mm^2. *In the 1 hour class 2 fundus colour image, the lesion site is superimposed by an optical reflex, but the lesion itself is ophthalmoscopically invisible (see also Figure 1). n. a.: image not available.

OCT image after 1 month is the most sensitive, followed by IR (6 months) and fundus images (1 hour). Notably, about 1/3 of class 0 lesions, that could be detected neither on the fundus image nor in OCT, caused an altered IR reflectance after 6 months.

Immediate visibility rates during treatment were lower than after 1 hour, as whitening increases over hours after lesion application. Compared to clinical treatment conditions, our detection sensitivity was optimized due to digital upscaling, contrast enhancement, and threefold evaluation by independent investigators. Consequently, lesion classes 1, 2, and possibly 3 would have been considered subvisible in clinical routine evaluation during the treatment. All classes 1 and 2 lesions became, by definition, detectable in OCT images, which gives evidence that they do induce structural retinal damage.

3.5. OCT GLD over Time (Figure 5). Figure 5 shows the greatest linear diameters (GLD) as measured in OCT at the time points 1 hour, 1 month, 3 months, and 6 months after the treatment. The corresponding mean values are given numerically in the supplementary table in the Supplementary

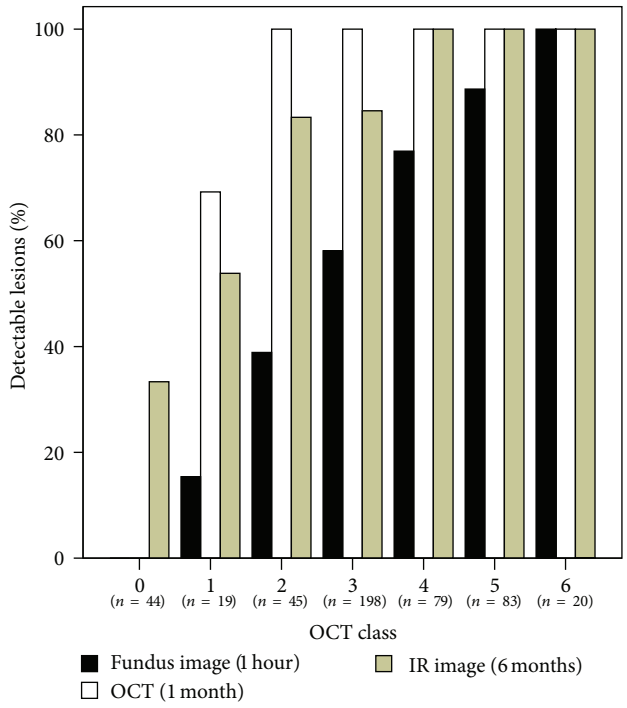

Figure 4: showing percentages of lesion visibilities for the different OCT classes in different examinations. All of OCT class 1 lesions were by definition visible in OCT images after 1 week. Several of these very mild lesions were no longer detectable after 1 month, which explains that less than 100% were detected. Sample sizes for each group are given below the X-axis.

Material available online at http://dx.doi.org/10.1155/2014/492679. Stratification according to irradiation diameter is shown in Figure 5(a), according to exposure-time in Figure 5(b), and according to OCT class in Figure 5(c). Lesions that were not detectable in OCT images (GLD = 0 at any time point) were excluded from the analysis. Consequently, class 1 lesions are not displayed.

The greatest change of GLD was a relevant decrease from 1 hour to 1 month after the treatment. There were only small changes after 1 month. From month 3 to 6, slight growth may be suspected in stronger lesions.

The influence of all three examined factors (irradiation diameter, irradiation time, and OCT class) on the GLD is significant ($P < 0.001$), but OCT classes create the greatest bandwidth of GLD's after 1 hour (177 μm in class 2 to 717 μm in class 6), compared to diameter strata (243 μm in 100 μm lesions to 404 μm in 300 μm lesions) and exposure-time strata (239 μm in 20 ms exposures to 438 μm in 200 ms exposures).

The statistical interaction was significant for GLD changes and irradiation diameter ($P < 0.001$) and GLD changes and OCT class ($P < 0.001$), but not for GLD changes and irradiation time ($P = 0.054$). This indicates that GLD changes similarly over time irrespective of irradiation time, but differently for different irradiation diameters or OCT classes. The statistical evaluation of IR lesion area development over time gave similar results (not shown).

Notice that, in Figure 5(b), the 100 ms lesions were all applied at 100 μm irradiation diameter, which produces a bias toward smaller GLD values. The vast majority of 200 ms lesions, in contrast, were applied at 300 μm irradiation diameter (192/234), which produces a bias toward larger GLD values.

3.6. Power: Intensity Correlation (Figure 6). Figure 6 shows laser powers that achieved different OCT classes, and data are stratified for exposure-times. As expected by clinical experience and theoretically described by the Arrhenius theory [29], longer exposures require lower power to achieve a given damage intensity or OCT class, respectively. This correlation is best appreciated in the class 3 data set. For increasing classes at a given exposure-time, increasing mean power values are expected and indeed found for 20 ms, classes 1–4 lesions. In other groups, such as 200 ms, classes 4–6 lesions, we did not encounter this correlation. Low lesion classes 1 and 2 and all 20 ms lesions have large confidence intervals, which indicates that a given power setting may create highly variable lesions in these subgroups, and that these subgroups cannot be reliably controlled by conventional power control. The data show the limitation of power-dependent retrospective laser control and give evidence of the high impact of transmission and pigmentation variation, which accounts for variable effects of lesions applied with identical power. Temperature data of the same set of lesions, which we have published before [23], underline that the inaccuracy is indeed owed to effect variation at constant powers, not to intensity assessment inaccuracy.

4. Discussion

In this study we evaluated the laser-induced retinal changes of 488 CW photocoagulation lesions from 20 patients. We varied exposure-time, irradiation diameter, and lesion intensity systematically and observed the lesions over 6 months. Our parameter variations included the clinically most important sets, with exposure-times of 20–200 ms and irradiation diameters of 100 and 300 μm. As influence variables, we examined exposure-time, irradiation diameter, OCT lesion class, and treatment laser power. Outcome measures were obtained in ophthalmoscopy and OCT and IR images and included lesion visibility, diameter, and area. The study addressed the questions which imaging modality was most sensitive and which early parameter was most suitable to estimate the retinal defect size after 6 months.

OCT has been used to display photocoagulation lesions as early as 1995, when Toth et al. applied OCT for a histological correlation of photocoagulation lesions [30]. Detection of subthreshold photocoagulation lesions by higher quality spectral domain OCT has been introduced in 2008 [31] and repeatedly published since then [21, 23, 32, 33]. It has been shown that OCT is capable of detecting lesions that are ophthalmoscopically invisible, and that lesions may be invisible in early OCT images but appear later in follow-up

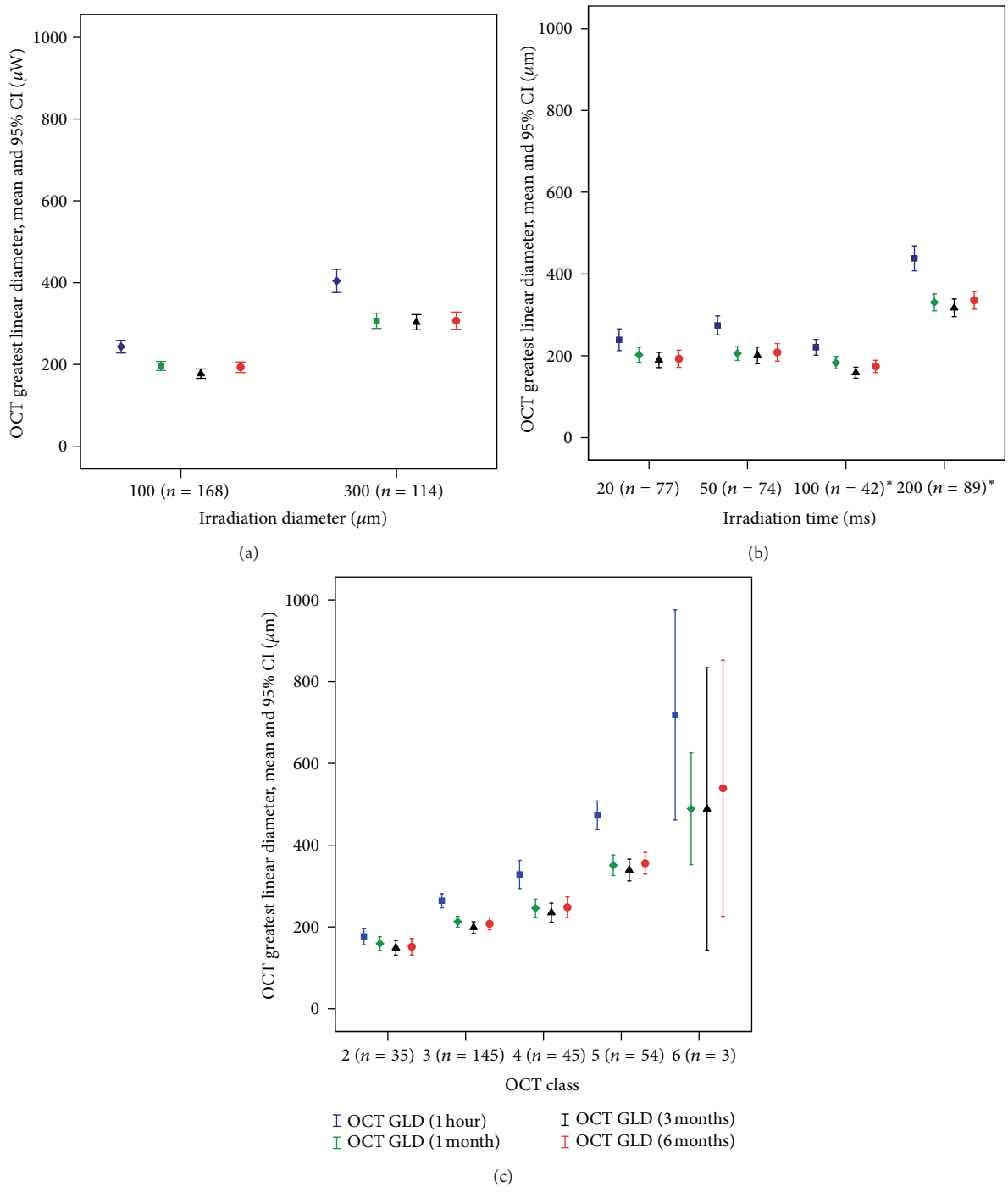

Figure 5: (a)–(c) show OCT GLD from 1 hour to 6 months after treatment. The symbols indicate mean values, and error bars indicate 95% confidence intervals of the mean (CI). In (a), values are grouped in strata of different irradiation diameters, in (b), in strata of different exposure-times, and, in (c), in strata of different OCT classes. *Y*-axes are commonly scaled in all 3 graphs. Sample sizes are indicated at the *X*-axis. *Please note that, in (b), 100 ms lesions were all applied with 100 μm irradiation diameter, and 200 ms lesions, mostly with 300 μm diameter, which leads to a bias of GLD.

OCT images. OCT has also been used in animal experiments to monitor photocoagulation in real time [34, 35]. Since OCT changes appear with a temporal delay, as do ophthalmoscopic changes, the applicability of OCT might be limited for real-time laser control. In our systematic comparison of mild and subthreshold photocoagulation lesions, IR imaging after 6 months was very sensitive and detected changes in one third of lesions that never became visible in OCT images. OCT images were more sensitive than ophthalmoscopy after 1 hour. Among OCT images, sensitivity after 1 week [23] or

1 month was highest and facilitated objective classification of lesions.

We graded lesions' intensities according to a morphological OCT classifier [23], which is universally applicable to lesions with different irradiation diameters and irradiation times. It was developed with 532 nm CW lesions but would most likely be applicable to differently created lesions as well, which is confirmed by findings of Mojana et al. who observed some similar OCT changes in "subthreshold" lesions created with an IR micropulse laser [21]. The OCT classifier includes two different subvisible intensity grades, which were in this case created with a CW photocoagulator. We have proven the validity of the OCT classifier on short-term follow-up data before [23]. In the present study, we show that lesion intensity is the key measure to describe the tissue effect of photocoagulation, as its predictive value concerning the 6-month lesion GLD (152–539 μm) and area is much better than that of power (Figure 6), irradiation diameter, or irradiation time (193–336 μm, Figure 5). OCT lesion intensity classification includes the impact of local and individual transmission and pigmentation as well. The presented lesion assessment has the potential to define common treatment endpoints that would be universally applicable to different photocoagulators (CW versus pulsed and different wavelengths) and protocols (irradiation times and duty cycles).

Numerous studies have investigated photocoagulation lesions after clinical treatment protocols, partly with long clinical follow-up, but with low parameter variation [19, 21, 22, 32, 36–40]. Mojana et al. evaluated subvisible IR-laser lesions in OCT images and discriminated 3 different lesion classes, some of which were comparable to ours, but which did not cover the entire intensity range [21]. Fewer OCT studies varied lesion parameters systematically [19, 20, 24, 41]. The lesion intensities displayed in those studies match our classes 3 (barely visible in [24]/subvisible in [20, 41]) to 6 (moderate grade in [24]/suprathreshold in [20, 41]), while our 2012 publication was the first systematic investigation that described subthreshold classes 1 and 2 [23].

Muqit et al. investigated 120 photocoagulation lesions of 392 μm diameter after 20, 100, or 200 ms irradiations at four different ophthalmoscopic endpoints. They observed decreasing GLD particularly for shorter exposed or less intense lesions in direct comparison of 1 hour and 6 month OCT images [41]. Lavinsky et al. analysed 100–400 μm, 10–200 ms lesions in OCT images over one year [20]. These authors emphasize the advantages of shortly exposed, smaller lesions when controlled by ophthalmoscopic visibility. In contrast, we believe that microstructural lesion intensity is the key measure which is correlated with clinical efficacy and biological response to laser irradiation. In fact, the lack of interaction of exposure-time and GLD development over time gives a clue that exposure-time might not be an adequate measure to differentiate lesions with different growth behaviour.

Photocoagulation scars grow frequently. Reported incidences range from 5.4% of eyes after mild macular treatment [42] to 70% of lesions after strong subretinal neovascularization treatment. Growth occurred at any time point after the treatment, resulted in geographic retinochoroidal

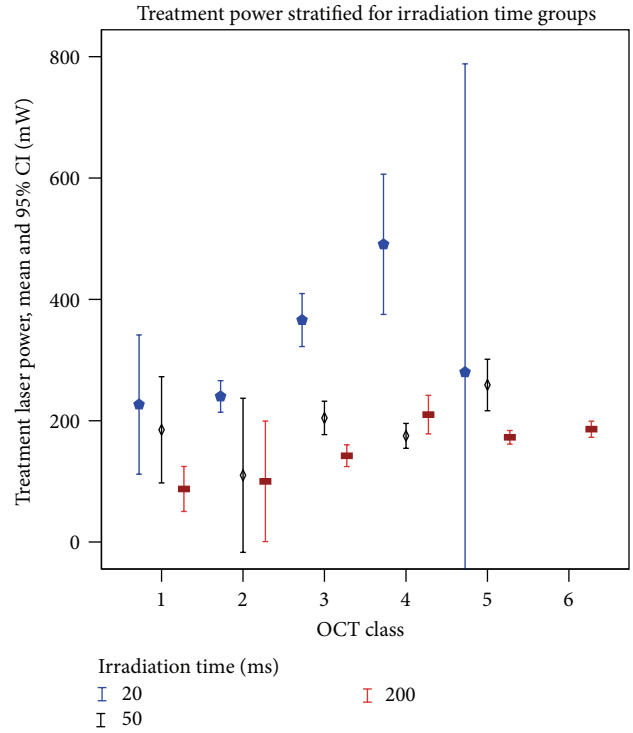

Figure 6: showing laser powers that achieved different OCT classes. Symbols indicate mean values, and error bars indicate CI. Class 5 lesions were rarely achieved by 20 ms exposures, and the low sample size of only 2 lesions limits the validity of the subgroup data shown.

atrophy [4], and can be detrimental in macular lesions [42]. On the other hand, complete retinal restoration after mild photocoagulation has been described and controversially discussed as well [19–22, 43, 44]. In our study, we did not encounter complete lesion disappearance in OCT images except for 5/488 (1%) lesions, in spite of the lowest possible lesion intensity. Concerning growth, obviously either the 6-month time frame of this study was too short to see significant growth or the lesions were too mild to grow substantially.

Lavinsky et al. have previously shown that short exposure or mild panretinal treatment affects a smaller area of retina if compared to standard panretinal treatment, and that there is an inverse correlation of the totally affected retinal area and clinical effectiveness [14, 24]. The lesion they show in [24] as an example of standard ETDRS treatment would be class 6 according to our classification (final GLD 539 μm). In our study, the classes 3 and 4 final GLD was 225 μm, which is 42% of the class 6 diameter. Hence, the treated area of classes 3-4 lesions is about 18% (0.42^2) of class 6 lesions. The final GLD of class 2 lesions was 150 μm, which is 28% of the class 6 diameter, and their treated area is about 8% (0.28^2) of class 6 lesions. In order to treat the same retinal area, about 5 times as many class 3 or 4 lesions and 12 times as many class 1 or 2 lesions would be necessary.

The physical laser parameters are only loosely correlated with the intensity of a retinal lesion, and even the ophthalmoscopic lesion appearance gives limited information on how severe a lesion is on a cellular level. Figure 3 demonstrates

the strong ophthalmoscopic similarity of different OCT-class lesions. In our previous study, we examined 35 lesions that had been applied with 100 μm diameter and 100 ms exposure-time in mild macular treatment, and of these, 12 (34%) were class 3 and 23 (66%) were class 4 [23]. 300 μm, 200 ms lesions were mostly class 5 (59%) but included some class 6 (31%) and few classes 3 and 4 lesions (each 5%) as well, although all lesions aimed at a common ophthalmoscopic endpoint. An ongoing, unpublished study shows that lesion intensities are highly variable within the same treatment session and between different physicians and different patients treated by the same physician. Obviously, ophthalmoscopic lesion evaluation is not very reliable.

5. Conclusions

Therefore, assessment of OCT lesion classes as investigated in this study would, for the first time, facilitate comparability of differently created photocoagulation lesions across different studies. It would also allow a predictive estimation of the clinical effect by the presented correlation with the final lesions sizes and enable calculation of necessary lesion numbers on the basis of a much more reliable measure than ophthalmoscopic lesion class.

Conflict of Interests

The authors declare that there is no conflict of interests regarding the publication of this paper.

Acknowledgment

The authors gratefully acknowledge the support of this collaborative project by the German Ministry of Education and Research (BMBF) according to the Innovation Award for Advancing Medical Technology 2006, Grant no. 01EZ0734, Department of Ophthalmology, University of Kiel.

References

[1] A. M. Shah, N. M. Bressler, and L. M. Jampol, "Does laser still have a role in the management of retinal vascular and neovascular diseases?" *American Journal of Ophthalmology*, vol. 152, no. 3, pp. 332.e1–339.e1, 2011.

[2] M. A. Mainster, "Decreasing retinal photocoagulation damage: principles and techniques," *Seminars in Ophthalmology*, vol. 14, no. 4, pp. 200–209, 1999.

[3] D. S. Fong, A. Girach, and A. Boney, "Visual side effects of successful scatter laser photocoagulation surgery for proliferative diabetic retinopathy: A Literature Review," *Retina*, vol. 27, no. 7, pp. 816–824, 2007.

[4] C. M. Morgan and H. Schatz, "Atrophic creep of the retinal pigment epithelium after focal macular photocoagulation," *Ophthalmology*, vol. 96, no. 1, pp. 96–103, 1989.

[5] P. Lanzetta, G. Dorin, A. Pirracchio, and F. Bandello, "Theoretical bases of non-ophthalmoscopically visible endpoint photocoagulation," *Seminars in Ophthalmology*, vol. 16, no. 1, pp. 8–11, 2001.

[6] J. Roider, R. Brinkmann, C. Wirbelauer, H. Laqua, and R. Birngruber, "Retinal sparing by selective retinal pigment epithelial photocoagulation," *Archives of Ophthalmology*, vol. 117, no. 8, pp. 1028–1034, 1999.

[7] G. Dorin, "Subthreshold and micropulse diode laser photocoagulation," *Seminars in Ophthalmology*, vol. 18, no. 3, pp. 147–153, 2003.

[8] Y. M. Paulus, A. Jain, H. Nomoto et al., "Selective retinal therapy with microsecond exposures using a continuous line scanning laser," *Retina*, vol. 31, no. 2, pp. 380–388, 2011.

[9] M. M. K. Muqit, J. C. B. Gray, G. R. Marcellino et al., "Barely visible 10-millisecond pascal laser photocoagulation for diabetic macular edema: observations of clinical effect and burn localization," *American Journal of Ophthalmology*, vol. 149, no. 6, pp. 979–986, 2010.

[10] J. Roider, S. H. M. Liew, C. Klatt et al., "Selective retina therapy (SRT) for clinically significant diabetic macular edema," *Graefe's Archive for Clinical and Experimental Ophthalmology*, vol. 248, no. 9, pp. 1263–1272, 2010.

[11] S. Koinzer, H. Elsner, C. Klatt et al., "Selective retina therapy (SRT) of chronic subfoveal fluid after surgery of rhegmatogenous retinal detachment: three case reports," *Graefe's Archive for Clinical and Experimental Ophthalmology*, vol. 246, no. 10, pp. 1373–1378, 2008.

[12] C. Klatt, M. Saeger, T. Oppermann et al., "Selective retina therapy for acute central serous chorioretinopathy," *British Journal of Ophthalmology*, vol. 95, no. 1, pp. 83–88, 2011.

[13] J. K. Luttrull, D. C. Musch, and C. A. Spink, "Subthreshold diode micropulse panretinal photocoagulation for proliferative diabetic retinopathy," *Eye*, vol. 22, no. 5, pp. 607–612, 2008.

[14] D. Lavinsky, J. A. Cardillo, L. A. S. Melo Jr., A. Dare, M. E. Farah, and R. Belfort Jr., "Randomized clinical trial evaluating mETDRS versus normal or high-density micropulse photocoagulation for diabetic macular edema," *Investigative Ophthalmology & Visual Science*, vol. 52, no. 7, pp. 4314–4323, 2011.

[15] J. K. Luttrull and C. J. Spink, "Serial optical coherence tomography of subthreshold diode laser micropulse photocoagulation for diabetic macular edema," *Ophthalmic Surgery Lasers and Imaging*, vol. 37, no. 5, pp. 370–377, 2006.

[16] S. Vujosevic, E. Bottega, M. Casciano, E. Pilotto, E. Convento, and E. Midena, "Microperimetry and fundus autofluorescence in diabetic macular edema: subthreshold micropulse diode laser versus modified early treatment diabetic retinopathy study laser photocoagulation," *Retina*, vol. 30, no. 6, pp. 908–916, 2010.

[17] S. Koinzer, K. Schlott, L. Ptaszynski et al., "Temperature controlled retinal photocoagulation—a step toward automated laser treatment," *Investigative Ophthalmology & Visual Science*, vol. 53, pp. 3605–3614, 2012.

[18] J. Figueira, J. Khan, S. Nunes et al., "Prospective randomised controlled trial comparing sub-threshold micropulse diode laser photocoagulation and conventional green laser for clinically significant diabetic macular oedema," *British Journal of Ophthalmology*, vol. 93, no. 10, pp. 1341–1344, 2009.

[19] M. M. K. Muqit, J. C. B. Gray, G. R. Marcellino et al., "In vivo laser-tissue interactions and healing responses from 20- vs 100-millisecond pulse pascal photocoagulation burns," *Archives of Ophthalmology*, vol. 128, no. 4, pp. 448–455, 2010.

[20] D. Lavinsky, J. A. Cardillo, Y. Mandel et al., "Restoration of retinal morphology and residual scarring after photocoagulation," *Acta Ophthalmologica*, vol. 91, pp. e315–e323, 2013.

[21] F. Mojana, M. Brar, L. Cheng, D.-U. G. Bartsch, and W. R. Freeman, "Long-term SD-OCT/SLO imaging of neuroretina and retinal pigment epithelium after subthreshold infrared laser treatment of drusen," *Retina*, vol. 31, no. 2, pp. 235–242, 2011.

[22] G. Deák, M. Bolz, S. Prager et al., "Photoreceptor layer regeneration is detectable in the human retina imaged by SD OCT after laser treatment using sub-threshold laser power," *Investigative Ophthalmology & Visual Science*, vol. 53, pp. 7019–7025, 2012.

[23] S. Koinzer, K. Schlott, L. Portz et al., "Correlation of temperature rise and optical coherence tomography characteristics in patient retinal photocoagulation," *Journal of Biophotonics*, vol. 5, pp. 889–902, 2012.

[24] D. Palanker, D. Lavinsky, M. S. Blumenkranz, and G. Marcellino, "The impact of pulse duration and burn grade on size of retinal photocoagulation lesion: implications for pattern density," *Retina*, vol. 31, no. 8, pp. 1664–1669, 2011.

[25] "Recommendation of the Retinological Society, the German Ophthalmological Society and the Professional Association of Ophthalmologists in Germany: treatment of diabetic maculopathy," *Klinische Monatsblätter für Augenheilkunde*, vol. 228, pp. 446–459, 2011.

[26] "Statement of the German Ophthalmological Society, the Retinological Society and the Professional Association of German Ophthalmologists on Therapy for Macular Oedema in Cases of Retinal Vein Occlusion," *Klinische Monatsblätter für Augenheilkunde*, vol. 227, pp. 542–556, 2010.

[27] W. Weinberg, V.-P. Gabel, and R. Birngruber, "Time sequence of the white hue correlated with the extent of damage in photocoagulation of the retina," *Berichte der Deutschen Ophthalmologischen Gesellschaft*, vol. 78, pp. 603–606, 1981.

[28] S. Koinzer, M. Saeger, C. Hesse et al., "Correlation with OCT and histology of photocoagulation lesions in patients and rabbits," *Acta Ophthalmologica*, vol. 91, pp. e603–e611, 2013.

[29] R. Birngruber, F. Hillenkamp, and V.-P. Gabel, "Theoretical investigations of laser thermal retinal injury," *Health Physics*, vol. 48, no. 6, pp. 781–796, 1985.

[30] C. Toth, R. Birngruber, J. Fujimoto et al., "Correlation between optical coherence tomography, clinical examination and histopathology of macular laser lesions," *Investigative Ophthalmology & Visual Science*, vol. 36, pp. 188–198, 1995.

[31] P. Lanzetta, A. Polito, and D. Veritti, "Subthreshold Laser," *Ophthalmology*, vol. 115, no. 1, p. 216.e1, 2008.

[32] C. Framme, A. Walter, P. Prahs et al., "Structural changes of the retina after conventional laser photocoagulation and selective retina treatment (SRT) in spectral domain OCT," *Current Eye Research*, vol. 34, no. 7, pp. 568–579, 2009.

[33] G. G. Deák, M. Bolz, S. Prager et al., "Photoreceptor layer regeneration is detectable in the human retina imaged by SD-OCT after laser treatment using subthreshold laser power," *Investigative Ophthalmology & Visual Science*, vol. 53, pp. 7019–7025, 2012.

[34] D. Veritti, V. Sarao, and P. Lanzetta, "Online optical coherence tomography during subthreshold laser irradiation," *European Journal of Ophthalmology*, vol. 22, pp. 575–579, 2012.

[35] H. H. Müller, L. Ptaszynski, K. Schlott et al., "Imaging thermal expansion and retinal tissue changes during photocoagulation by high speed OCT," *Biomedical Optics Express*, vol. 3, pp. 1025–1046, 2012.

[36] M. Nagpal, S. Marlecha, and K. Nagpal, "Comparison of laser photocoagulation for diabetic retinopathy using 532-nm standard laser versus multispot pattern scan laser," *Retina*, vol. 30, no. 3, pp. 452–458, 2010.

[37] H. Kang, L. Su, H. Zhang, X. Li, L. Zhang, and F. Tian, "Early histological alteration of the retina following photocoagulation treatment in diabetic retinopathy as measured by spectral domain optical coherence tomography," *Graefe's Archive for Clinical and Experimental Ophthalmology*, vol. 248, no. 12, pp. 1705–1711, 2010.

[38] M. Bolz, K. Kriechbaum, C. Simader et al., "In vivo retinal morphology after grid laser treatment in diabetic macular edema," *Ophthalmology*, vol. 117, no. 3, pp. 538–544, 2010.

[39] K. Kriechbaum, M. Bolz, G. G. Deak, S. Prager, C. Scholda, and U. Schmidt-Erfurth, "High-resolution imaging of the human retina in vivo after scatter photocoagulation treatment using a semiautomated laser system," *Ophthalmology*, vol. 117, no. 3, pp. 545–551, 2010.

[40] J. K. Luttrull, C. Sramek, D. Palanker, C. J. Spink, and D. C. Musch, "Long-term safety, high-resolution imaging, and tissue temperature modeling of subvisible diode micropulse photocoagulation for retinovascular macular edema," *Retina*, vol. 32, no. 2, pp. 375–386, 2012.

[41] M. M. K. Muqit, J. Denniss, V. Nourrit et al., "Spatial and spectral imaging of retinal laser photocoagulation burns," *Investigative Ophthalmology and Visual Science*, vol. 52, no. 2, pp. 994–1002, 2011.

[42] H. Schatz, D. Madeira, H. R. McDonald, and R. N. Johnson, "Progressive enlargement of laser scars following grid laser photocoagulation for diffuse diabetic macular edema," *Archives of Ophthalmology*, vol. 109, no. 11, pp. 1549–1551, 1991.

[43] Y. M. Paulus, A. Jain, R. F. Gariano et al., "Healing of retinal photocoagulation lesions," *Investigative Ophthalmology and Visual Science*, vol. 49, no. 12, pp. 5540–5545, 2008.

[44] P. E. Stanga and M. M. K. Muqit, "Re: comparison of laser photocoagulation for diabetic retinopathy using 532-nm standard laser versus multispot pattern scan laser," *Retina*, vol. 30, no. 10, pp. 1749–1751, 2010.